Model-based formulation of amorphous solid dispersions made by hot-melt extrusion

Dissertation

zur

Erlangung des Doktorgrades (Dr. rer. nat.)

der

Mathematisch-Naturwissenschaftlichen Fakultät

der

Rheinischen Friedrich-Wilhelms-Universität Bonn

vorgelegt von

Esther Sophia Bochmann

aus

Hannover

Bonn 2018

Angefertigt mit Genehmigung der Mathematisch-Naturwissenschaftlichen
Fakultät der Rheinischen Friedrich-Wilhelms-Universität Bonn

Promotionskommission:

Erstgutachter:	Prof. Dr. Karl-Gerhard Wagner
Zweitgutachter:	Prof. Dr. Alf Lamprecht
Drittgutachter:	Prof. Dr. Karsten Mäder
Fachnaher Gutachter:	Prof. Dr. Gerd Bendas
Fachfremder Gutachter:	Prof. Dr. Barbara Kirchner

Tag der Promotion: 13. Mai 2019
Erscheinungsjahr: 2019

Danksagung

An erster Stelle möchte ich mich bei Prof. Dr. Karl G. Wagner für die stets hilfreichen Ratschläge und Denkanstöße bedanken und natürlich für die jederzeit engagierte und umfangreiche Betreuung meiner Promotionsarbeit. Besonders danke ich auch Andreas Gryczke und Dr. Dirk Neumann für die zahlreichen konstruktiven Gespräche und wissenschaftlichen Diskussionen. Ich danke beiden für ihr offenes Ohr und für die freundliche Unterstützung in allen Belangen, welche meine Arbeit maßgeblich geprägt haben.

Ein weiterer herzlicher Dank gilt Rachel Evans für ihre wissenschaftliche Diskussionsbereitschaft und die Hilfe in der englischen Sprache. Auch danke ich meiner Kollegin Kristina Steffens, meiner Masterandin Elgin Üstüner und meinen Wahlpflichtfächlern Noreen Schütz, Rafael Bachmeier und Kevin Kayser für ihre tatkräftige Unterstützung. Großer Dank gilt ebenfalls Thorsten Cech, wie auch Florian Bang und Thorsten Agnese, für ihre umfangreiche Hilfe und die Möglichkeit, weiterhin meine Messungen am Rheometer der BASF SE durchführen zu dürfen.

Außerdem danke ich meinen Bürokollegen Bernadette Kettel, Maryam Shetab-Bousheri, Pia Steinlein und Simone Putzke. Eure liebe Hilfe und die außerordentlich schöne gemeinsame Zeit werden mir immer in guter Erinnerung bleiben. Großen Dank auch an meinen Arbeitskreis und Martina Gerlitz für die netten Abende und Gespräche abseits vom Institutsalltag. An dieser Stelle möchte ich mich ebenfalls bei allen weiteren Angehörigen und Kollegen des Instituts für ihre Hilfsbereitschaft und die sehr gute Zusammenarbeit bedanken.

Am Ende zu den wichtigsten Menschen meines Lebens: Meiner Familie, auf die ich mich blind verlassen kann und die mir immer zur Seite steht, unabhängig von Situation und Umständen. Und besonders Lukas, der mich manchmal besser zu kennen scheint, als ich mich selbst. Danke.

TABLE OF CONTENT:

1 Introduction and theoretical background

Computation chemistry and high throughput screening are two procedures which enable the identification of new chemical entities (NCEs) with an improved receptor interaction. In most cases, the increase in specificity to the target receptor, are often connected with a higher lipophilicity and a respective poor water solubility of the NCE. In dependence of the desired doses of the active pharmaceutical ingredient (API), the poor water solubility causes a low oral bioavailability of the new drug. To overcome this solubility-dependent low bioavailability, the use of so-called “enabling technologies” is gaining more and more attention over the recent years. One of these new techniques is the molecular dispersive embedment of poorly water-soluble APIs in polymeric matrices to form an amorphous solid dispersion (ASD) by means of hot-melt extrusion (HME). Especially the formation of intermolecular interactions between API and polymer are important for producing a stable ASD over the shelf life. For forming ASD, a soluble API/polymer combination lead to a thermodynamically stable system, which would be superior in durability. Otherwise, an only kinetically stabilized ASD with a respective insoluble API/polymer combination would be prone to recrystallization during shelf life. Furthermore, the strength of this API-polymer interactions and HME process conditions dictates the API weight fraction which can be embedded amorphously in the polymeric matrix [1–11]. A better understanding of the specific interactions between API and polymer, which enable a “molecular dispersive” solubilization, is vital to evaluate whether a solubility prediction of APIs in polymer melts is feasible. In the early stage of HME formulation development, the available API amount is very limited or expensive. Therefore, a theoretical consideration or preselection of excipients for HME is beneficial. Especially HME, with its high throughput of material even at small-scale, a reduction of trials due to process simulation and prediction of solubility within the polymer matrix is desirable. The use of HME numerical simulation depends on the available physicochemical data of the ASD under consideration. An easy approach to short cut this long-lasting characterization of ASD would simplify the use of such simulation software and it reduces the effort in early HME formulation and process development. It would encourage researchers to consider hot-melt extrusion as a formulation technology in early drug product development [8–11].

1.1 Solubility prediction of APIs in polymeric matrices

In literature most publications are using the Hansen solubility theory, partially in combination with the Flory-Huggins lattice theory or molecular dynamics simulations [12–15].

1.1.1 Hansen solubility parameter, group contribution method

The Hansen solubility parameters (or cohesive energy parameters) are dividing the cohesive forces between two molecules into three different forces, namely: hydrogen bonding, dipole forces and dispersive forces. If the solubility parameters of two substances are similar, miscibility is likely. In most cases, the cohesive forces are described by means of a mathematical model in which a numerical value is given to every molecular group in the respective substance (group contribution method, GCM) [12,14,16–26]. The application of the Hansen solubility parameters for the solubility prediction of APIs in polymer melts has been validated several times, in some cases with adjustment of the original Hansen parameter calculation [16–18,27,28]. The adjustments comprises inter alia the splitting of hydrogen bonding into proton-donators and proton-acceptors [28] or changes / alternatives in the common GCM data set [15,16,21,29].

1.1.2 Flory-Huggins lattice theory

Another assumption to estimate the solubility of APIs in polymeric matrices is based on the Flory-Huggins lattice theory for polymer solution with its interaction parameter χ. By using a mathematical term for the mixing entropy, the difference in molecular size between polymer and solvent can be considered [13,14]. If the free energy of mixing between two substances is negative, the miscibility of both components is likely. To adapt the original Flory-Huggins lattice theory for ASDs, several procedures has been published. The adaptions comprises the inclusion of the activation coefficient for the evaluation of the free mixing energy [22,25,26], molecular dynamic simulations [15,27,30–32], identification of changes in Gibbs energy by using heat capacity [33], evaluation of the temperature dependency [20,24,34,35] and the adoption to hot-melt extruded materials [19]. In the case of molecular dynamic simulations, the software PC-SAFT from Sadowski and co-workers is one of the promising newly developed

methods [27,36–38]. Using PC-SAFT, not only binary mixtures of different API/polymer combinations were investigated [27,36], but also the influence of humidity on the long-term physical stability of ASD [37] or amorphous-amorphous phase separations [38] were evaluated.

1.1.3 **Limitations of the common solubility predictions**

The general assumption of the two named solubility prediction theories is based on liquid, highly diluted organic systems [12,13]. Regarding polymer melts, the solute (API) is substantially smaller than the "solvent" (polymer) and it is not diluted infinitively. Thus, an adaption of the original solubility theories to an amorphous API-polymer melt is questionable. Another disadvantage is the low consideration of specific API-polymer interactions and a missing energy term for breaking crystal lattices. Therefore, both solubility theories are only dealing with a possible exchange of energy due to deviations in the intermolecular cohesive forces of already amorphous systems, but they do not handle the solubility of a crystalline API in a polymer melt [24]. Especially the Hansen solubility parameters have its limitation concerning the prediction of the general polarity from a chemical structure and the formation of hydrogen bonding. Thus only qualitative statements can be made without quantitative considerations [16]. The Hansen solubility parameters are only depict the enthalpy of such system which limits the application per se, since a term for entropy is missing [27]. A further disadvantage of both assumptions is that the melt viscosity of the polymeric matrix, which is limiting miscibility during the HME process, remains unconsidered [17]. In the case of the Flory-Huggins lattice theory, the minor influence of variations in molecular chain length of the polymer on the interaction parameter χ might be an indication of an insufficient consideration of molecular chain length effects (e.g. hydrogen bonding) on the interactions and miscibility of a system [39,40].

1.1.4 **Limitations in selection of substances in literature**

A common procedure in the published literature, where Hansen solubility parameters or Flory-Huggins lattice theory has been investigated, is the evaluation of only one "model substance" [19–21,24,34,35,39–41]. In rare cases the amount of employed substances exceeded ten [16,23,42]. Furthermore, a systemic selection of molecules to establish a general valid prediction model has been rarely investigated [16,18,23],

whereby Just et al. had conducted a selection of similar structures and considered less a high variance in molecular structures. Another limitation in literature is the use of identical model substances to validate the prediction model (e.g. Indomethacin [17,21,24,25,33,40,43–46], Ibuprofen [15,18,25,41,45–47], Naproxen [16,18,23,39,45,46], Nifedipine [25,26,43,44,46]). To validate a general solubility prediction model, covering most parts of the molecular space of APIs is mandatory but rarely used.

1.1.5 **Limitations in conclusive experimental data in literature**

A very common measuring technique to examine the solubility of API in polymeric matrices is the differential scanning calorimetry (DSC). Especially the melting point depression method by evaluating the endset of the API melting peak needs an adequate low heating rate and API particle size [44,48], which has not been considered in some publications [18,27]. Furthermore, the evaluation of the API melting/dissolution peak onset is questionable, since this indicates only the temperature where the API starts to dissolve. At this temperature point it is unknown, if the entire API weight fraction would dissolve or if it is just partially stable. Furthermore at low crystalline API weight fractions, the onset becomes broader and lower, which decreases the accuracy of onset determination [19,21,23]. Thus, a robust and fast measuring technique to determine the solubility of API in polymeric matrices is needed. Especially, a method which enables a fast equilibration of an API/polymer mixture at a certain measuring temperature, thus the method would be less sensitive to the applied DSC heating rate or to the obtained particle size during sample preparation, is beneficial. Rational formulation development of hot-melt extrusion would be helpful.

In formulation development of amorphous solid dispersions (ASDs) by means of hot-melt extrusion (HME), the process is generally API-consuming and expensive in terms of time and personal [11,49–51]. Especially when the API availability is limited, one of the major drawbacks of HME is the high material throughput. Furthermore, the various process parameters (screw speed, screw configuration, throughput, temperature profile, etc.) lead to a complex multivariable process, which is challenging to optimize or scale-up [52,53]. Therefore, several solutions to simplify the use of HME in early formulation development had already been investigated to enable a rational process and formulation development of ASD by means of HME.

1.1.6 **Mini- and micro-scale testing methods and procedures for HME**

A very common example to reduce the batch size for first HME trials to as little as 5 g is the use of small-scale co-rotating twin-screw extruders (e.g. 9 mm screw diameter) prior to the production scale [52,54–56]. It enables a solid dispersion formulation screening but due to the fundamental differences to larger scale extruders, a rational process development or scale-up is not feasible [57]. For process development and scale-up, crucial process characteristics (e.g. residence time distribution (RTD) and specific mechanical energy (SME)) have to be measured accurately [53,57–59]. Therefore, extruders of 10-12 mm or larger screw diameters are needed but this will require throughputs of 50 g/h up to 20 kg/h. Since the extruder needs equilibration time for the set process conditions (approx. 15-30 min), the required material quantity to conduct extrusion experiments and to gain HME process information would increase drastically.

In terms of rational solid dispersion formulation screening with a very low required batch-size, thermoanalytical techniques, such as differential scanning calorimetry (DSC) [21,24,39,43,44,46,60], hot-stage microscopy [52,57] or melt rheology (please see section 1.2.2) are often investigated. DSC can either be used for the glass transition temperature (T_g) determination for process development [57,61] or for the characterization of the API-solubility within the polymeric matrix (please see section 1.1). Furthermore, the miscibility of compounds can be determined by hot-stage microscopy, which additionally enables the assessment of the potential temperature range for processing in HME [52,57].

In general, thermoanalytical techniques are only providing hints for a subsequent production of ASD by means of hot-melt extrusion. Especially, the determination of process conditions is limited, and subsequent HME process results may differ from previous thermoanalytical findings. Therefore, mini-scale twin-screw extruders are needed to obtain better process information, however the cost of an increased batch size might be limiting in early formulation development.

1.1.7 **Melt viscosity as a material characteristic**

In HME, melt rheology is one of the crucial material characteristics which defines the applicable process conditions for a required formulation, such as screw speed, pressure and temperature profile [52,58,62–65]. It influences the addition of plasticizer, energy input or viscous heat dissipation, torque (motor load) and hence the entire extrusion performance [4,53,58]. Even more, melt rheology can be used for the definition of the applicable and optimal process window for HME [64,66–69] or as a formulation screening tool [70].

In addition, melt viscosity is also one of the crucial input parameters for HME process simulation. By using melt viscosity in combination with HME simulation, the experimental effort for defining the optimal HME process conditions can be minimized. Furthermore, especially for thermo-sensitive APIs, the required long-lasting rheological measurement for HME simulation might be not feasible. Hence, a simple way to gain the rheological behavior as a function of shear and temperature for a required formulation is needed.

1.1.8 **Numerical computation of hot-melt extrusion process**

To get a better insight and understanding of the extrusion process, numerical HME simulation is a valid and often used tool [52,63,71,72]. It identifies temperature, pressure and shear profiles along the screws which is helpful to determine the process window of HME to manufacture ASD [73]. The two major applications of HME numerical simulation are the optimization of screw configuration and the scale-up from small-scale to production-scale extruders.

Several research works have already been conducted with HME simulation for a better process understanding. For example, the quantification of the mixing capability of mixing elements and kneading blocks as a function of staggering angle has been investigated [74]. It was found that the quality of mixing is not significantly higher of a mixing element than of a normal conveying element. Regarding suspensions, the erosion and break-up of fillers in the HME process has also been investigated [75]. It was shown, that this filler behavior can accurately predicted by HME simulation software and it can

be used to design the optimal mixing equipment. For suspensions, the pressure-dependent wall slippage at barrel and screw surfaces could be characterized [76]. Furthermore, the optimization of the screw configuration was performed with the help of multi-objective evolutionary algorithms or genetic algorithms which were able to deal with this multi-objective and multimodal issue [72,77]. Another important process parameter of HME, which was investigated several times, is the residence time distribution (RTD). Several influencing factors, such as throughput and screw speed, have been identified and simulation models for RTD profiles were established [78–81]. In the case of pharmaceutical development, HME simulation has already been investigated to perform a rational development, process up-scaling and formulation screening to form ASDs [52,59]. Especially for up-scaling, adiabatic process conditions are favorable. If non-adiabatic conditions at large-scale extruders occur, viscous dissipation will lead to a process which goes off the course [82]. Due to the high influence of barrel heating and cooling at small-scale extruders, non-adiabatic conditions can be compensated and thus they are difficult to detect. HME numerical simulation is one solution to address this scale issue between small- and large-scale extruders. In general, there are two different types of computation: (i) one dimensional and (ii) three dimensional simulation [71,73]. A 3D model for HME simulation is more accurate, especially in terms of detecting hot-spots and quality of mixing. However, the computation is numerically too expensive and long-lasting for simulating an entire twin-screw extruder. Thus, a more practical but still sufficient approach in HME formulation development is a 1D model which is faster and does not need any specific computerization. However, the 3D model can be used additionally to compute a specific part of the twin-screw extruder or for particle tracking to calculate the mixing capability. For both simulation types, the main drawback is the need of experimental input variables, especially melt viscosity which might not be easy to access. Furthermore, the use of HME simulation in early formulation screening is limited, since the physicochemical characteristics has to be measured for every physical mixture under consideration prior to any simulation work.

1.2 References

[1] K. Mäder, U. Weidenauer, D. Allhenn, eds., Innovative Arzneiformen: ein Lehrbuch für Studium und Praxis; mit 59 Tabellen, Wiss. Verl.-Ges, Stuttgart, 2010.

[2] M.A. Repka, N. Langley, J. DiNunzio, eds., Melt Extrusion, Springer New York, New York, NY, 2013. http://link.springer.com/10.1007/978-1-4614-8432-5 (accessed September 24, 2015).

[3] J. Breitenbach, Melt extrusion: from process to drug delivery technology, Eur. J. Pharm. Biopharm. 54 (2002) 107–117.

[4] S. Shah, S. Maddineni, J. Lu, M.A. Repka, Melt extrusion with poorly soluble drugs, Int. J. Pharm. 453 (2013) 233–252. doi:10.1016/j.ijpharm.2012.11.001.

[5] W.L. Chiou, S. Riegelman, Pharmaceutical Applications of Solid Dispersion Systems, J. Pharm. Sci. 9 (1971) 1281–1301.

[6] S. Janssens, G. Van den Mooter, Review: physical chemistry of solid dispersions, J. Pharm. Pharmacol. 61 (2009) 1571–1586. doi:10.1211/jpp/61.12.0001.

[7] K. Kolter, K. Matthias Karl, Andreas Gryczke, Hot-Melt Extrusion with BASF Pharma Polymers, 2. Auflage, BASF, Ludwigshafen, 2012. http://www.pharma-ingredients.basf.com/documents/enp/brochure/en/03_120803%20hot%20melt%20extrusion%20with%20basf%20pharma%20polymers.pdf (accessed September 24, 2015).

[8] M. Stanković, H.W. Frijlink, W.L.J. Hinrichs, Polymeric formulations for drug release prepared by hot melt extrusion: application and characterization, Drug Discov. Today. 20 (2015) 812–823. doi:10.1016/j.drudis.2015.01.012.

[9] H. Liu, L.S. Taylor, K.J. Edgar, The role of polymers in oral bioavailability enhancement; a review, Polymer. (2015). doi:10.1016/j.polymer.2015.09.026.

[10] Y. He, C. Ho, Amorphous Solid Dispersions: Utilization and Challenges in Drug Discovery and Development, J. Pharm. Sci. 104 (2015) 3237–3258. doi:10.1002/jps.24541.

[11] J.S. LaFountaine, J.W. McGinity, R.O. Williams, Challenges and Strategies in Thermal Processing of Amorphous Solid Dispersions: A Review, AAPS PharmSciTech. (2015). doi:10.1208/s12249-015-0393-y.

[12] C.M. Hansen, Hansen solubility parameters: a user's handbook, 2nd ed, CRC Press, Boca Raton, 2007.

[13] P.J. Flory, Principles of polymer chemistry, 19. print, Cornell Univ. Press, Ithaca, NY, 2006.

[14] D.W. van Krevelen, Properties of polymers: their correlation with chemical structure: their numerical estimation and prediction from additive group contributions, 4th, completely rev. ed ed., Elsevier, Amsterdam, 2009.

[15] M. Maus, K.G. Wagner, A. Kornherr, G. Zifferer, Molecular dynamics simulations for drug dosage form development: thermal and solubility characteristics for hot-melt extrusion, Mol. Simul. 34 (2008) 1197–1207. doi:10.1080/08927020802411695.

[16] S. Just, F. Sievert, M. Thommes, J. Breitkreutz, Improved group contribution parameter set for the application of solubility parameters to melt extrusion, Eur. J. Pharm. Biopharm. 85 (2013) 1191–1199. doi:10.1016/j.ejpb.2013.04.006.

[17] A. Forster, J. Hempenstall, I. Tucker, T. Rades, Selection of excipients for melt extrusion with two poorly water-soluble drugs by solubility parameter calculation and thermal analysis, Int. J. Pharm. 226 (2001) 147–161.

[18] J. Albers, K. Matthée, K. Knop, P. Kleinebudde, Evaluation of predictive models for stable solid solution formation, J. Pharm. Sci. 100 (2011) 667–680. doi:10.1002/jps.22313.

[19] J. Djuris, I. Nikolakakis, S. Ibric, Z. Djuric, K. Kachrimanis, Preparation of carbamazepine–Soluplus® solid dispersions by hot-melt extrusion, and prediction of drug–polymer miscibility by thermodynamic model fitting, Eur. J. Pharm. Biopharm. 84 (2013) 228–237. doi:10.1016/j.ejpb.2012.12.018.

[20] C. Donnelly, Y. Tian, C. Potter, D.S. Jones, G.P. Andrews, Probing the Effects of Experimental Conditions on the Character of Drug-Polymer Phase Diagrams Constructed Using Flory-Huggins Theory, Pharm. Res. 32 (2015) 167–179. doi:10.1007/s11095-014-1453-9.

[21] J. Gupta, C. Nunes, S. Vyas, S. Jonnalagadda, Prediction of Solubility Parameters and Miscibility of Pharmaceutical Compounds by Molecular Dynamics Simulations, J. Phys. Chem. B. 115 (2011) 2014–2023. doi:10.1021/jp108540n.

[22] T. Lindvig, M.L. Michelsen, G.M. Kontogeorgis, A Flory-Huggins model based on the Hansen solubility parameters, Fluid Phase Equilibria. 203 (2002) 247–260.

[23] S. Thakral, N.K. Thakral, Prediction of drug-polymer miscibility through the use of solubility parameter based flory-huggins interaction parameter and the experimental validation: PEG as model polymer, J. Pharm. Sci. 102 (2013) 2254–2263. doi:10.1002/jps.23583.

[24] Y. Zhao, P. Inbar, H.P. Chokshi, A.W. Malick, D.S. Choi, Prediction of the thermal phase diagram of amorphous solid dispersions by flory-huggins theory, J. Pharm. Sci. 100 (2011) 3196–3207. doi:10.1002/jps.22541.

[25] P.J. Marsac, T. Li, L.S. Taylor, Estimation of Drug–Polymer Miscibility and Solubility in Amorphous Solid Dispersions Using Experimentally Determined Interaction Parameters, Pharm. Res. 26 (2009) 139–151. doi:10.1007/s11095-008-9721-1.

[26] P.J. Marsac, S.L. Shamblin, L.S. Taylor, Theoretical and Practical Approaches for Prediction of Drug–Polymer Miscibility and Solubility, Pharm. Res. 23 (2006) 2417–2426. doi:10.1007/s11095-006-9063-9.

[27] A. Prudic, Y. Ji, G. Sadowski, Thermodynamic Phase Behavior of API/Polymer Solid Dispersions, Mol. Pharm. 11 (2014) 2294–2304. doi:10.1021/mp400729x.

[28] E. Stefanis, C. Panayiotou, A new expanded solubility parameter approach, Int. J. Pharm. 426 (2012) 29–43. doi:10.1016/j.ijpharm.2012.01.001.

[29] C.M. Hansen, 50 Years with solubility parameters—past and future, Prog. Org. Coat. 51 (2004) 77–84. doi:10.1016/j.porgcoat.2004.05.004.

[30] K. Pajula, M. Taskinen, V.-P. Lehto, J. Ketolainen, O. Korhonen, Predicting the Formation and Stability of Amorphous Small Molecule Binary Mixtures from Computationally Determined Flory−Huggins Interaction Parameter and Phase Diagram, Mol. Pharm. 7 (2010) 795–804. doi:10.1021/mp900304p.

[31] K. Pajula, L. Wittoek, V.-P. Lehto, J. Ketolainen, O. Korhonen, Phase Separation in Coamorphous Systems: *in Silico* Prediction and the Experimental Challenge of Detection, Mol. Pharm. 11 (2014) 2271–2279. doi:10.1021/mp400712m.

[32] M. Maniruzzaman, M.J. Snowden, M.S. Bradely, D. Douroumis, Studies of intermolecular interactions in solid dispersions using advanced surface chemical analysis, RSC Adv. 5 (2015) 74212–74219. doi:10.1039/C5RA13176F.

[33] R.A. Bellantone, P. Patel, H. Sandhu, D.S. Choi, D. Singhal, H. Chokshi, A.W. Malick, N. Shah, A method to predict the equilibrium solubility of drugs in solid polymers near room temperature using thermal analysis, J. Pharm. Sci. 101 (2012) 4549–4558. doi:10.1002/jps.23319.

[34] D. Lin, Y. Huang, A thermal analysis method to predict the complete phase diagram of drug–polymer solid dispersions, Int. J. Pharm. 399 (2010) 109–115. doi:10.1016/j.ijpharm.2010.08.013.

[35] K. Bansal, U.S. Baghel, S. Thakral, Construction and Validation of Binary Phase Diagram for Amorphous Solid Dispersion Using Flory–Huggins Theory, AAPS PharmSciTech. (2015). doi:10.1208/s12249-015-0343-8.

[36] A. Prudic, T. Kleetz, M. Korf, Y. Ji, G. Sadowski, Influence of Copolymer Composition on the Phase Behavior of Solid Dispersions, Mol. Pharm. 11 (2014) 4189–4198. doi:10.1021/mp500412d.

[37] K. Lehmkemper, S.O. Kyerematen, O. Heinzerling, M. Degenhardt, G. Sadowski, Long-Term Physical Stability of PVP- and PVPVA-Amorphous Solid Dispersions, Mol. Pharm. 14 (2017) 157–171. doi:10.1021/acs.molpharmaceut.6b00763.

[38] C. Luebbert, F. Huxoll, G. Sadowski, Amorphous-Amorphous Phase Separation in API/Polymer Formulations, Molecules. 22 (2017) 296. doi:10.3390/molecules22020296.

[39] A. Paudel, J. Van Humbeeck, G. Van den Mooter, Theoretical and Experimental Investigation on the Solid Solubility and Miscibility of Naproxen in Poly(vinylpyrrolidone), Mol. Pharm. 7 (2010) 1133–1148. doi:10.1021/mp100013p.

[40] M.M. Knopp, N.E. Olesen, P. Holm, P. Langguth, R. Holm, T. Rades, Influence of Polymer Molecular Weight on Drug-Polymer Solubility: A Comparison between Experimentally Determined Solubility in PVP and Prediction Derived from Solubility in Monomer, J. Pharm. Sci. 104 (2015) 2905–2912. doi:10.1002/jps.24410.

[41] D.J. Greenhalgh, A.C. Williams, P. Timmins, P. York, Solubility parameters as predictors of miscibility in solid dispersions, J. Pharm. Sci. 88 (1999) 1182–1190. doi:10.1021/js9900856.

[42] Y.T. Bao, N.K.P. Samuel, C.G. Pitt, The prediction of drug solubilities in polymers, J. Polym. Sci. Part C Polym. Lett. 26 (1988) 41–46.

[43] Y. Sun, J. Tao, G.G.Z. Zhang, L. Yu, Solubilities of crystalline drugs in polymers: An improved analytical method and comparison of solubilities of indomethacin and nifedipine in PVP, PVP/VA, and PVAc, J. Pharm. Sci. (2010) n/a-n/a. doi:10.1002/jps.22251.

[44] J. Tao, Y. Sun, G.G.Z. Zhang, L. Yu, Solubility of Small-Molecule Crystals in Polymers: d-Mannitol in PVP, Indomethacin in PVP/VA, and Nifedipine in PVP/VA, Pharm. Res. 26 (2009) 855–864. doi:10.1007/s11095-008-9784-z.

[45] R. Haddadin, F. Qian, S. Desikan, M. Hussain, R.L. Smith, Estimation of Drug Solubility in Polymers via Differential Scanning Calorimetry and Utilization of the Fox Equation, Pharm. Dev. Technol. 14 (2009) 19–27. doi:10.1080/10837450802409370.

[46] S.O. Kyerematen, M. Pudlas, G.H. Woehrle, A Fast and Reliable Empirical Approach for Estimating Solubility of Crystalline Drugs in Polymers for Hot Melt Extrusion Formulations, J. Pharm. Sci. 103 (2014) 2847–2858. doi:10.1002/jps.23941.

[47] M. Maniruzzaman, J. Pang, D.J. Morgan, D. Douroumis, Molecular Modeling as a Predictive Tool for the Development of Solid Dispersions, Mol. Pharm. 12 (2015) 1040–1049. doi:10.1021/mp500510m.

[48] A. Mahieu, J.-F. Willart, E. Dudognon, F. Danède, M. Descamps, A New Protocol To Determine the Solubility of Drugs into Polymer Matrixes, Mol. Pharm. 10 (2013) 560–566. doi:10.1021/mp3002254.

[49] H. Patil, R.V. Tiwari, M.A. Repka, Hot-Melt Extrusion: from Theory to Application in Pharmaceutical Formulation, AAPS PharmSciTech. 17 (2016) 20–42. doi:10.1208/s12249-015-0360-7.

[50] R.V. Tiwari, H. Patil, M.A. Repka, Contribution of hot-melt extrusion technology to advance drug delivery in the 21st century, Expert Opin. Drug Deliv. 13 (2016) 451–464. doi:10.1517/17425247.2016.1126246.

[51] A. Newman, G. Knipp, G. Zografi, Assessing the performance of amorphous solid dispersions, J. Pharm. Sci. 101 (2012) 1355–1377. doi:10.1002/jps.23031.

[52] D.E. Zecevic, K.G. Wagner, Rational Development of Solid Dispersions via Hot-Melt Extrusion Using Screening, Material Characterization, and Numeric Simulation Tools, J. Pharm. Sci. 102 (2013) 2297–2310. doi:10.1002/jps.23592.

[53] J. Thiry, F. Krier, B. Evrard, A review of pharmaceutical extrusion: Critical process parameters and scaling-up, Int. J. Pharm. 479 (2015) 227–240. doi:10.1016/j.ijpharm.2014.12.036.

[54] T. Sakai, M. Thommes, Investigation into mixing capability and solid dispersion preparation using the DSM Xplore Pharma Micro Extruder: Small-scale HME, J. Pharm. Pharmacol. 66 (2014) 218–231. doi:10.1111/jphp.12085.

[55] S. Guns, V. Mathot, J.A. Martens, G. Van den Mooter, Upscaling of the hot-melt extrusion process: Comparison between laboratory scale and pilot scale production of solid dispersions with miconazole and Kollicoat® IR, Eur. J. Pharm. Biopharm. 81 (2012) 674–682. doi:10.1016/j.ejpb.2012.03.020.

[56] P. Piccinni, Y. Tian, A. McNaughton, J. Fraser, S. Brown, D.S. Jones, S. Li, G.P. Andrews, Solubility parameter-based screening methods for early-stage formulation development of itraconazole amorphous solid dispersions, J. Pharm. Pharmacol. 68 (2016) 705–720. doi:10.1111/jphp.12491.

[57] A.M. Agrawal, M.S. Dudhedia, E. Zimny, Hot Melt Extrusion: Development of an Amorphous Solid Dispersion for an Insoluble Drug from Mini-scale to Clinical Scale, AAPS PharmSciTech. 17 (2016) 133–147. doi:10.1208/s12249-015-0425-7.

[58] B. Lang, J.W. McGinity, R.O. Williams, Hot-melt extrusion – basic principles and pharmaceutical applications, Drug Dev. Ind. Pharm. 40 (2014) 1133–1155. doi:10.3109/03639045.2013.838577.

[59] D.E. Zecevic, Solid dispersion via hot melt extrusion - formulation and process aspects, Dissertation, Eberhard Karls Universität, 2014.

[60] E.S. Bochmann, D. Neumann, A. Gryczke, K.G. Wagner, Micro-scale prediction method for API-solubility in polymeric matrices and process model for forming amorphous solid dispersion by hot-melt extrusion, Eur. J. Pharm. Biopharm. 107 (2016) 40–48. doi:10.1016/j.ejpb.2016.06.015.

[61] S.-Y. Chan, S. Qi, D.Q.M. Craig, An investigation into the influence of drug–polymer interactions on the miscibility, processability and structure of polyvinylpyrrolidone-based hot melt extrusion formulations, Int. J. Pharm. 496 (2015) 95–106. doi:10.1016/j.ijpharm.2015.09.063.

[62] A. Eitzlmayr, J. Khinast, G. Hörl, G. Koscher, G. Reynolds, Z. Huang, J. Booth, P. Shering, Experimental characterization and modeling of twin-screw extruder elements for pharmaceutical hot melt extrusion, AIChE J. 59 (2013) 4440–4450. doi:10.1002/aic.14184.

[63] J. Rantanen, J. Khinast, The Future of Pharmaceutical Manufacturing Sciences, J. Pharm. Sci. 104 (2015) 3612–3638. doi:10.1002/jps.24594.

[64] J. Aho, J.P. Boetker, S. Baldursdottir, J. Rantanen, Rheology as a tool for evaluation of melt processability of innovative dosage forms, Int. J. Pharm. 494 (2015) 623–642. doi:10.1016/j.ijpharm.2015.02.009.

[65] J. Lyons, P. Blackie, C. Higginbotham, The significance of variation in extrusion speeds and temperatures on a PEO/PCL blend based matrix for oral drug delivery, Int. J. Pharm. 351 (2008) 201–208. doi:10.1016/j.ijpharm.2007.09.041.

[66] S.S. Gupta, T. Parikh, A.K. Meena, N. Mahajan, I. Vitez, A.T.M. Serajuddin, Effect of carbamazepine on viscoelastic properties and hot melt extrudability of Soluplus®, Int. J. Pharm. 478 (2015) 232–239. doi:10.1016/j.ijpharm.2014.11.025.

[67] H. Liu, X. Zhang, H. Suwardie, P. Wang, C.G. Gogos, Miscibility studies of indomethacin and Eudragit® E PO by thermal, rheological, and spectroscopic analysis, J. Pharm. Sci. 101 (2012) 2204–2212. doi:10.1002/jps.23075.

[68] S.M. Maru, M. de Matas, A. Kelly, A. Paradkar, Characterization of thermal and rheological properties of zidovidine, lamivudine and plasticizer blends with ethyl cellulose to assess their suitability for hot melt extrusion, Eur. J. Pharm. Sci. 44 (2011) 471–478. doi:10.1016/j.ejps.2011.09.003.

[69] F. Yang, Y. Su, J. Zhang, J. DiNunzio, A. Leone, C. Huang, C.D. Brown, Rheology Guided Rational Selection of Processing Temperature To Prepare Copovidone–Nifedipine Amorphous Solid Dispersions via Hot Melt Extrusion (HME), Mol. Pharm. 13 (2016) 3494–3505. doi:10.1021/acs.molpharmaceut.6b00516.

[70] M.S. Dudhedia, A.M. Agrawal, Rheological study of copovidone and solid dispersion blend used for hot melt extrusion, J. Appl. Polym. Sci. 133 (2016) n/a-n/a. doi:10.1002/app.43278.

[71] J. Grimard, L. Dewasme, A. Vande Wouwer, A Review of Dynamic Models of Hot-Melt Extrusion, Processes. 4 (2016) 19. doi:10.3390/pr4020019.

[72] A. Gaspar-Cunha, A. Poulesquen, B. Vergnes, J.A. Covas, Optimization of processing conditions for polymer twin-screw extrusion, Int. Polym. Process. 17 (2002) 201–213.

[73] A. Durin, P. De Micheli, H.-C. Nguyen, C. David, R. Valette, B. Vergnes, Comparison between 1D and 3D Approaches for Twin-Screw Extrusion Simulation, Int. Polym. Process. 29 (2014) 641–648.

[74] A. Sarhangi Fard, P.D. Anderson, Simulation of distributive mixing inside mixing elements of co-rotating twin-screw extruders, Comput. Fluids. 87 (2013) 79–91. doi:10.1016/j.compfluid.2013.01.030.

[75] T. Lozano, P.G. Lafleur, M. Grmela, B. Vergnes, Modeling filler dispersion along a twin-screw extruder, Int. Polym. Process. 18 (2003) 12–19.

[76] M. Malik, D.M. Kalyon, J.C. Golba Jr, Simulation of co-rotating twin screw extrusion process subject to pressure-dependent wall slip at barrel and screw surfaces: 3D FEM Analysis for combinations of forward-and reverse-conveying screw elements, Int. Polym. Process. 29 (2014) 51–62.

[77] A. Gaspar-Cunha, J.A. Covas, B. Vergnes, Defining the configuration of co-rotating twin-screw extruders with multiobjective evolutionary algorithms, Polym. Eng. Sci. 45 (2005) 1159–1173. doi:10.1002/pen.20391.

[78] X.-M. Zhang, L.-F. Feng, S. Hoppe, G.-H. Hu, Local residence time, residence revolution, and residence volume distributions in twin-screw extruders, Polym. Eng. Sci. 48 (2008) 19–28. doi:10.1002/pen.20812.

[79] J. Gao, G.C. Walsh, D. Bigio, R.M. Briber, M.D. Wetzel, Residence-time distribution model for twin-screw extruders, AIChE J. 45 (1999) 2541–2549.

[80] J. Gao, G.C. Walsh, D. Bigio, R.M. Briber, M.D. Wetzel, Mean residence time analysis for twin screw extruders, Polym. Eng. Sci. 40 (2000) 227–237.

[81] Y. Gao, F.J. Muzzio, M.G. Ierapetritou, A review of the Residence Time Distribution (RTD) applications in solid unit operations, Powder Technol. 228 (2012) 416–423. doi:10.1016/j.powtec.2012.05.060.

[82] D.E. Zecevic, R.C. Evans, K. Paulsen, K.G. Wagner, From benchtop to pilot scale–experimental study and computational assessment of a hot-melt extrusion scale-up of a solid dispersion of dipyridamole and copovidone, Int. J. Pharm. 537 (2018) 132–139. doi:10.1016/j.ijpharm.2017.12.033.

2 Aims and scope

Regarding hot-melt extrusion in early formulation and process development, techniques and procedures are needed to simplify the application which decrease the required time and material (please see section 1). This would encourage researchers to validate, whether HME might be the right processing option for their final formulation without the drawback of an expensive and long-lasting process and formulation evaluation in early stage development. As a first step to identify the optimal and stable formulation for forming amorphous solid dispersions, a reliable theoretical polymer screening is needed. It would reduce the experimental effort prior conducting any hot-melt extrusion trials. Furthermore, the identification of a soluble API/polymer system would lead to an ASD which is thermodynamically stable enabling a prolonged shelf life. Secondly, a theoretical consideration of process conditions would further reduce the number of trials needed to optimize and scale-up the HME process to achieve the required amorphous solid dispersion.

Concerning the two major challenges in early formulation development of amorphous solid dispersions by means of hot-melt extrusion, e.g. polymer selection and process optimization, following aims in this thesis have been investigated:

- Defining a robust and fast API solubility determination in polymeric matrices to create a wide API solubility data set for further investigations by means of differential scanning calorimetry (see chapter 3)
- A general overview of published measuring techniques for the solubility of APIs in the polymeric matrix at room temperature and the comparison to our own solubility prediction assumption (see chapter 4).
- Evaluation and validation of a possible connection of glass transition temperature (T_g) and melt viscosity of an amorphous solid dispersion (see chapter 5)
- Investigating the T_g-viscosity correlation for HME numerical simulation purposes, in which model-based viscosity can be used instead of the actual melt viscosity (see chapter 6).

- Validation of the T_g-viscosity correlation and its general applicability in numerical simulation of hot-melt extrusion processes. It would short-cut rheological measurements and simplify the application of HME numerical simulation in early stage process and formulation development for amorphous solid dispersions (see chapter 7).

3 Micro-scale prediction method for API-solubility in polymeric matrices and process model for forming amorphous solid dispersion by hot-melt extrusion

Esther S. Bochmann [a]; Dirk Neumann [a,b]; Andreas Gryczke [c]; Karl G. Wagner [a,1]

[a] Department of Pharmaceutical Technology and Biopharmaceutics, University of Bonn, Bonn, Germany

[b] Scientific Consilience GmbH, Saarbrücken, Germany

[c] Global Technical Marketing Solubilization, BASF SE, Ludwigshafen, Germany

This part was published as

E.S. Bochmann, D. Neumann, A. Gryczke, K.G. Wagner, Micro-scale prediction method for API-solubility in polymeric matrices and process model for forming amorphous solid dispersion by hot-melt extrusion, European Journal of Pharmaceutics and Biopharmaceutics. 107 (2016) 40–48. doi:10.1016/j.ejpb.2016.06.015.

3.1 Graphical abstract

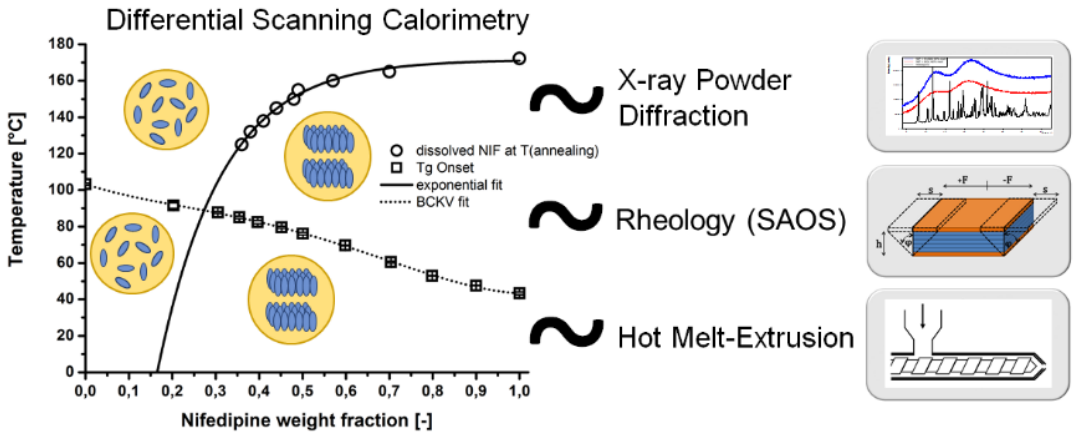

3.2 Abstract

A new predictive micro-scale solubility and process model for amorphous solid dispersions (ASDs) by hot-melt extrusion (HME) is presented. It is based on DSC measurements consisting of an annealing step and a subsequent analysis of the glass transition temperature (T_g). The application of a complex mathematical model (BCKV-equation) to describe the dependency of T_g on the active pharmaceutical ingredient (API)/polymer ratio, enables the prediction of API solubility at ambient conditions (25 °C). Furthermore, estimation of the minimal processing temperature for forming ASDs during HME trials could be defined and was additionally confirmed by X-ray powder diffraction data. The suitability of the DSC method was confirmed with melt rheological trials (small amplitude oscillatory system). As an example, ball milled physical mixtures of dipyridamole, indomethacin, itraconazole and nifedipine in poly(vinylpyrrolidone-co-vinylacetate) (copovidone) and polyvinyl caprolactam-polyvinyl acetate-polyethylene glycol graft copolymer (Soluplus®) were used.

3.3 Keywords

amorphous solid dispersion, DSC, hot-melt extrusion, melt rheology, solubility

3.4 Chemical compounds studied in this article

Dipyridamole (PubChem CID: 3108); Indomethacin (PubChem CID: 3715); Itraconazole (PubChem CID: 55283); Nifedipine (PubChem CID: 4485)

3.5 Introduction

Today, one of the major challenges in pharmaceutical research is the increasing number of active pharmaceutical ingredients (APIs) which belong to class II or IV of the Biopharmaceutical Classification System (BCS) and exhibit low solubility [1,2]. To overcome poor solubility hot-melt extrusion (HME), spray drying and cyclodextrin-complexation are commonly used [3,4]. HME is a solvent-free, fast and continuous manufacturing process. The solubility enhancement by HME is based on forming an amorphous solid dispersion (ASD) [5–9], where the API is molecularly dispersed in a polymeric matrix. As no energy is needed to overcome the crystal lattice energy of the API, solubility is improved. Some of the disadvantages especially for HME, are the time- and material-consuming trials that have to be conducted to set the manufacturing process variables [10]. Furthermore, predictive micro-scale assays are needed to determine if an ASD is mandatory to overcome solubility issues [11,12]. For this purpose, differential scanning calorimetry (DSC) is often used to evaluate the API solubility in polymers and their respective physical stability [13]. The physical stability of an ASD is not only promoted by a polymer of high glass transition temperature (T_g), but also by the solubility of the API in the polymer matrix [10,11,13,14].

Various approaches to predict the solubility of APIs in polymer melts can be found in the literature. They are based on either DSC trials or measurements in low molecular weight analogues of the polymer by neglecting the influence of molecular weight and steric hindrance [15,16]. DSC involves the melting or softening of the materials and thus is related to the HME process. Typical DSC methods are the melting point depression method [17–19] and the dissolution end point method [20–22]. Both DSC methods are based on the API melting point determination with low heating rates using either the onset or the endset of the dissolution endotherm or rather melting tempera-

ture (T_m) peak signal. By using the onset of T_m, influences of particle size and production of the physical mixtures can be neglected. However, the onset only indicates the starting point of API-dissolution in the polymer without knowing whether the entire fraction of API present in the mixture can be dissolved at that respective temperature [23–25]. In contrast, the dissolution endpoint method enables the measurement of the endpoint of the dissolution step and thus might be more accurate. The disadvantage of this method is its strong dependence on the particle size. If the particle size is not sufficiently small, the melt is not able to reach its equilibrium state during heating and the $T_{m,Endset}$ for the dissolution is shifted to higher temperatures [22]. In addition, an evaporation-based DSC technique was reported [26], in which samples were prepared by evaporating the organic solvent and further analyzing the recrystallization at elevated temperatures. Due to the use of the evaporation technique, results might not be similar to the melting methods or representative of HME processes [27].

Furthermore, most techniques identify the equilibrium state of the physical mixture during DSC method by prolonging the annealing time or decreasing the heating rate. If a melt is not close to equilibrated conditions after such a procedure, the blend will not reach its equilibrium in an investigable period of time. Consequently, proof of suitable conditions for DSC trials is needed.

In order to evaluate a micro-scale solubility and process model for ASDs by hot-melt extrusion, a new DSC approach for the API solubility estimation in a polymer matrix was investigated. It consists of an annealing step and a subsequent analysis of the glass transition temperature. The application of a complex mathematical model (BCKV-equation [28]) to describe the course of T_g dependency on the API:polymer ratio enables the prediction of API solubility at ambient conditions (25 °C). Suitable annealing in time and temperature were analyzed by melt rheology with small amplitude oscillatory system (SAOS) measurements. Furthermore, an estimate of the minimal processing temperature (T_{min}) for forming ASDs during HME trials could be defined and was additionally confirmed by x-ray powder diffraction (XRPD) data.

3.6 Material and methods

3.6.1 Material

Dipyridamole (DPD) was obtained from Sigma-Aldrich Chemical Co. (St. Louis, MO, USA). Indomethacin (IMC) and itraconazole (ITZ) were purchased from Alfa Aesar (Karlsruhe, Germany) and nifedipine (NIF) was obtained from Cayman Chemical (Ann Arbor, MI, USA). Poly(vinylpyrrolidone-co-vinylacetate) (copovidone, KVA64) and polyvinyl caprolactam-polyvinyl acetate-polyethylene glycol graft copolymer (Soluplus®, SOL) were kindly donated by BASF SE (Ludwigshafen, Germany) (Fig. 3.1).

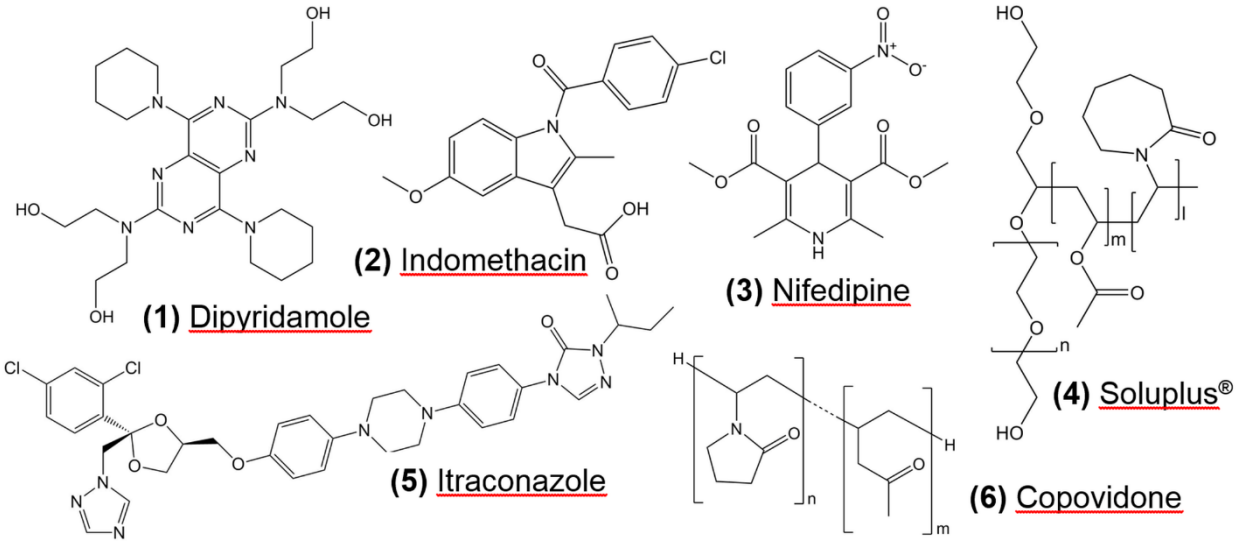

Figure 3.1 *Chemical structures of the substances investigated.*

3.6.2 Methods

3.6.2.1 Preparation of physical mixtures

For DSC and XRPD measurements, 400 mg of physical mixture, consisting of one polymer and API in various weight fractions (10 – 90 % w/w), was ball milled with a MM400 from Retsch GmbH (Haan, Germany) with up to 30 Hz for 6 times 5 min. In between the milling cycles a pause of 5 min was kept for minimization of thermal energy intake. Due to a smaller sample size for DSC, the reduction of the particles size by ball milling was needed however, DSC measurements with the unmilled pure sub-

stances showed no change in solid state. For rheological measurements, physical mixtures of 20 % API in copovidone were prepared by mortar and pestle which were subsequently homogenized using a Turbula mixer (Willy A. Bachofen AG – Maschinenfabrik, Muttenz, Swiss) for 10 min at 22 rpm.

3.6.2.2 X-ray powder diffraction (XRPD)

XRPD measurements were performed in reflection mode (X'Pert MRD Pro, PANalytical, Almelo, Netherlands) with an X'Celerator detector and nickel filtered CuKα1 radiation (λ=1.5406 Å) at 45 kV and 40 mA. Physical mixtures were analyzed at a scanning rate of 1.41 2Θ/min before and after annealing in a drying oven under the same conditions as the DSC method dictated.

3.6.2.3 Differential Scanning Calorimetry (DSC)

A DSC 2 from Mettler Toledo (Gießen, Germany) with nitrogen cooling, nitrogen as purge gas (30 ml/min) and an auto sampler was used. The system was calibrated with indium and zinc standards. At least three samples of approximately 10 mg from each mixture were analyzed using 40 µl aluminum pans with a pierced lid. Glass transition temperatures (T_g) and melting temperatures (T_m) of the pure polymers and APIs were analyzed via heating-cooling-heating cycles at 10 K/min (Table 3.1). In addition, heat capacities were determined by using TOPEM® (modulated DSC) with 1 K pulse height, 15–30 second pulse width and an underlying heating and cooling rate of 2 K/min.

Table 3.1 *Properties of the APIs and polymers investigated, in which T_m, T_g and ΔC_p were determined via DSC. Mean values ± standard deviation.*

Substance	M_w [g/mol]	T_m [°C] (± S.D.)	T_g [°C] (± S.D.)	ΔC_p [J/(g*K)] (± S.D.)
Copovidone	45,000-70,000	-	107.1 (± 0.02)	0.40 (± 0.042)
Soluplus®	90,000-140,000	-	71.1 (± 0.63)	0.30 (± 0.038)
Dipyridamole	504.626	167.1 (± 0.11)	38.2 (± 1.36)	0.68 (± 0.045)
Indomethacin	357.79	160.1 (± 0.24)	44.4 (± 0.20)	0.33 (± 0.054)
Itraconazole	705.63	165.8 (± 0.01)	57.7 (± 0.61)	0.44 (± 0.015)
Nifedipine	346.33	172.2 (± 0.11)	44.3 (± 0.88)	0.34 (± 0.039)

3.6.2.4 Rheometer (SAOS)

An oscillatory rheometer (Haake® MARS® III, Thermo Scientific, Karlsruhe, Germany) with a plate-plate geometry (d = 20 mm) and a gap height of 0.75 mm was used. All experiments were conducted at least in triplicate and in the controlled deformation AutoStrain mode (CD AutoStrain mode). An amplitude of 5.5 % was applied and was verified by an amplitude sweep. Frequency sweeps were conducted in 10 K steps in the suitable temperature range from at least 10 Hz to 0.1 Hz. Subsequently the frequency sweeps in which the specimen was thermorheologically simple, were horizontally shifted into one master curve at a previously defined reference temperature by means of Time Temperature Superposition (TTS). The resulting viscosity profile from the master curves were fit to the Carreau-Yasuda equation (CY-equation, Eq. (3.1)) [29–32],

$$\eta = \eta_\infty + (\eta_0 - \eta_\infty) \cdot [1 + (\lambda\dot{\gamma})^a]^{(n-1)/a} \tag{3.1}$$

where η_0 and η_∞ are the zero shear and infinite shear viscosity, λ is the characteristic time, n is the Power law index and a is the Yasuda constant. To obtain a more accurate curve fitting, η_∞ was set to zero (Eq. (3.2)).

$$\eta = \eta_0 \cdot [1 + (\lambda\dot{\gamma})^a]^{(n-1)/a} \tag{3.2}$$

During TTS, shift factor a_T for each frequency sweep under investigation were obtained and were adjusted to a Williams-Landel-Ferry fit (WLF-fit, Eq. (3.3)) [29–32],

$$\log(a_T) = \frac{-C_1\,(T-T_0)}{C_2+(T-T_0)} \tag{3.3}$$

where C_1 and C_2 are constants, T is the intended temperature and T_0 is the reference temperature. This WLF-fit was needed to describe the temperature dependency of λ (Eq. (3.4)) and η_0 (Eq. (3.5)) of the CY-equation (Eq. (3.1)),

$$a_T = \frac{\eta_T}{\eta_0} \tag{3.4}$$

$$a_T = \frac{\lambda_T}{\lambda_0} \tag{3.5}$$

where index T denotes the intended temperature and index 0 the reference temperature of the master curve. In summary, the CY-equation and WLF-fit enable the extrapolation of data by means of angular frequency and temperature within a limited range [33]. As an example, the results from fitting these parameters for KLVA64-blends with 20 % API at 150 °C are shown in Table 3.2.

Table 3.2 *Extrapolated Carreau-Yasuda and WLF fits at 150 °C for different blends resulting from oscillatory measurements. Mean values ± standard error*.*

Substance	Carreau-Yasuda fit			WLF fit		
	η_0 [Pa·s] (± S.E.)	λ [s] (± S.E.)	n (± S.E.)	a (± S.E.)	C_1 (± S.E.)	C_2 (± S.E.)
Copovidone	61,005.8 (± 1,472.2)	1.356 (± 0.445)	0.577 (± 0.042)	0.756 (± 0.103)	10.04 (± 2.73)	147.40 (± 37.92)
Soluplus®	17,156.37 (± 58.82)	0.757 (± 0.027)	0.567 (±0.005)	0.782 (±0.013)	4.75 (± 0)	104.67 (± 0)
KVA64 + 20% DPD	11,360.7 (± 367.4)	0.393 (± 0.226)	0.598 (± 0.076)	0.767 (± 0.162)	8.78 (± 0.50)	135.98 (± 7.31)
KVA64 + 20% IMC	6,555.5 (± 142.0)	0.288 (± 0.075)	0.620 (± 0.031)	0.807 (± 0.106)	8.87 (± 2.20)	142.36 (± 31.15)
KVA64 + 20% ITZ	25,630.6 (± 683.3)	0.850 (± 0.534)	0.645 (± 0.067)	0.741 (± 0.159)	4.74 (± 0.25)	46.99 (± 3.05)
KVA64 + 20% NIF	12,357.9 (± 227.7)	0.542 (± 0.110)	0.612 (± 0.025)	0.806 (± 0.085)	9.01 (± 3.51)	127.26 (± 53.96)

* Please see the supplementary data for other temperatures (Table 3.A.2)

3.6.2.5 Solubility determination via DSC

The DSC method consists of an annealing step and a subsequent analysis of the T_g and determination of the ratio of the solubilized API to polymer using a calibration curve for T_g. As a first step, Couchman-Karasz equation (CK-equation, Eqs. (3.6) & (3.7)) [34] was employed to predict the T_g of API:polymer physical mixtures by using the properties of pure materials only,

$$T_g = \frac{w_1 T_{g,1} + k_{CK}(1-w_1) T_{g,2}}{w_1 + k_{CK}(1-w_1)} \qquad \text{with} \quad \Delta T_g = T_{g,2} - T_{g,1} \tag{3.6}$$

$$k_{CK} = \frac{\Delta C_{p,2}}{\Delta C_{p,1}} \tag{3.7}$$

where w is the weight fraction, k_{CK} is the Couchman-Karasz constant, C_p the heat capacity step at glass transition and the indices 1 and 2 refer to API and polymer, respectively. The calculated glass transition temperature of the physical mixtures was then

taken into account in order to set the right annealing temperature, ensuring a sufficient dissolution of the API into the polymeric matrix by a low viscous melt. To confirm a suitable annealing in time and temperature, rheological trials were conducted with samples of 20 % API in KVA64 as well as the pure polymers. Furthermore, this should allow to estimate the minimal processing temperature for hot-melt extrusion. Finally, XRPD measurements were performed to check complete dissolution of the API as reported by DSC.

After annealing, the physical mixtures were analyzed in terms of glass transition temperature ($T_{g,1}$), resulting from the annealing step (Fig. 3.2). Subsequently, the samples were reheated to temperatures above their melting points and the glass transitions ($T_{g,2}$) of these completely amorphous systems were determined (Fig. 3.2). This glass transition temperature ($T_{g,2}$) obtained from the second heating step was used to determine the solubilized API fraction at the respective annealing temperature ($T_{Annealing}$) by employing the Brostow Chiu Kalogeras Vassilikou-Dova equation [28] (BCKV-equation, Eq. (3.8)). The BCKV-equation was used to fit the dependence of $T_{g,2}$ on the fraction of API in the system,

$$T_g = w_1 T_{g,1} + (1 - w_1) T_{g,2} + w_1(1 - w_1)[a_0 + a_1(2w_1 - 1) + a_2(2w_1 - 1)^2] \quad (3.8)$$

with a_0, a_1 and a_2 as fitting constants. Due to its polynomial form, it enables the consideration of positive and negative deviations from the CK-equation (Eq. (3.6)). To predict a phase diagram and to characterize the solubility at ambient conditions (25 °C), the soluble API fractions and the respective temperatures $T_{Annealing}$ were used. An exponential fit of the free parameters was performed using Eq. (3.9).

$$T_{Annealing} = y_0 + A * e^{R_0 * x} \quad (3.9)$$

Here, x is the soluble API fraction at $T_{Annealing}$, A and R_0 are fit parameters and y_0 corresponds to T_m of the API, but was set as a variable parameter. The result from the fit was employed to extrapolate x to 25 °C.

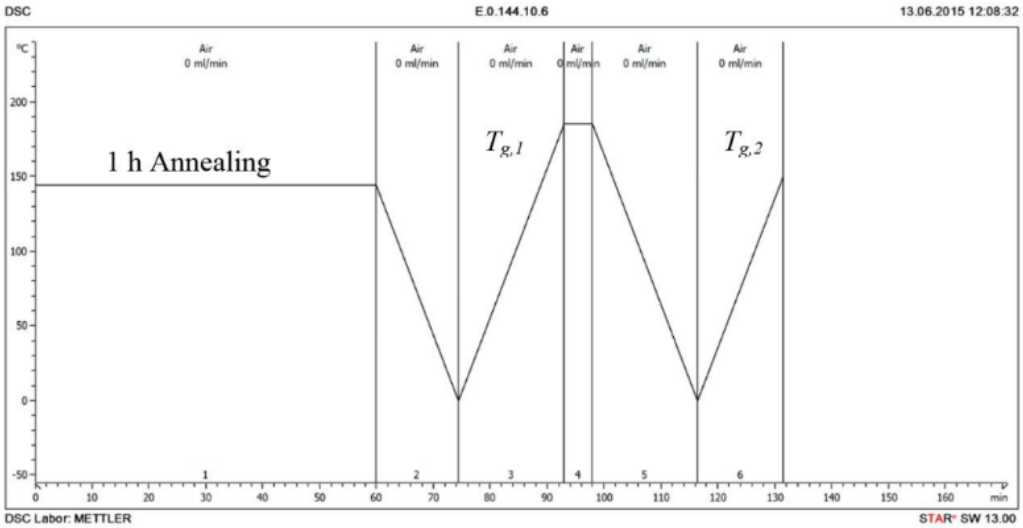

Figure 3.2 *Example for the DSC temperature program (40% NIF-copovidone blend).*

3.6.2.6 Data processing

All mathematical operations and curve fittings were conducted via Origin® Pro 8G of OriginLab (Northampton, MA, USA). The adjusted correlation coefficient (r^2) of the equations describes the goodness of the performed fits by including the degree of freedom (or number of variables) of the equation used.

3.7 Results & Discussion

3.7.1 Couchman-Karasz equation versus BCKV-equation

Properties of the pure substances for employing the Couchman-Karasz equation (Eq. (3.6), (3.7)) for physical mixtures are listed in Table 3.1. In most cases, the experimental T_g differed from the CK-equation, indicating specific interactions between the API and the polymer which cannot be explained by simple combinatorial mixing (Fig. 3.3a-d, Table 3.3).

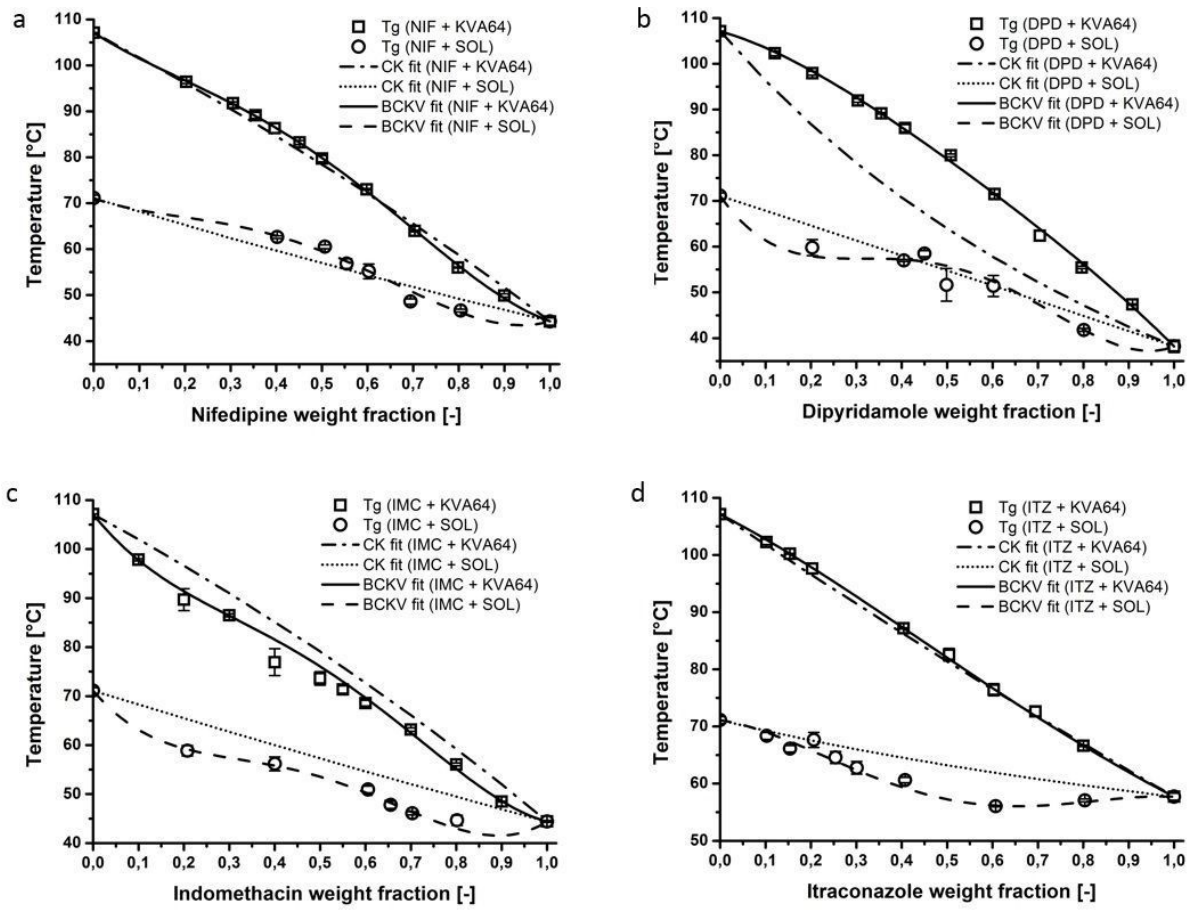

Figure 3.3a-d *Glass transition temperatures and resulting CK- and BCKV-fits of (a) NIF, (b) DPD), (c) IMC and (d) ITZ) in SOL and KVA64. Mean values ± standard deviation.*

Table 3.3 *Deviation and shape discrepancies between CK- and BCKV-fit of the mixtures.*

API	Polymer	Max. absolute deviation of BCKV-fit from CK-model [±K]	Oscillating curve shape
NIF	KVA64	2	Yes
	SOL	3	Yes
DPD	KVA64	9	No
	SOL	6	Yes
IMC	KVA64	4	Yes
	SOL	6	Yes
ITZ	KVA64	1	No
	SOL	6	No

For the nifedipine physical mixtures, the experimental T_g of SOL and KVA64 systems oscillated around the CK-equation to a different extent (Fig. 3.3a, Table 3.3). Due to the higher oscillation of NIF-SOL around the CK-fit, specific interactions between NIF and SOL might be stronger than between NIF and KVA64. The interaction of NIF and SOL might be related to hydrogen bonding between the nitrogen group of NIF and hydroxyl groups of SOL [35]. In NIF-KVA64 blends, interactions were suggested between carbonyl groups of copovidone and the secondary amine group of NIF [36].

In the case of dipyridamole, the T_g-values calculated with the CK-equation exhibited equally strong deviations (± 6-9 K) from the experimental values for both physical mixtures with KVA64 and SOL, although, interestingly, with a different curve shape (Fig. 3.3b, Table 3.3). In the case of DPD-KVA64, the deviation suggested hydrogen bonding between carbonyl groups of the KVA64 and the hydroxyl group of DPD as suggested by Chem. et. al. [37]. Concerning DPD-SOL, hydrogen bonding between the hydroxyl group of DPD and the vinyl acetate groups of SOL are likely.

Regarding physical mixtures of indomethacin, glass transitions calculated with the CK-equation were continuously shifted towards higher temperature values compared to the measured T_gs (±6 K) (Fig. 3.3c, Table 3.3). This resulted in a poor fit of the CK-model for IMC-SOL blends; however, the BCKV-model fitted the experimental data almost perfectly. The discrepancy between measured T_g and CK-equation can be explained by the inhibition of the dimerization of IMC and specific interaction between IMC acting as a proton donor and SOL acting as a proton acceptor via the amide carbonyl group [38]. In the case of IMC-KVA64, hydrogen bonding between carbonyl groups of copovidone and the carboxylic group of IMC, which had its maximum at 20–30 % IMC, might cause the strong discrepancy at this concentration range (±4 K) [36,39].

In the case of ITZ comprising no proton donor groups and KVA64 with its proton acceptor property via carbonyl groups, specific interactions (hydrogen bonding), was absent (Fig. 3.3d, Table 3.3) [40]. This was indicated by no significant differences between CK-fit and measured T_g. Slightly positive T_g differences at low ITZ fractions in KVA64 might be a result of improved packing of the polymeric chains, which hinders

its movements. However, ITZ-SOL blends exhibited continuously lower T_g values than predicted via the CK-model (±6 K), which suggested hydrogen bonding as well as weak lipophilic interactions between the substances [41].

Regarding the ability of the two mathematical models to describe the course of the composition-dependent glass transition, BCKV-fit offers higher flexibility (Table 3.3). Due to its polynomial form, the BCKV-model was able to adjust to deviations from the purely mixing ratio based CK-model caused by specific interactions. All BCKV-fits exhibited adjusted correlation coefficients r^2 close to 1. However, BCKV-fits for KVA64-mixtures featured a slightly higher goodness of fit ($0.99 \leq r^2$) than for SOL-mixtures ($0.98 \leq r^2$). On the other hand, the CK-equation is more appropriate for estimates prior to conducting experimental measurements because only the knowledge of the pure substances is needed. After the performing trials, the BCKV-model should be used instead. However in our proposed method, CK-equation was used to determine the desired $T_{Annealing}$ by using the T_g of the physical mixture under investigation (Tab. 3.A.1). This enabled a fast processing of the API:polymer solubility determination because no experimental trials with the physical mixtures were needed. The inaccuracy of the CK-model for predicting the T_g was already considered in setting $T_{Annealing}$.

The chemical structures of KVA64 and SOL (Fig. 3.1) suggest that both polymers usually act as hydrogen acceptors, and therefore the miscibility with APIs via hydrogen bonding is favorable for those APIs featuring a hydrogen donor site. Additionally, Soluplus® might act as a hydrogen donor or favor lipophilic interactions, although to a minor extent. In addition, a higher recorded T_g than that predicted by the CK-equation may be explained by improved packing of the polymeric chains, which would hinder its movements, increasing T_g while at the same time decreasing the true density [40]. As seen in the ITZ-copovidone system, deviations from the CK-fit can not only be due to specific interactions between API and polymer, but also may be caused by changing mobility and flexibility of the polymeric chains in general [40].

3.7.2 **Validation of the solubility estimation method by Small Amplitude Oscillatory System (SAOS) trials**

In SAOS trials, every copovidone mixture reached its equilibrium viscosity state within 2 h at temperatures approximately 60 °C above the $T_{g,Blend}$ predicted by the CK-equation (Table 3.4). In the case of copovidone mixtures, this temperature ($T_{g,Blend}$ + 60 °C) resulted in low zero shear viscosity values (η_0 < 11,400 Pa·s, Table 3.4) facilitating the dissolution of the API in the polymer matrix until the solubility within the polymer is reached. Since the equilibration time prior to a frequency sweep in SAOS trials was set to 2 h, the same duration was also a starting point for setting the annealing time for the DSC experiment to measure the T_g. However, a comparison between 1 and 2 hours annealing revealed no significant differences in T_g and annealing was reduced to 1 hour. This reduction in annealing time was enabled by smaller particle sizes obtained upon ball milling of the API / polymer mixtures prior to DSC measurements. Please see the supplementary data for specific annealing conditions of each physical mixture in DSC (Table 3.A.1). As a result of the KVA64 trials, a 2 h equilibrium period (melting of powder sample at $T = T_g$ + 60 °C) prior to the frequency sweep measurements and an annealing time of 1 h for mixtures of a zero-shear viscosity below 11,500 Pa·s were set as parameters for solubility detection of API in polymer. Zero shear viscosities at $T_{g,Blend}$ + 60 °C obtained by extrapolation of API-KVA64 blends data, according to Eqs. (3.2) and (3.3), were compared and revealed viscosities in the same viscosity range (11,361 – 2,481 Pa·s, Table 3.4). It should be mentioned that differences in zero shear viscosity between 2,461 and 6,178 Pa·s are negligible for rheological effects; macroscopic effects will start to be pronounced for changes of a decade or higher [42]. However, in the case of dipyridamole, zero shear viscosity resulted in a higher η_0-value than the other API-KVA64 mixtures. This can be explained by the high positive discrepancy between CK-equation and measured T_g at 20 % DPD. However, even the DPD-KVA64 blend reached its equilibrium within 2 h during SAOS trials and 1 h annealing during DSC measurements. Consequently, deviations from the CK-equation had a negligible influence on the accuracy of the DSC trials and the DSC method evaluated was regarded to be generally valid for KVA64 blends.

Table 3.4 *Glass transition temperatures and viscosities of Soluplus® copovidone, and 20% API-copovidone blends. Mean values ± standard deviation.*

Substance	$T_{g,\,CK}$ [°C]	$T_{g,\,experimental}$ [°C] (± S.D.)	$T_{g,CK}$ + 60 °C [°C]	η_0 [Pa*s] at $T_{g,CK}$ + 60 °C
Copovidone	107.1	107.1 (± 0.02)	167	5,573
Soluplus®	71.1	71.1 (± 0.63)	131	194,038
KVA64 + 20% DPD	86.8	97.9 (± 0.38)	147	11,361
KVA64 + 20% IMC	96.6	88.02 (± 1.01)	157	2,481
KVA64 + 20% ITZ	96.6	97.6 (± 0.89)	157	6,178
KVA64 + 20% NIF	96.2	96.4 (± 0.35)	156	4,861

In the case of Soluplus® mixtures, the verification of sufficient annealing was conducted similarly to KVA64. SOL exhibited a two decades higher zero shear viscosity at $T_{g,Blend}$ + 60 °C than KVA64 blends (Table 3.4). One reason may be the very broad glass transition range in DSC of 27.45 K (±2.57 K) for Soluplus® compared to 8.49 K (±0.30 K) for copovidone. Consequently, the annealing temperature had to be increased to 90-100 °C above $T_{g,Blend}$ where SOL exhibited a zero-shear viscosity of 2,731-5,994 Pa·s. This condition will facilitate the dissolution and diffusion of the API in the molten polymeric matrix. The same temperature should enable HME processes [43]. Trials with Soluplus® blends at $T_{g,Blend}$ + 90-100 °C with elongated annealing time showed no significant difference in glass transition and 1 h annealing was set for all SOL DSC measurements.

In summary, the annealing step in the DSC method is able to promote the dissolution of the API into the molten polymer matrix to its equilibrium state. One drawback is that the annealing depends heavily on the rheological properties of the polymer. Therefore, the annealing process should be performed at a temperature at which the viscosity is below 12,000 Pa·s.

3.7.3 Estimation of the lowest processing temperature for ASDs in hot-melt extrusion

In rheological trials at ~60 °C above $T_{g,Blend}$, the zero-shear viscosity was suggested to be low enough for enabling hot-melt extrusion trials to form ASD (Table 3.4) [43]. The

identified dissolved API concentrations in the polymer matrix at the relevant extrusion temperature are given in Table 3.5. This temperature is defined as where $T_{g,1}$ and $T_{g,2}$ were identical and no melting peak occurred (Fig. 3.4). Data were confirmed with XRPD trials. An example is shown for NIF-KVA64 mixtures in Figure 3.5a-b. Please see the supplementary data for further XRPD data of the physical mixtures before and after annealing (Fig. 3.A.1). Differences in DSC and XRPD data are due to the different sensitivities of the measuring systems: because XRPD is able to detect remaining crystals even at very low concentrations [44], the soluble concentrations can be up to 10 % lower than in DSC trials.

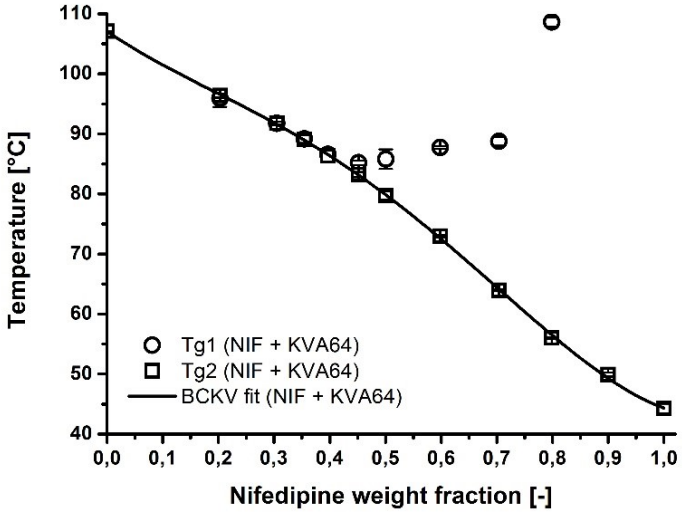

Figure 3.4 *T_g of annealed and completely molten samples at T_g+60°C of NIF-copovidone blends. Mean values ± standard deviation.*

However, HME trials would be necessary to reach sufficient time and shear rate for dissolving the API in the polymer melt at this lowest processing temperature. The presence of high shear is reducing the melt viscosity [29,30], which is likely to decrease the dissolution rate of the API in the polymer melt. Extrusion trials for the confirmation of this statement are currently conducted.

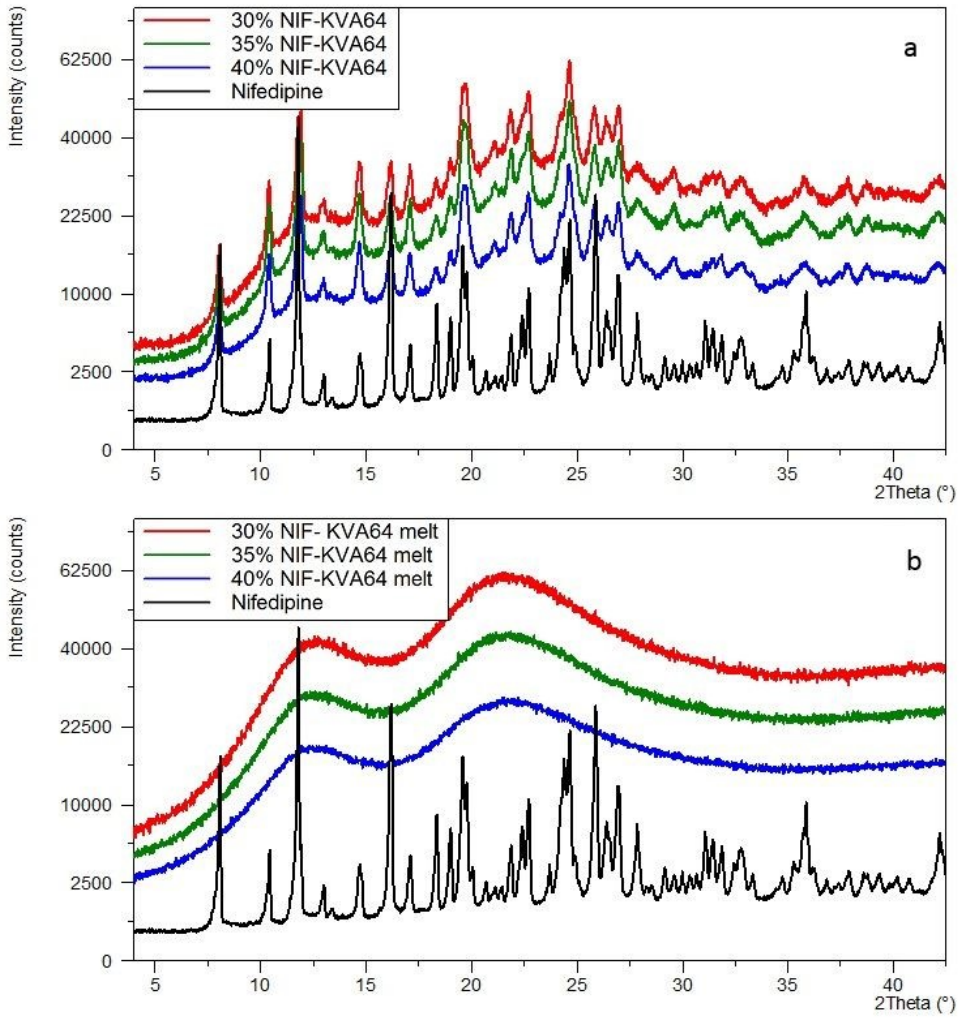

Figure 3.5a-b *XPRD data of NIF-KVA64 physical mixtures containing 30%, 35% and 40% of API (a) prior and (b) after annealing where 30% was identified as completely soluble.*

3.7.4 **Prediction of phase diagrams and solubilities at 25 °C**

To obtain a more accurate estimate of the solubility at 25 °C, that is for stability predictions, additional solubility values were measured at temperatures up to 5–10 °C below the melting point of the API. If the solubility temperature (T_S) was higher than the melting point of the API, solubility values were determined up to the respective highest temperature value. By using an exponential fit (Eq. (3.9)), the predicted solubility of the APIs at the various annealing temperatures was extrapolated to ambient conditions (25 °C) (Fig. 3.6a-b, Table 3.5). The measured T_g values were excellently fitted via the BCKV-model in the case of KVA64 (Fig. 3.6a). For SOL, the BCKV-fits were slightly

less accurate but still more than acceptable. Only NIF-SOL blends should be carefully regarded. Due to the relatively high zero shear viscosity of the system and the solubility behavior of the API in the polymer, measurement of more annealing temperatures for a better extrapolation were not feasible.

Table 3.1 *Solubilized weight fractions at T_{HME} determined via DSC or XRPD and predicted solubilities at ambient condition.*

Substance	Weight fraction [-] T_{HME} / DSC	Weight fraction [-] T_{HME} / XRPD	Prediction for 25 °C [-] via DSC
DPD + KVA64	0.30 (138°C)	0.20 (147°C)	0.03
IMC + KVA64	0.55 (136°C)	0.55 (136°C)	0.36
ITZ + KVA64	0.15 (159°C)	0.05 (165°C)	0
NIF + KVA64	0.40 (144°C)	0.30 (150°C)	0.19
DPD + SOL	0.40 (152°C)	0.40 (152°C)	0.18
IMC + SOL	0.60 (145°C)	0.55 (146°C)	0.26
ITZ + SOL	0.15 (158°C)	0.15 (158°C)	0
NIF + SOL	0.50 (157°C)	0.40 (160°C)	0.23

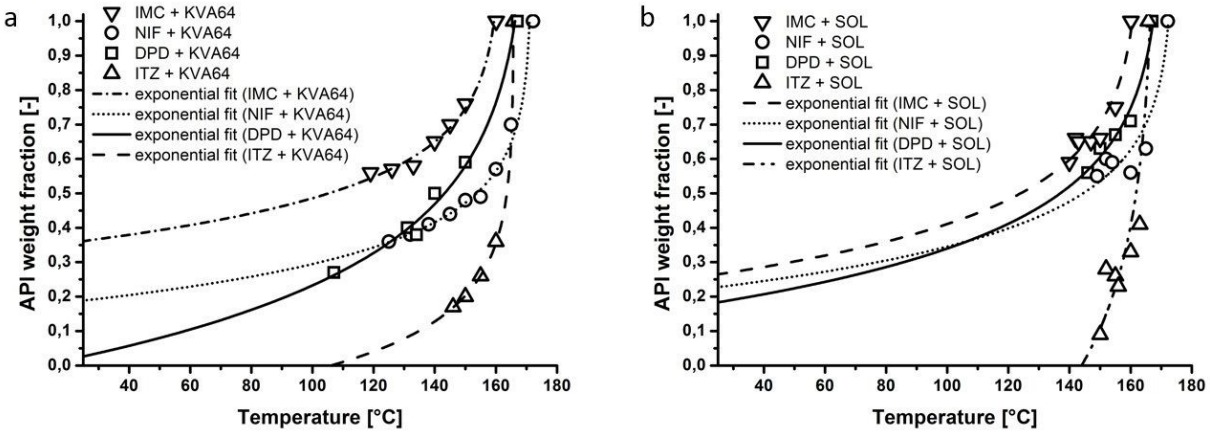

Figure 3.6a-b *Solubilities of IMC, NIF, DPD and ITZ in (a) KVA64 (a) and (b) SOL in temperature and weight fraction dependence.*

Although less deviation from the CK-model was found for NIF (Fig. 3.3a), it was soluble in KVA64 and SOL by favoring hydrogen bonding. The data hint at a slightly better miscibility at 25 °C with SOL than with KVA64. Due to a less accurate exponential fit, this finding is not entirely convincing, however is likely, if the extent of deviation from the CK-equation is considered. In addition, the dissolution endpoint method of other

authors suggests similar results for KVA64 [20–22]. For DPD, mixtures with SOL showed increased solubility compared to mixtures with KVA64 (Fig. 3.6a-b). It increased from 3 % to 18 %, indicating more specific interaction with SOL than with KVA64. However, T_g of KVA64 blends deviated to a higher extent from the CK-equation than SOL systems but with a different curve shape (Fig. 3.3b).

IMC was the best miscible substance with both polymers in this investigation. In KVA64, IMC exhibited a solubility of 36 % and in SOL 26 % were dissolved at 25 °C (Fig. 3.6a-b). Hence, KVA64 seemed to be the better partner for hydrogen bonding or less sterically hindered. The solubility identified correlated to the deviation from the CK-model (Fig. 3.3c). Furthermore, results from a dissolution endpoint method achieved similar outcomes [20–22].

In contrast, ITZ blends were the only immiscible systems at an extrapolation to ambient temperature (Fig. 3.6a-b). As it is generally discussed [13] that no deviation from the CK-equation is indicative for a poor solubility of the mixture components or rather the absence of specific interactions, this could be the reason for the observed immiscibility of our ITZ-KVA64 blends. However, although a great negative deviation for ITZ-SOL blends from the CK-equation was observed, the system was still immiscible at ambient conditions (Fig. 3.3d). Therefore, hydrogen bonding and lipophilic interaction were too weak to promote the dissolution of ITZ in Soluplus® or copovidone to a high extent. A comparison to the dissolution endpoint method revealed similar results [20].

In summary, deviations from the CK-model did not automatically lead to the conclusion of soluble systems or vice versa. Specific interactions between two compounds which favor mixing seem to be only one reason for the deviation from the CK-equation. Interestingly, blends that have an oscillating course were more miscible than systems which exhibited only one broad maximum / minimum, such as ITZ-SOL and DPD-KVA64 mixtures. Except for ITZ-KVA64, which did not deviate from the CK-equation, these were the immiscible or borderline miscible systems under investigation. Further evaluated immiscible systems, like carbamazepine and griseofulvin in Soluplus® or copovidone, confirm this result (data not shown). In conclusion, not only the extent of deviation from the CK-equation but also the shape should be regarded.

To predict phase diagrams we employed the BCKV-fit of $T_{g,Onset}$, and the exponential fit of the temperature dependent solubility. An example of the resulting diagram for the NIF-KVA64 is shown in Figure 3.7. The $T_{g,Onset}$ was used in this study because this is the point at which systems transform into a kinetically unstable state. The resulting phase diagram can be divided into kinetically and/or thermodynamically stable areas [20]. Therefore, it enables the evaluation of the formulation prior to extrusion experiments in order to produce solid amorphous dispersions. In conclusion, the estimate of the temperature limit for the formation of an amorphous system can be applied. Furthermore, the thermodynamically stable API fraction in the polymer matrix at ambient conditions can be predicted, but no statement for kinetically stabilized (thus thermodynamically unstable) systems and hence the shelf life could be made.

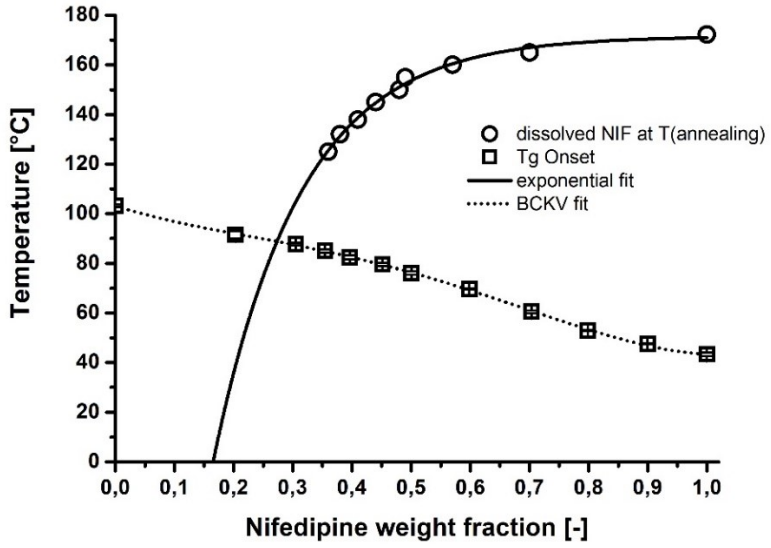

Figure 3.7 *Predicted phase diagram for NIF-copovidone blends. Mean values ± standard deviation.*

3.8 Conclusion

A micro-scale solubility and process model for forming ASDs by hot-melt extrusion and the API solubility prediction in a polymer based on DSC measurements was developed. The model includes an annealing step and the analysis of the glass transition temperatures (T_g). The application of a complex mathematical model (BCKV-equation)

enables the identification of the soluble API content within the polymer matrix by employing the API/polymer ratio dependent T_g course. Our methodology showed good accuracy for predicting the thermodynamically stabilized API content in the polymer at ambient conditions. An estimate of the minimal processing temperature to form ASDs during an HME trial (where the API is completely soluble within the polymeric matrix) could additionally be defined. Moreover, it was seen that not only the deviation from the Couchman-Karasz equation but also the course shape of T_g should be judged in order identify the presence of specific interactions and resulting solubility of two compounds. The above mentioned DSC findings were confirmed by XRPD and melt rheological trials. Rheological investigations revealed that annealing steps should be adapted to the melt rheological properties of the polymer in order to reach its equilibrium state prior to analyzing the soluble API fraction during DSC measurements. In summary, our proposed method is able to reduce HME trials for the production of ASDs and thus it may lower costs and the time required to establish an HME process. To minimize the effort, XRPD to confirm data and SAOS for adjustment of $T_{Annealing}$ might be neglected. In case of $T_{Annealing}$, the broadness of T_g can be used instead of rheological trials to receive information about the viscosity of the polymer in the molten state. However, if the minimal processing temperature should be determined, rheological information at least for the pure polymer melt might be useful.

3.9 Acknowledgement

The authors would like to thank BASF SE greatly, especially Thorsten Cech, for their support and providing access to the rheometer. Further warm thanks to Fritz Soergel for always being available concerning rheology and Rachel C. Evans for reviewing the manuscript. This research did not receive any specific grant from funding agencies in the public, commercial, or not-for-profit sectors.

3.10 References

[1] S. Janssens, G. Van den Mooter, Review: physical chemistry of solid dispersions, J. Pharm. Pharmacol. 61 (2009) 1571–1586. doi:10.1211/jpp/61.12.0001.

[2] C.A. Lipinski, F. Lombardo, B.W. Dominy, P.J. Feeney, Experimental and computational approaches to estimate solubility and permeability in drug discovery and development settings, Adv. Drug Deliv. Rev. 64 (2012) 4–17. doi:10.1016/j.addr.2012.09.019.

[3] H. Liu, L.S. Taylor, K.J. Edgar, The role of polymers in oral bioavailability enhancement; a review, Polymer. (2015). doi:10.1016/j.polymer.2015.09.026.

[4] M. Stanković, H.W. Frijlink, W.L.J. Hinrichs, Polymeric formulations for drug release prepared by hot melt extrusion: application and characterization, Drug Discov. Today. 20 (2015) 812–823. doi:10.1016/j.drudis.2015.01.012.

[5] J. Breitenbach, Melt extrusion: from process to drug delivery technology, Eur. J. Pharm. Biopharm. 54 (2002) 107–117.

[6] Z. Dong, A. Chatterji, H. Sandhu, D.S. Choi, H. Chokshi, N. Shah, Evaluation of solid state properties of solid dispersions prepared by hot-melt extrusion and solvent co-precipitation, Int. J. Pharm. 355 (2008) 141–149. doi:10.1016/j.ijpharm.2007.12.017.

[7] A. Forster, J. Hempenstall, I. Tucker, T. Rades, Selection of excipients for melt extrusion with two poorly water-soluble drugs by solubility parameter calculation and thermal analysis, Int. J. Pharm. 226 (2001) 147–161.

[8] H. Liu, P. Wang, X. Zhang, F. Shen, C.G. Gogos, Effects of extrusion process parameters on the dissolution behavior of indomethacin in Eudragit® E PO solid dispersions, Int. J. Pharm. 383 (2010) 161–169. doi:10.1016/j.ijpharm.2009.09.003.

[9] S. Janssens, G. Van den Mooter, Review: physical chemistry of solid dispersions, J. Pharm. Pharmacol. 61 (2009) 1571–1586. doi:10.1211/jpp/61.12.0001.

[10] Y. He, C. Ho, Amorphous Solid Dispersions: Utilization and Challenges in Drug Discovery and Development, J. Pharm. Sci. 104 (2015) 3237–3258. doi:10.1002/jps.24541.

[11] F. Meng, V. Dave, H. Chauhan, Qualitative and quantitative methods to determine miscibility in amorphous drug–polymer systems, Eur. J. Pharm. Sci. 77 (2015) 106–111. doi:10.1016/j.ejps.2015.05.018.

[12] D.E. Zecevic, K.G. Wagner, Rational Development of Solid Dispersions via Hot-Melt Extrusion Using Screening, Material Characterization, and Numeric Simulation Tools, J. Pharm. Sci. 102 (2013) 2297–2310. doi:10.1002/jps.23592.

[13] J.A. Baird, L.S. Taylor, Evaluation of amorphous solid dispersion properties using thermal analysis techniques, Adv. Drug Deliv. Rev. 64 (2012) 396–421. doi:10.1016/j.addr.2011.07.009.

[14] F. Qian, J. Huang, M.A. Hussain, Drug-polymer solubility and miscibility: Stability consideration and practical challenges in amorphous solid dispersion development, J. Pharm. Sci. (2010) n/a-n/a. doi:10.1002/jps.22074.

[15] P.J. Marsac, T. Li, L.S. Taylor, Estimation of Drug–Polymer Miscibility and Solubility in Amorphous Solid Dispersions Using Experimentally Determined Interaction Parameters, Pharm. Res. 26 (2009) 139–151. doi:10.1007/s11095-008-9721-1.

[16] P.J. Marsac, S.L. Shamblin, L.S. Taylor, Theoretical and Practical Approaches for Prediction of Drug–Polymer Miscibility and Solubility, Pharm. Res. 23 (2006) 2417–2426. doi:10.1007/s11095-006-9063-9.

[17] J. Gupta, C. Nunes, S. Vyas, S. Jonnalagadda, Prediction of Solubility Parameters and Miscibility of Pharmaceutical Compounds by Molecular Dynamics Simulations, J. Phys. Chem. B. 115 (2011) 2014–2023. doi:10.1021/jp108540n.

[18] A. Paudel, J. Van Humbeeck, G. Van den Mooter, Theoretical and Experimental Investigation on the Solid Solubility and Miscibility of Naproxen in Poly(vinylpyrrolidone), Mol. Pharm. 7 (2010) 1133–1148. doi:10.1021/mp100013p.

[19] Y. Zhao, P. Inbar, H.P. Chokshi, A.W. Malick, D.S. Choi, Prediction of the thermal phase diagram of amorphous solid dispersions by flory-huggins theory, J. Pharm. Sci. 100 (2011) 3196–3207. doi:10.1002/jps.22541.

[20] S.O. Kyerematen, M. Pudlas, G.H. Woehrle, A Fast and Reliable Empirical Approach for Estimating Solubility of Crystalline Drugs in Polymers for Hot Melt Extrusion Formulations, J. Pharm. Sci. 103 (2014) 2847–2858. doi:10.1002/jps.23941.

[21] Y. Sun, J. Tao, G.G.Z. Zhang, L. Yu, Solubilities of crystalline drugs in polymers: An improved analytical method and comparison of solubilities of indomethacin and nifedipine in PVP, PVP/VA, and PVAc, J. Pharm. Sci. (2010) n/a-n/a. doi:10.1002/jps.22251.

[22] J. Tao, Y. Sun, G.G.Z. Zhang, L. Yu, Solubility of Small-Molecule Crystals in Polymers: d-Mannitol in PVP, Indomethacin in PVP/VA, and Nifedipine in PVP/VA, Pharm. Res. 26 (2009) 855–864. doi:10.1007/s11095-008-9784-z.

[23] C. Donnelly, Y. Tian, C. Potter, D.S. Jones, G.P. Andrews, Probing the Effects of Experimental Conditions on the Character of Drug-Polymer Phase Diagrams Constructed Using Flory-Huggins Theory, Pharm. Res. 32 (2015) 167–179. doi:10.1007/s11095-014-1453-9.

[24] A. Prudic, Y. Ji, G. Sadowski, Thermodynamic Phase Behavior of API/Polymer Solid Dispersions, Mol. Pharm. 11 (2014) 2294–2304. doi:10.1021/mp400729x.

[25] M. Yang, P. Wang, H. Suwardie, C. Gogos, Determination of acetaminophen's solubility in poly(ethylene oxide) by rheological, thermal and microscopic methods, Int. J. Pharm. 403 (2011) 83–89. doi:10.1016/j.ijpharm.2010.10.026.

[26] A. Mahieu, J.-F. Willart, E. Dudognon, F. Danède, M. Descamps, A New Protocol To Determine the Solubility of Drugs into Polymer Matrixes, Mol. Pharm. 10 (2013) 560–566. doi:10.1021/mp3002254.

[27] M.M. Knopp, N.E. Olesen, P. Holm, K. LÖBmann, R. Holm, P. Langguth, T. Rades, Evaluation of Drug-Polymer Solubility Curves Through Formal Statistical Analysis: Comparison of Preparation Techniques, J. Pharm. Sci. 104 (2015) 44–51. doi:10.1002/jps.24207.

[28] W. Brostow, R. Chiu, I.M. Kalogeras, A. Vassilikou-Dova, Prediction of glass transition temperatures: Binary blends and copolymers, Mater. Lett. 62 (2008) 3152–3155. doi:10.1016/j.matlet.2008.02.008.

[29] D.W. Clegg, A.A. Collyer, Rheological measurement, Chapman & Hall, London; New York, 1998.

[30] U. Eisele, Introduction to Polymer Physics, Springer Berlin Heidelberg, Berlin, Heidelberg, 1990. http://dx.doi.org/10.1007/978-3-642-74434-1 (accessed November 27, 2015).

[31] D.W. van Krevelen, Properties of polymers: their correlation with chemical structure: their numerical estimation and prediction from additive group contributions, 4th, completely ed ed., Elsevier, Amsterdam, 2009.

[32] R.I. Tanner, Engineering rheology, 2nd ed, Oxford University Press, New York, 2000.

[33] R.K. Jena, X. Chen, C.Y. Yue, Y.C. Lam, Viscosity of COC polymer (TOPAS) near the glass transition temperature: Experimental and modeling, Polym. Test. 29 (2010) 933–938. doi:10.1016/j.polymertesting.2010.08.007.

[34] P.R. Couchman, F.E. Karasz, A classical thermodynamic discussion of the effect of composition on glass-transition temperatures, Macromolecules. 11 (1978) 117–119. http://pubs.acs.org/doi/abs/10.1021/ma60061a021 (accessed November 3, 2015).
[35] S. Keratichewanun, Y. Yoshihashi, N. Sutanthavibul, K. Terada, J. Chatchawalsaisin, An Investigation of Nifedipine Miscibility in Solid Dispersions Using Raman Spectroscopy, Pharm. Res. 32 (2015) 2458–2473. doi:10.1007/s11095-015-1638-x.
[36] A. Forster, J. Hempenstall, T. Rades, Characterization of glass solutions of poorly water-soluble drugs produced by melt extrusion with hydrophilic amorphous polymers, J. Pharm. Pharmacol. 53 (2001) 303–315. http://onlinelibrary.wiley.com/doi/10.1211/0022357011775532/abstract (accessed February 2, 2015).
[37] S. Chen, J. Zhu, F. Ma, Q. Fang, Y. Li, Preparation and Characterization of Solid Dispersions of Dipyridamole with a Carrier "Copolyvidonum Plasdone®S-630," Drug Dev. Ind. Pharm. 33 (2007) 888–899. doi:10.1080/03639040701199209.
[38] S.-Y. Lin, H.-L. Lin, Y.-T. Chi, Y.-T. Huang, C.-Y. Kao, W.-H. Hsieh, Thermoanalytical and Fourier transform infrared spectral curve-fitting techniques used to investigate the amorphous indomethacin formation and its physical stability in Indomethacin-Soluplus® solid dispersions, Int. J. Pharm. (2015). doi:10.1016/j.ijpharm.2015.10.042.
[39] T. Matsumoto, G. Zografi, Physical Properties of Solid Molecular Dispersions of Indemethacin with Poly(vinylpyrrolidone) and Poly(vinylpyrrolidone-co-vinylacetate) in Relation to Indomethacin Crystallization, Pharm. Res. 16 (1999) 1722–1728.

3.11 Supplementary data

Table 3.A.1 *Measured physical mixtures in DSC and the annealing temperatures, respectively. The annealing temperature corresponds to $T_{g,CK}$ + 60 °C for KVA64 blends and to $T_{g,CK}$ + 90 or 100 °C for SOL blends.*

Substance	$T_{Annealing}$ [°C]	Substance	$T_{Annealing}$ [°C]
DPD + KVA64		**DPD + SOL**	
20%	147	**20%**	159
30%	138	**40%**	152
35%	134	**45%**	150
40%	131	**50%**	148

60%	118	**60%**	146
80%	107	**80%**	142
IMC + KVA64		**IMC + SOL**	
20%	155	**20%**	166
40%	145	**40%**	150
50%	139	**60%**	145
55%	136	**65%**	143
60%	133	**70%**	142
70%	126	**80%**	140
80%	119		
ITZ + KVA64		**ITZ + SOL**	
10%	160	**10%**	159
15%	159	**15%**	158
20%	157	**20%**	158
40%	146	**25%**	157
50%	141	**30%**	156
60%	137	**40%**	155
70%	132	**60%**	152
80%	127	**80%**	150
NIF + KVA64		**NIF + SOL**	
20%	156	**40%**	160
30%	150	**50%**	157
35%	147	**55%**	156
40%	144	**60%**	154
45%	142	**70%**	152
50%	138	**80%**	149
60%	132		
70%	125		
80%	118		
90%	111		

Table 3.A.2 *Carreau-Yasuda and WLF-Fits for different blends resulting from oscillatory measurements and employing TTS. Mean values ± standard error.*

T	Carreau-Yasuda fit				WLF fit	
[°C]	η_0 [Pa·s] (± S.E.)	λ [s] (± S.E.)	n (± S.E.)	a (± S.E.)	C_1 (± S.E.)	C_2 (± S.E.)
Copovidone						
140	329,203.2 (± 9,414.6)	7.151 (± 2.810)	0.574 (± 0.050)	0.748 (± 0.119)	10.77 (± 0.58)	137.35 (± 7.93)
150	61,005.8 (± 1,472.2)	1.356 (± 0.445)	0.577 (± 0.042)	0.756 (± 0.103)	10.04 (± 2.73)	147.40 (± 37.92)
160	14,038.6 (± 319.3)	0.316 (± 0.097)	0.578 (± 0.039)	0.758 (± 0.097)	9.42 (± 2.25)	157.60 (± 33.64)
170	3,842.8 (± 78.9)	0.085 (± 0.024)	0.577 (± 0.036)	0.757 (± 0.088)	8.86 (± 1.37)	167.63 (± 22.03)
180	1,228.9 (± 23.0)	0.027 (± 0.007)	0.577 (± 0.033)	0.757 (± 0.080)	8.26 (± 1.06)	176.25 (± 18.22)
190	465.2 (± 8.2)	0.010 (± 0.002)	0.579 (± 0.031)	0.765 (± 0.077)	7.44 (± 0.82)	180.74 (± 15.08)
Soluplus®						
150	17,156.37 (± 58.82)	0.757 (± 0.027)	0.567 (±0.005)	0.782 (±0.013)	4.75 (± 0)	104.67 (± 0)
160	6,707.56 (± 23.00)	0.292 (± 0.011)	0.567 (±0.005)	0.782 (±0.013)	4.34 (± 0)	114.77 (± 0)
170	2,959.77 (± 10.15)	0.131 (± 0.005)	0.567 (±0.005)	0.782 (±0.013)	3.98 (± 0)	124.48 (± 0)
Copovidone + 20% Dipyridamole						
140	56,917.0 (± 1,362.6)	1.942 (± 0.836)	0.600 (± 0.056)	0.771 (± 0.122)	9.47 (± 0.12)	126.01 (± 1.71)
150	11,360.7 (± 367.4)	0.393 (± 0.226)	0.598 (± 0.076)	0.767 (± 0.162)	8.78 (± 0.50)	135.98 (± 7.31)
160	2,841.1 (± 88.6)	0.096 (± 0.054)	0.595 (± 0.074)	0.765 (± 0.156)	8.19 (± 0.31)	146.15 (± 4.84
170	849.0 (± 24.5)	0.030 (± 0.015)	0.600 (± 0.067)	0.775 (± 0.148)	7.64 (± 0.27)	155.75 (± 4.56)
Copovidone + 20% Indomethacin						
130	185,056.5 (± 4,782.0)	7.981 (± 2.513)	0.618 (± 0.038)	0.798 (± 0.123)	10.40 (± 0.55)	123.32 (± 7.05)

140	30,662.6 (± 687.9)	1.358 (± 0.366)	0.621 (± 0.032)	0.810 (± 0.110)	9.62 (± 2.84)	133.44 (± 36.99)
150	6,555.5 (± 142.0)	0.288 (± 0.075)	0.620 (± 0.031)	0.807 (± 0.106)	8.87 (± 2.20)	142.36 (± 31.15)
160	1,686.0 (± 34.1)	0.076 (± 0.018)	0.623 (± 0.029)	0.821 (± 0.102)	8.54 (± 1.70)	155.67 (± 25.81)
170	517.2 (± 10.5)	0.023 (± 0.006)	0.621 (± 0.029)	0.812 (± 0.100)	7.99 (± 1.39)	165.26 (± 22.66)
Copovidone + 20% Itraconazole						
150	25,630.6 (± 683.3)	0.850 (± 0.534)	0.645 (± 0.067)	0.741 (± 0.159)	4.74 (± 0.25)	46.99 (± 3.05)
160	3,746.1 (± 67.1)	0.131 (± 0.054)	0.651 (± 0.044)	0.763 (± 0.114)	3.90 (± 1.35)	56.85 (± 16.46)
170	992.9 (± 11.3)	0.035 (± 0.009)	0.652 (± 0.028)	0.770 (± 0.074)	3.18 (± 1.20)	65.13 (± 17.51)
180	340.3 (± 3.5)	0.012 (± 0.003)	0.654 (± 0.025)	0.773 (± 0.066)	3.14 (± 0.81)	80.27 (± 13.44)
Copovidone + 20% Nifedipine						
150	12,357.9 (± 227.7)	0.542 (± 0.110)	0.612 (± 0.025)	0.806 (± 0.085)	9.01 (± 3.51)	127.26 (± 53.96)
160	2,728.7 (± 92.1)	0.121 (± 0.044)	0.613 (± 0.045)	0.811 (± 0.157)	*8.28 (± 14.30)*	*136.06 (± 220.70)*
170	737.9 (± 22.2)	0.033 (± 0.011)	0.613 (± 0.400)	0.815 (±0.141)	7.72 (± 5.92)	146.18 (± 98.80)

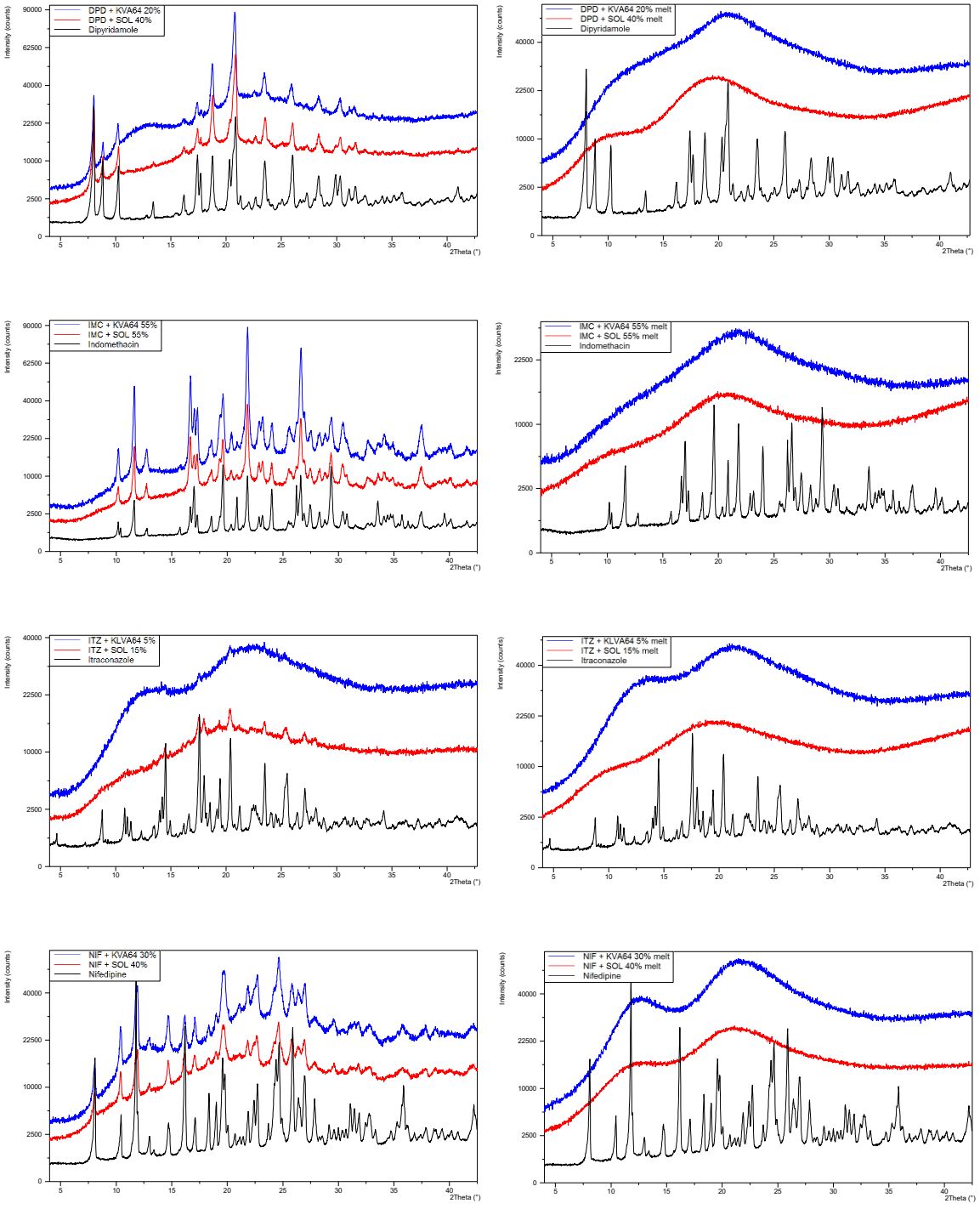

Figure 3.A.1 *XRPD diagrams of the physical mixtures (DPD, IMC, ITZ, NIF in KVA64 or SOL) before and after annealing which were amorphous after the annealing step.*

4 Predicting the solubility of active pharmaceutical ingredients in polymeric matrices

Esther S. Bochmann [a]; Dirk Neumann [a,b]; Andreas Gryczke [c]; Karl G. Wagner [a]

[a] Department of Pharmaceutical Technology and Biopharmaceutics, University of Bonn, Bonn, Germany

[b] Scientific Consilience GmbH, Saarbrücken, Ludwigshafen, Germany

[c] AbbVie Deutschland GmbH & Co. KG, Ludwigshafen, Germany

This part was submitted as

E.S. Bochmann, A. Gryczke, K.G. Wagner, Predicting the solubility of active pharmaceutical ingredients in polymeric matrices, European Journal of Pharmaceutics and Biopharmaceutics.

4.1 Graphical Abstract

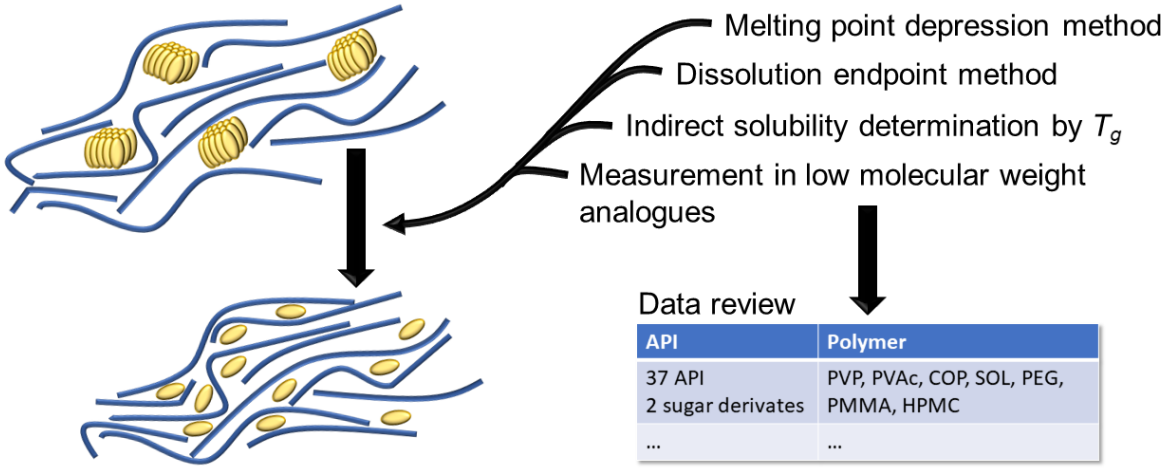

4.2 Abstract

The number of models for predicting the solubility of active pharmaceutical ingredients (APIs) in polymeric matrices on the one hand and the extent of available associated data on the other hand has been rising steadily in the past few years. However, according to our knowledge an overview on the methods used for prediction and the respective experimental data is missing. Therefore, we compiled experimental data, the techniques used for their determination and the models used for predicting the solubility. Our focus was on polymers commonly used in spray drying and hot-melt extrusion to form amorphous solid dispersions (ASDs), namely polyvinylpyrrolidone grades (PVP), polyvinyl acetate (PVAc), vinylpyrrolidone-vinyl acetate copolymer (copovidone, COP), polyvinyl caprolactam-polyvinyl acetate-polyethylene glycol graft polymer (Soluplus®, SOL), different types of methacrylate copolymers (PMMA), polyethylene glycol grades (PEG) and hydroxypropyl-methylcellulose grades (HPMC). The literature data were further supplemented by our own results. The final data set included 37 APIs and two sugar derivatives. The majority of the prediction models was constituted by the melting point depression method, dissolution endpoint measurements, indirect solubility determination by T_g and the use of low molecular weight analogues. We observed that the API solubility depended more on the working group which conducted the experiments than on the measuring technique used. Furthermore, this compilation should assist researchers in choosing a prediction method suited for

their investigations. Finally, the data set should help researchers in training their own solubility prediction models.

4.3 Keywords

solubility, data review, amorphous solid dispersion, prediction model

4.4 Chemical compounds studied in this article

Bisacodyl (PubChem CID: 2391); Carbamazepine (PubChem CID: 2554); Celecoxib (PubChem CID: 2662); Cilostazol (PubChem CID: 2754); Clozapine (PubChem CID: 2818); Dipyridamole (PubChem CID: 3108); Felodipine (PubChem CID: 3333); Gliclazide (PubChem CID: 3475); Griseofulvin (PubChem CID: 441140); Indomethacin (PubChem CID: 3715); Itraconazole (PubChem CID: 55283); Lamotrigine (PubChem CID: 3878); Loratadine (PubChem CID: 3957); Nifedipine (PubChem CID: 4485); Naproxen (PubChem CID: 156391); Posaconazole (PubChem CID: 468595); Praziquantel (PubChem CID: 4891); Probucol (PubChem CID: 4912); Ritonavir (PubChem CID: 392622); Telmisartan (PubChem CID: 65999); Verapamil-HCl (PubChem CID: 62969); Copovidone (PubChem CID: 25086-89-9)

4.5 Introduction

In recent years, the increasing number of poorly soluble active pharmaceutical ingredients (APIs) led to the requirement of new and innovative strategies and dosage forms in drug formulation development [1]. One of the so-called enabling technologies to overcome poor API-solubility is the formation of amorphous solid dispersions (ASDs), either by solvent evaporation or by melting techniques (e.g. spray drying or hot-melt extrusion) [2–4]. In ASDs, the API is amorphously embedded (molecularly dispersed) in a polymeric matrix and often kinetically stabilized, especially if a supersaturated state at room temperature is achieved. Due to the absence of a crystal lattice, the API rate and extent of dissolution in aqueous media are increased and thus, the respective bioavailability is enhanced [5–8]. The drawback of a metastable amorphous API form, which is mainly kinetically stabilized in a polymeric matrix, is the overall reduced stability due to potential recrystallisation over the shelf life and the ensuing decrease in

bioavailability [5,9]. Therefore, a thermodynamically embedded amorphous API in a polymeric matrix, which is entirely soluble without supersaturation at room temperature, is favorable. This can be achieved if the API content in an (dissolved) ASD is completely soluble in the investigated polymeric matrix at ambient conditions [10,11]. It leads not only to a kinetically but more to a thermodynamically stabilized system which prevents recrystallization and thus prolongs the shelf life of the entire drug formulation [3,12–14]. However, the measurement of the API solubility is challenging and a direct determination at room temperature is obstructed by the high viscosity of the overall system [12]. The slow kinetics of such systems result in unrealistically long periods to observe recrystallization and determine the limit of API solubility, respectively. Therefore, either the use of surrogate systems with a low weight analogue to the respective polymer or measurements at elevated temperatures and subsequent extrapolation to room temperature are used to obtain the desired information on an experimental basis [9,15–17].

Several techniques and assumptions, with corresponding data sets, are available in the literature which can be used to elucidate the solubility of an API in a given polymeric matrix [5,10,12,15]. Commonly used techniques are based on differential scanning calorimetry (DSC) methods or measurements in low molecular weight analogues. The most widely investigated DSC methods include DSC measurements, the melting point depression method [10,17,18] and the dissolution endpoint method [19–21]. During measurement and while applying a sufficiently low heating rate to the specimen, either the onset or the endset of the melting endotherm can be analyzed. Furthermore, indirect measurements of the API solubility in polymeric matrices by using the glass transition temperature (T_g) of recrystallized or annealed samples have been reported [22,23]. Further measuring techniques, which make use of heat capacity differences between the solid solution and its unmixed components, solution calorimetry or high-energy mechanical milling on processed solid dispersions have also been investigated [24–26]. In the case of measurements in low molecular weight analogous, the limiting factor of the high viscosity of an ASD at room temperature is circumvented by employing the polymer's low molecular weight analogue and extrapolating the obtained solubility to the polymer of interest [27,28].

However, most of the data sets used to train solubility prediction methods encompass only one or a limited number of APIs. Thus, the overall applicability of such prediction

model is questionable. The aim of our study is 1) to compare the available data sets and models published so far and 2) to supplement these data with our own work and data on predicting API solubility in polymeric matrices. This leads to a compilation of API-polymer solubility data, which should assist researchers in choosing an adequate prediction method and should provide researchers with a data set for training solubility prediction models. Finally, we were able to prove the validity of our own DSC method by comparing it to a wide data set, based on other methods presented in literature.

4.6 Material and methods

4.6.1 **Material**

Bisacodyl, dipyridamole, gliclazide, naproxen and verapamil-HCl were received from Sigma-Aldrich Chemical Co. (St. Louis, MO, USA). Griseofulvin, indomethacin and itraconazole were obtained from Alfa Aesar GmbH & Co. KG (Karlsruhe, Germany). Clozapine, ritonavir and posaconazole were received from Swapnroop Drug and Pharmaceuticals (Aurangabad, India). Loratadine and telmisartan were purchased from sris Pharmaceuticals (Telangana, India). Nifedipine and probucol were from Cayman Chemical (Ann Arbor, MI, USA). Celecoxib was purchased from Cadila Pharmaceuticals Ltd. (Ahmedabad, India) and cilostazol was received from Amsal Chem Pvt Ltd. (Mumbai, India). Felodipine was obtained from Molekula Limited (Newcastle, UK), lamotrigine was received from Maps Laboratories Pvt. Ltd. (Gujarat, India), praziquantel was received from Divis Laboratories Ltd. (Telangana India). Vinylpyrrolidone-vinyl acetate copolymer (copovidone, Kollidon® VA 64, COP), polyvinyl caprolactam-polyvinyl acetate-polyethylene glycol graft polymer (Soluplus®, SOL) and carbamazepine were kindly donated by BASF SE (Ludwigshafen, Germany) (Table 4.1).

Table 4.1 *Physicochemical properties of substances under investigation. Molecular weight was taken from PubChem Substance and Compound databases [29], all other parameters were experimentally determined.*

Substance	*Mw* [g/mol]	T_m [°C]	T_g [°C]	C_p step at T_g [J/g·K]	*Soluble in COP at 100 °C*
Bisacodyl	361.4	133.6	16.1	0.36	Yes
Carbamazepine	236.3	175.1 190.2	52.7	0.38	No
Celecoxib	381.4	160.9	56.8	0.39	Yes
Cilostazol	369.5	158.6	31.2	0.46	No
Clozapine	326.8	182.1	59.7	0.35	No
Dipyridamole	504.6	167.1	38.2	0.68	Yes
Felodipine	384.3	144.2	45.0	0.30	Yes
Gliclazide	323.4	170.5	39.6	0.48	No
Griseofulvin	352.8	218.3	88.9	0.30	No
Indomethacin	357.8	160.1	44.4	0.33	Yes
Itraconazole	705.6	165.8	57.7	0.44	No
Lamotrigine	256.1	215.8	93.3	0.54	No
Loratadine	382.9	134.6	34.9	0.30	No
Naproxen	230.3	156.1	6.7*	0.31*	Yes
Nifedipine	346.3	172.2	44.3	0.34	Yes
Posaconazole	700.8	167.7	59.8	0.43	No
Praziquantel	312.4	138.3	35.9	0.37	No
Probucol	516.8	126.3	25.6	0.46	Yes
Ritonavir	720.9	121.8	48.6	0.46	Yes
Telmisartan	514.6	268.3	129.5	0.35	No
Verapamil-HCl	491.1	142.3	55.2	0.51	No
Copovidone (COP)	45,000 - 70,000	-	107	0.40	-
Soluplus® (SOL)	90,000 – 140,000	-	71.1	0.30	-

** measured with 10% COP weight fraction due to APIs recrystallization tendency.*

4.6.2 **Methods**

4.6.2.1 Differential Scanning Calorimetry (DSC)

A DSC 2 from Mettler Toledo (Gießen, Germany) was used to analyze glass transition temperatures (T_gs), heat capacity steps at T_g and the API solubility in polymer melts. The system was equipped with an auto sampler, nitrogen cooling and nitrogen as

purge gas (30 ml/min). Calibration of the DSC was performed by using n-octane, indium and zinc standards. Every investigated material was analyzed in triplicate placing approx. 10 mg sample in a 40 µl aluminum pan with a pierced lid and using 10 K/min as heating and cooling rate. In the case of heat capacities, measurements were conducted against a sapphire standard and in TOPEM® mode (modulated DSC) with 1 K pulse height, 15-30 s pulse width and an underlying heating rate of 2 K/min. For heat capacity measurement, the samples were annealed prior to analysis to enable homogeneous API-distribution in the polymeric matrix. Before conducting any DSC measurement, samples were prepared by using a MM400 ball mill of Retsch GmbH (Haan, Germany) with 30 Hz and 3x 5 min milling cycles.

4.6.2.2 Solubility determination via DSC

The solubility determination of APIs in COP and SOL were conducted by using a protocol of our recent work [23]. The method was based on an indirect measurement of the API solubility by using the T_g. First, the sample was annealed at a certain temperature, were the melt viscosity of the specimen allowed the API to dissolve. Secondly, the T_g of this annealed sample was determined and a further T_g analysis of the respective amorphous system with the completely dissolved API fraction was conducted. This procedure was repeated at different API/polymer weight fractions. Further, the second analyzed T_gs served for the determination of the weight fraction-dependent curve progression of T_g by employing the Brostow Chiu Kalogeras Vassilikou-Dova fit (BCKV-fit, Eq. 4.1),

$$T_g = w_1 T_{g,1} + (1 - w_1) T_{g,2} + w_1(1 - w_1)[a_0 + a_1(2w_1 - 1) + a_2(2w_1 - 1)^2] \quad (4.1)$$

where at $T_{g,1}$ and $T_{g,2}$ are the T_gs of API and polymer, respectively, w_1 is the weight fraction of the API and a_0, a_1 and a_2 are variables [30]. Due to its polynomial form, the BCKV-fit is able to consider positive and negative deviations from the Couchman-Karasz fit [31]. Thus, it was appropriate to identify the solubilized API fraction of the annealed samples by employing the API weight fraction-dependent curve progression of glass transition temperature. Finally, for predicting the API solubility phase diagram, Equation 2 was fitted to the solubility curve progression,

$$T_{Annealing} = y_0 + A * e^{R_0 * x} \quad (4.2)$$

where x is the soluble API fraction ($w_{API}/w_{polymer}$) at the respective temperature, A and R_0 are fitting constants and y_0 corresponds to the API melting point but was set as a variable. All API solubility results were further confirmed with XRPD measurements (data not shown).

4.6.2.3 Empirical model of solubility in COP

In short, to predict if the solubility in COP at 100°C is at least 0.20 (w/w), we used R, a freely available language and environment for statistical computing and graphics [32]. Molecular descriptors of the API in COP in Table 4.1 of the manuscript were computed with MOE [33]. These descriptors were enriched with data obtained from experiments and the PubChem database [29]. Features that had no value or had the same value for 50% or more of the compounds were removed. Features were not standardized at the beginning of the computations. Instead, standardization was performed prior to any model training.

An initial estimate of the necessary number of descriptors was obtained using the package glmnet [34], whereas selection of features was performed using the LiblineaR package [35], which provides a wrapper for the LIBLINEAR C/C++ library for machine learning [36]. The predictive accuracy was assessed using balanced accuracy computed by the package caret [37].

Features were selected using recursive feature elimination [38]. The optimal value of the hyperparameter of each regularized logistic regression model was estimated by a leave-one out crossvalidation. To assess the predictive accuracy of our models for unseen data, we performed nested crossvalidation: in an additional outer loop we employed leave-one out crossvalidation to compute the balanced accuracy for test samples. The selection of the features for the final model was based on the full set of compounds.

A more detailed description of our approach is given in the supplementary material (Appendix A).

4.7 Results & Discussion

The data of API solubility in polymeric matrices from literature, together with our own results, are given in Table 4.2. In general, solubility data were given in weight fractions ($w_{API}/w_{polymer}$). Regarding the data set, the focus was on polymers which were commonly known for their application in hot-melt extrusion and on solubility determinations, which were based on experimental results. The following polymers occurred frequently enough in literature to warrant inclusion in our compilation: polyvinylpyrrolidone grades (PVP), polyvinyl acetate (PVAc), vinylpyrrolidone-vinyl acetate copolymer (copovidone, COP), polyvinyl caprolactam-polyvinyl acetate-polyethylene glycol graft polymer (Soluplus®, SOL), different types methacrylate copolymers (PMMA), polyethylene glycol (PEG) and hydroxypropyl-methylcellulose grades (HPMC). To expand the data set, solubility data of further 20 APIs in COP and SOL of our own work were added. In total, the final data set was comprised of 37 APIs and 2 sugar derivatives with a varying extent of available polymer data and several measuring techniques to obtain the API solubility in polymeric matrices. A detailed compilation of the physicochemical characteristics of the APIs and sugar derivatives under investigation is listed in the supplementary section (Appendix B). Although different measuring techniques were used, the majority of techniques were based on DSC. Observed differences in the solubilities for the same substance likely depended on both the measuring technique, obviously, but also on the working group which conducted the measurements.

4.7.1 Measuring techniques

In the data set presented in Table 4.2, only API solubilities which were derived from experimental values were considered. The index next to the solubility value depicts the measuring technique used. They were divided into melting point depression methods by using the onset of the melting point (T_m) (index 1), dissolution endpoint methods using the endset of T_m (index 2), indirect measurements via the glass transition temperatures (index 3), measurements in low molecular weight analogues (index 4) and further measuring techniques (index 5). The fifth category of measuring techniques includes for example, a technique based on a thermodynamic model to calculate the

Gibbs energy change while forming a drug-polymer solution [24], using solution calorimetry to determine enthalpies of mixing [25] or investigating the stability of ASDs against high-energy mechanical milling [26].

Melting point depression method

In the case of the melting point depression method, an adequately low heating rate (approx. 0.2-2 K/min) is applied to a physical mixture and the onset of the melting endotherm characterizes the temperature which enables the dissolution of the entire API fraction [10,17,18]. Employing the Flory-Huggins lattice theory and the proposed calculation of the interaction parameter χ by Marsac et al. was able to extrapolate the API solubility to ambient temperatures using the melting point depression of a soluble API/polymer system [39,40]. One of the drawbacks of this method is that at a low crystalline API weight fraction, the melting peak becomes more broad and flat, making it challenging to define the onset accurately [10,41,42]. Furthermore, the onset only characterizes the starting point of the API dissolution within the polymeric matrix. It remains unknown whether the entire API fraction would dissolve at this temperature or probably at temperatures above the onset [43–45]. However, this method is more robust against the sample preparation method used. While for the dissolution endpoint method a certain maximal particle size of the specimen needs to be defined for an appropriate solubility determination, this drawback is less critical for the melting point depression method [19,22].

Dissolution endpoint method

Regarding the dissolution endpoint method, a cryo-milled physical mixture and the application of an adequately low heating rate (approx. 0.2-2 K/min) enables the accurate characterization of the melting endotherm endset, which serves as the temperature point where the API fraction is entirely soluble within the polymeric matrix [19–21]. This method is prone to errors due to measurements in a non-equilibrated state as a result of high heating rates (>2 K/min) or insufficiently large particle sizes, as cryo-milling seemed to be necessary for an accurate determination of the melting point endset [19,22]. Due to the strong dependency of the resulting solubility on the preparation

method, this method is prone to error. The extrapolation to ambient temperature can either be performed by using the Flory-Huggins lattice theory [39,40], the empirical assumption of Kyerematenge et.al. [21] or the relatively new PC-SAFT (perturbed-chain statistical associating fluid theory) software from Sadowski and co-workers, which is based on a perturbation theory for chain molecules [44,46–48]. In the case of PC-SAFT, not only binary mixtures of different API/polymer combinations were investigated [44,46], but also the influence of humidity on the long-term physical stability of ASD [47] as well as amorphous-amorphous phase separations [48] were evaluated.

Indirect solubility determination by T_g

Indirect measurements of the API solubility in a polymeric matrix are based on analysis of annealed or recrystallized samples [22,23]. We employed this approach in our own studies. For detailed information, the reader is kindly referred to subsection 4.6.2.2.. In the case of the recrystallization method, a supersaturated amorphous solid dispersion is prepared by solvent evaporation and annealed at different temperatures. Subsequently, the T_g of the annealed sample is analyzed and compared to the API weight fraction-dependent course of T_g by employing the Gordon-Taylor equation [49]. Extrapolation to room temperature was conducted by employing the Flory-Huggins lattice theory [39,40]. Due to the use of the Gordon-Taylor equation to identify the soluble API weight fraction, the weight fraction-dependent course of T_g has to follow this equation. Otherwise a regression can only be performed between two measuring points which is statistically questionable [50]. However, the comparability of this indirect measurement to melting point depression techniques has already been proven [51].

Measurement in low molecular weight analogues

In this method, the measurement is performed in the low molecular weight analogue monomer (e.g. 1-ethyl-2-pyrrolidone instead of PVP) of a desired polymer [27,39]. Regarding copolymers, the measurements are conducted separately in the respective analogous monomers and in dependence of the composition of the copolymer, the solubility is calculated. By using a liquid analogue, the API solubility in the low molecular weight analogue can be directly determined at room temperature and it is further

extrapolated to the polymer of interest. Therefore, difficulties in achieving an equilibrated state during solubility measurements of a highly viscous ASD are circumvented. However, whether the effect of the polymer's molecular weight and probable steric hindrances are negligible at all times is questionable. Hints of an existing threshold for the influence of molecular mobility have already been found [50].

4.7.1.1 Comparison of the common measuring techniques

Upon investigation of the deviation due to different measuring techniques used to obtain API solubility data, no trend was observed to rank the measuring techniques according to their reliability (Table 4.2). Conducting the chosen measuring technique in an accurate way to ensure the sample is in its equilibrated state during analysis seems more important than the method itself. For example, the determined solubility ($w_{API}/w_{polymer}$) of felodipine in PVP seemed more dependent on the working group who conducted the experiments than on the measuring technique itself. The felodipine-PVP (K12-K90) solubility fraction determined by using the dissolution endpoint method ranged between 0.00 and 0.24 [43,52], whereas the use of low molecular weight analogues resulted in a solubility from 0.05 to 0.31 [39,53], independent of the PVP grade used. More striking is the discrepancy in solubility data for measurements with an indomethacin-COP system by Kyerematen et al. (0.32 at 25 °C) [21] and by Knopp et al. (0.06 at 25 °C) [53], both using the dissolution endpoint method. Although they used the same methodology, the obtained indomethacin solubility varied. In comparison to other publications, the obtained solubility by Kyerematen et al. seemed more consistent (Table 4.2) than the one of Knopp et al., leaving the accuracy in solubility determination in the last case questionable.

4.7.2 **Consistency of the obtained literature data set**

To evaluate the consistency within the solubility data in Table 4.2, APIs with a wide set of available data were chosen, namely acetaminophen, celecoxib, felodipine, indomethacin, naproxen and nifedipine. In most of the cases, the largest data sets were obtained for PVP and COP, therefore these two polymers served as the basis to judge the accuracy of solubility results.

In the case of acetaminophen, the solubility data were mainly derived by Rades and co-workers [53,54] or by Sadowski and co-workers [21,47,55]. Regarding the solubility of acetaminophen-PVP, it varied from 0.17 to 0.32, whereas the API was insoluble in PVAc. Consequently, the solubility in COP (6:4) decreased slightly to 0.21-0.28, compared to PVP. A further COP grade (3:7) with a lower PVP content led to a further reduction in solubility to 0.02-0.05. Therefore, a consistent data set in terms of acetaminophen could be presented, but with a slight variation in acetaminophen-PVP solubility. Regarding celecoxib, the entire data set for PVP, PVAc and COP was found in publications from Rades and co-workers [50,51,53,54], except two data points of our own work in COP and SOL. Our measured COP solubility was in good agreement with literature. However, the solubility in SOL seemed to be underestimated by our own approach. In general, celecoxib was found to be soluble in most of the investigated polymers, but its solubility in PVAc might be very low. In the case of felodipine, a wide data set reported by a variety of authors was found, namely the obtained solubility in PVP ranged from 0.00 to 0.31. Due to the low solubility in PVAc and the average solubility of 0.21 in COP, the higher solubilities in PVP might be more consistent with the overall data set. Furthermore, our results for the felodipine-COP system were in good accordance with the overall data set. For indomethacin, a comparably large data set to felodipine was obtained. As mentioned above for other APIs, the solubility in PVP was highly variable (0.08-0.54), which makes it difficult to comment about the solubility of indomethacin in PVP. However, the solubility in COP (6:4, PVP:PVAc) was reported in a narrow range of 0.31-0.36. Due to the insoluble indomethacin-PVAc system, a PVP-solubility which was higher than the COP-solubility would be plausible. In the case of naproxen, mainly two groups of authors had worked on its solubility, Paudel et al. [17] and Sadowski and co-workers [21,47,55]. Paudel et al. determined a solubility in PVP of 0.06 for naproxen, whereas the group of Sadowski exceeded a solubility of 0.31 to 0.36. With respect to the low solubility in PVAc and in comparison to the results for COP (6:4) in the range of 0.19-0.28, in which our own data point was included, the higher solubility of Sadowski and co-workers seemed more reliable. Regarding nifedipine, data from Marsac et al. (0.05-0.07 in PVP) [27,28], Kyerematen et al. (0.21 in PVP, 0.12 in COP) [21] and solubility of our own investigations (0.19 in COP) were obtained. Similar to the afore-mentioned APIs in PVP or COP, for a nifedipine-PVP system a solubility around 0.21 seems more plausible than a lower value. Otherwise

due to the insoluble nifedipine-PVAc system, the present solubility in COP would be unexplainably high. Furthermore, our determined solubility in COP (0.19) was in good accordance to literature values [21].

To conclude, in most of the regarded cases, a higher solubility in the respective polymer seemed to be more plausible than lower findings. The underestimation of API solubility might be a reason of measurements in a non-equilibrated state of the system under investigation. Therefore, before conducting measurements, the kinetic factor of melt viscosity must be considered, and it has to be assured that this is not influencing the desired solubility determination.

4.7.3 **Solubility in polymer-dependency**

The focus for this data review was on polymers which can be used to form ASD, either by spray-drying or by HME, namely PVP, PVAc, COP, SOL, PMMA, PEG and HPMC (Table 4.2). The largest data set was obtained for the various PVP grades, followed by COP, SOL and PVAc. Only limited publications were found for PMMA, PEG and HPMC.

For PVP, a variety of molecular weight grades from K12 (approx. 2,500 g/mol) to K90 (approx. 1,250,000 g/mol) were investigated. In general, no connection or tendency between molecular weight and API solubility could be made, which might be also a fact of the high variability in API solubility found in literature. However, PVP was the polymer which enabled the highest API solubility throughout the investigated polymers due to its high ability to form hydrogen bonds [56]. The highest solubility in PVP was found for celecoxib (up to 0.60), indomethacin (up to 0.54) and chloramphenicol (up to 0.52) [50,51,53]. In contrast, most APIs were sparely soluble in PVAc, due to the lack of specific interactions, especially hydrogen bonding [56]. The API solubility in PVAc did not exceeded 0.1 for the entire data set, except for celecoxib where a solubility of up to 0.16 was reported [54]. Regarding copovidone COP, consisting of PVP and PVAc in different weight ratios, the API solubility was slightly decreased in comparison to PVP. Furthermore, a decrease in PVP weight ratios always went hand in hand with a further reduction in the respective API solubility [46,50,57]. Therefore, regarding APIs in COP, the solubility of an API mainly depended on the hydrogen bonding capability

of PVP, whereas PVAc seemed more important for the processability of the copolymer than for improving the API solubility.

In the case of SOL, similar API solubilities compared to COP were achieved. The highest solubilities in SOL were found for celecoxib (0.34) naproxen (0.32) and indomethacin (0.31) [51]. Regarding the structure of SOL, it consists inter alia of PEG and PVAc units. As already stated, PVAc was sparely able to form specific interactions, e.g. hydrogen bonding, with a desired API. Thus, instead of the PVAc part, the PEG in SOL might be influencing or promoting the API solubility. In the case of indomethacin, the API solubilities in PEG (0.22-0.25) and SOL (0.20-0.31) were comparable. Furthermore, ketoconazole was insoluble in both polymers. However, discrepancies in solubility for sulfadimidine (SOL 0.00; PEG 0.12) and sulfathiazole (SOL 0.07; PEG 0.22) were found. Thus, due to the limits in the data set, no statement about the solubility-dependent polymer parts in SOL could be made, except that the PVAc fraction is unlikely to improve the API solubility. For PMMA and HPMC, again only a limited data set was found, which hindered any evaluation. However, the solubility in PMMA or HPMC was always lower or comparable to PVP.

4.7.4 **Empirical model of solubility in COP**

We performed an initial assessment of the number of features necessary to separate compounds exhibiting 0.2 (*w/w*) solubility at 100 °C in COP from those that are less soluble. The following 12 features were selected from the available 146 features (sorted by rank): PEOE_VSA_FPNEG, BCUT_SLOGP_0, std_dim2, b_rotR, a_don, SlogP_VSA6, E_tor, balabanJ, Tg, dens, SlogP_VSA8, E_ang. To better estimate the number of necessary features, we plotted the balanced accuracy of the models for unseen data obtained by recursive feature elimination versus the number of features used by the models (Figure 4.1). This plot indicates that the balanced accuracy levels off at 71% with 8 features. Further evaluation of the results using up to 12 features showed that celecoxib, dipyridamole, gliclazide, lamotrigine, loratadine and probucol were mispredicted in almost all cases. This hints at the existence of at least two clusters of compounds, since celecoxib, dipyridamole, gliclazide and lamotrigine were the only APIs with a positive deviation from the Couchman-Karasz equation [31] in the investigated data set. However, the connection between misprediction and positive

deviation from Couchman-Karasz fit remained unclear and could not be ascribed to a solubility measuring issue.

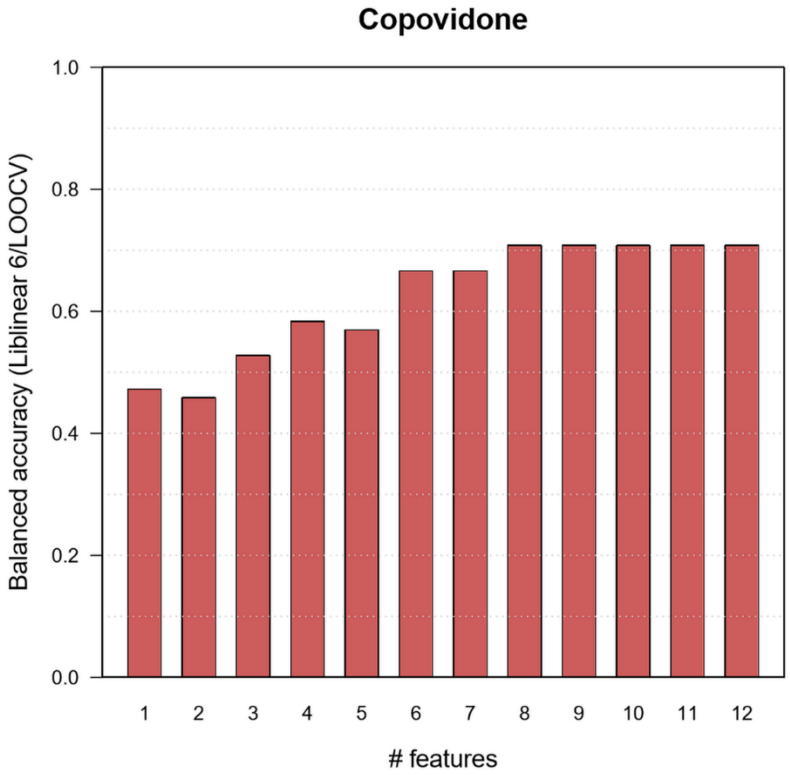

Figure 4.1 *Balanced accuracy for unseen data obtained by recursive feature elimination versus the number of features used by the models*.

Performing recursive feature elimination using all compounds resulted in selecting the following features (sorted by rank): a_don, SlogP_VSA8, Tg, PEOE_VSA_FPNEG, E_oop, b_rotR, SlogP_VSA6, BCUT_SLOGP_0.

Two different approaches were used in selecting the two sets given above, so differences between the two sets are possible. However, there is an overlap between both sets of selected features. Some of the computed features are of special interest. For example, a_don is the number of hydrogen bond donor atoms and PEOE_VSA_FPNEG is the fractional negative polar van der Waals surface area. Both these features may be important to describe the interaction between the compound and COP. b_rotR is the number of rotatable bonds divided by the total number of

bonds. Interestingly, the experimentally determined glass transition temperature is selected as well. Using only these 4 features and removing the putative outliers results in a training error of zero.

Further computations need to be carried out to confirm the existence of different subgroups of compounds and whether the set of four features may be replaced by other combinations with the same or even a lower cardinality.

Table 4.2 *Solubility review in (w/w) at 25 °C (Methods: Index 1= Melting point depression method; Index 2= Dissolution endpoint method; Index 3= Indirect solubility determination by T_g; Index 4= Measurement in low molecular weight analogues; Index 5= others; Polmers: PVP (K-value); COP (PVP:PVAc ratio); PEG (mol>ecular weight); PMMA (EPO: Eudragit® E PO/ E100: Eudragit® E100/ L100: Eudragit® L100); HPMC (E5: Ethocel® E5/ AS: HPMC acetate succinate)).*

API	Polymer						
	PVP	PVAc	COP	SOL	PEG	PMMA	HPMC
Aceclofenac				0.27[1] [58]			
Acetaminophen	0.17[5] (K17) [54]	0.004 [53]	0.21[2] (6:4) [21,47]	0.04[1] [54]			0.02[2] (AS) [55]
	0.18[4] (K17) [53]	0.011 [54]	0.28[2] (6:4) [47,55]	0.09[5] [54]			
	0.19[5] (K17) [54]	0.015 [54]		0.10[5] [54]			
	0.23[2] (K25) [21,47]	0.015 [54]	0.02[2] (3:7) [53]				
	0.29[1] (K17) [54]		0.03[3] (3:7) [53]				
	0.32[2] (K25) [47,55]		0.05[1] (3:7) [53]				
			0.05[4] (3:7) [53]				
Albendazole			0.04[1] (6:4) [59]	0.06[1] [59]		0.02[1] (EPO) [59]	
Bisacodyl			0.08[3] (6:4)	0.22[3]			
Carbamazepine	0.02[3] (K12) [51]		0.00[3] (6:4)	0.00[1] [42]			
				0.00[3]			
Celecoxib (1)	0.38[3] (K12) [51]	0.02[3] [60]	0.06[2] (6:4) [53]	0.09[3]		0.20[5] (EPO) [26]	0.25[3] [51]
	0.38[5] (K17) [54]	0.03[4] [53,60]	0.17[3] (6:4) [53]	0.23[5] [54]		0.41[1] (EPO) [26]	0.32[1] [51]
	0.38[5] (K17) [54]	0.08[1] [54]	0.25[1] (6:4) [53]	0.23[5] [54]			
	0.40[3] (K12) [60]	0.13[5] [54]	0.26[4] (6:4) [53]	0.25[1] [54]			
	0.41[4] (K17) [53]	0.16[5] [54]	0.33[3] (6:4)	0.29[1] [51]			

API	Polymer						
	PVP	**PVAc**	**COP**	**SOL**	**PEG**	**PMMA**	**HPMC**
Celecoxib (2)	0.43[1] (K17) [54]		0.33[3] (6:4) [60]	0.34[3] [51]			
	0.44[1] (K12) [51]		0.38[4] (6:4) [60]				
	0.60[4] (K12) [60]						
			0.08[3] (3:7) [60]				
			0.18[4] (3:7) [60]				
			0.20[3] (5:5) [60]				
			0.26[4] (5:5) [60]				
			0.36[3] (7:3) [60]				
			0.42[4] (7:3) [60]				
Chloramphenicole	0.39[5] (K17) [54]	0.00[4] [53]	0.05[2] (5:5) [53]	0.11[5] [54]			
	0.40[5] (K17) [54]	0.04[1] [54]	0.14[3] (5:5) [53]	0.14[1] [54]			
	0.40[1] (K17) [54]	0.05[5] [54]	0.15[1] (5:5) [53]	0.14[5] [54]			
	0.52[4] (K17) [53]	0.06[5] [54]	0.26[4] (5:5) [53]				
Cilostazol	0.00[1] (K29/32) [61]		0.00[1] (6:4) [61]	0.00[3]			0.00[1] (E5) [61]
			0.00[3] (6:4)				
Cinnarizine	0.01[1] (K30) [62]			0.00[1] [16]			
Clozapine			0.00[3] (6:4)	0.00[3]			
Curcumin	0.00[1] (K90) [63]				0.00[1] (8000) [63]	0.00[1] (EPO) [63]	0.00[1] (E5) [63]
Dipyridamole	0.00[1] (K30) [62]		0.03[3] (6:4) [23]	0.18[3] [23]			
Felodipine (1)	0.00[2] (K25) [43]	0.00[2] [65]	0.00[2] (6:4) [43]	0.00[2] [64]		0.00[2] (EPO) [66]	0.00[2] (AS) [64]
	0.03[2] (K15) [43]	0.04[4] [53]	0.11[2] (6:4) [65]	0.20[3]		0.20[5] (EPO) [26]	
	0.05[4] (K17) [53]		0.22[3] (6:4)			0.31[1] (EPO) [26]	

API	Polymer						
	PVP	PVAc	COP	SOL	PEG	PMMA	HPMC
Felodipine (2)	0.06[1] (K17) [53]		0.30[5] (6:4) [26]				
	0.07[2] (K12) [43]		0.42[1] (6:4) [26]				
	0.07[4] (K12) [27]						
	0.07[3] (K17) [53]						
	0.07[4] (K29/32) [27]						
	0.07[4] (K90) [27]						
	0.08[2] (K17) [53]						
	0.10[2] (K15) [64]						
	0.18[5] (K29/32) [25]						
	0.24[2] (K25) [65]						
	0.25[4] (K29/32) [39]						
	0.31[4] (K12) [39]						
Gliclazide			0.00[3] (6:4)	0.08[3]			
Griseofulvin	0.09[5] (K30) [24]		0.00[3] (6:4)	0.00[3]		0.09[5] (E100) [24]	
						0.12[5] (L100) [24]	
Ibuprofen	0.50[2] (K25) [65]	0.05[2] [65]	0.41[2] (6:4) [65]				
Ibuprofen sodium			0.00[2] (6:4) [21]	0.00[2] [21]			
Indomethacin (1)	0.08[5] (K30) [24]	0.00[1] [67]	0.31[1] (6:4) [67]	0.20[3] [51]	0.22[2] (6000) [44]	0.09[5] (E100) [24]	0.08[3] [51]
	0.13[4] (K90) [27]	0.00[2] [19–21]	0.32[2] (6:4) [19–21]	0.26[3] [23]	0.25[2] (35000) [44]	0.10[5] (L100) [24]	0.27[1] [51]
	0.13[4] (K29/32) [27]	0.01[2] [39]	0.33[1] (6:4) [18]	0.31[1] [51]			
	0.14[4] (K12) [27]	0.01[4] [46]	0.34[2] (6:4) [46]				
	0.20[1] (K30) [67]		0.36[3] (6:4) [23]				

API	Polymer						
	PVP	PVAc	COP	SOL	PEG	PMMA	HPMC
Indomethacin (2)	0.27[1] (K12) [67] 0.30[3] (K12) [22] 0.31[4] (K17) [53] 0.31[4] (K25) [68] 0.31[4] (K30) [68] 0.31[4] (K90) [68] 0.33[4] (K12) [68] 0.39[3] (K30) [68] 0.40[3] (K12) [68] 0.40[3] (K90) [68] 0.41[3] (K25) [68] 0.41[5] (K29/32) [25] 0.43[2] (K12, K15) [19–21] 0.43[2] (K25) [46] 0.54[1] (K12) [51] 0.54[3] (K12) [51]		0.06[2] (7:3) [53] 0.19[3] (7:3) [53] 0.22[4] (7:3) [53] 0.35[1] (7:3) [53] 0.21[2] (3:7) [46]				
Itraconazole	0.09[5] (K30) [24]		0.00[2] (6:4) [21] 0.00[3] (6:4) [23]	0.00[2] [21] 0.00[3] [23]	0.00[1] (6000) [62]	0.08[5] (E100) [24] 0.13[5] (L100) [24]	
Ketoconazole	0.01[4] (K12) [27] 0.01[4] (K29/32) [27] 0.01[4] (K90) [27]						0.00[2] [70]

API	Polymer						
	PVP	PVAc	COP	SOL	PEG	PMMA	HPMC
Lacidipine	0.00[1] (K12) [67] 0.00[1] (K30) [67]	0.00[1] [67]	0.00[1] (6:4) [67]		0.05[1] (8000) [67] 0.22[1] (10000) [67]		
Loratadine			0.00[3] (6:4)	0.00[3]			
Mannitol	0.00[2] (K12, K15) [19–21]						
Naproxen	0.06[4] (K12) [17] 0.06[4] (K25) [17] 0.06[4] (K90) [17] 0.31[2] (K25) [21,47] 0.31[2] (K25) [47,55] 0.36[2] (K25) [46]	0.01[2] [46]	0.19[2] (6:4) [46] 0.21[2] (6:4) [47,55] 0.25[3] (6:4) 0.28[2] (6:4) [21,47] 0.07[2] (3:7) [46]	0.32[3]			0.03[2] (AS) [55]
Nifedipine	0.05[4] (K12) [27] 0.05[4] (K29/32) [27] 0.05[4] (K90) [27] 0.06[4] (K29/32) [39] 0.07[4] (K12) [39] 0.21[2] (K12) [19–21]	0.00[2] [20,21]	0.12[2] (6:4) [19–21] 0.19[3] (6:4) [23]	0.05[1] [71] 0.23[3] [23]			
Posaconazole			0.00[3] (6:4)	0.00[3]			
Praziquantel			0.00[3] (6:4)	0.00[3]			
Probucol			0.14[3] (6:4)	0.13[3]			
Ritonavir (1)	0.26[1] (K12) [51]		0.03[3] (6:4)	0.00[3]			

API	Polymer						
	PVP	**PVAc**	**COP**	**SOL**	**PEG**	**PMMA**	**HPMC**
Ritonavir (2)				0.00[1] [51]			
Sucrose	0.02[4] (K12) [27] 0.02[4] (K29/32) [27] 0.02[4] (K90) [27]				0.00[1] (6000) [41]		
Sulfadiazine	0.00[2] (K17) [72]			0.00[2] [72]			
Sulfadimidine	0.18[2] (K17) [21,72]			0.00[2] [21,72]	0.12[2] (35000) [44]		
Sulfamerazine	0.11[2] (K17) [21,72]			0.00[2] [72]			
Sulfamethoxazole				0.13[1] [71]			
Sulfathiazole	0.27[2] (K17) [21,72]			0.07[2] [21,72]	0.22[2] (35000) [44]		
Tadalafil			0.25[3] (6:4) [13]				
Telmisartan	0.00[2] (K25) [73]		0.00[3] (6:4)	0.00[2] [73]		0.00[2] (E100) [73]	0.00[2] (E5) [73]
Temazepam	0.00[1] (K30) [74]				0.03[1] (6000) [74]		
Verapamil-HCl			0.00[3] (6:4)				

4.8 Conclusion

We compiled data available in literature on API solubility in polymers. The final data set comprises seven polymers (PVP, PVAc, COP, SOL, PEG, PMMA and HPMC), 37 APIs and two sugar derivatives in total. It also includes our own so far unpublished data set which was found to be consistent with previously published data. The majority of studies used the melting point depression method, dissolution endpoint measurements, indirect solubility determination by T_g or low molecular weight analogues. It appears that the resulting API solubility depended not only on the method used, but rather more on the working group and authors who conducted the measurements. The API solubility measurement itself is prone to bias due to difficulties in reaching the equilibrated state of a system prior any solubility determination. Hence, working group-specific analytical methods, once inadequately chosen, seemed to be maintained. Furthermore, no simple relation between API solubility and the molecular weight of PVP was observed. PVP always exhibited the highest API solubility, whereas APIs showed the poorest solubility in PVAc. This is underlined by the findings for COP, a copolymer of PVP and PVAc. Here, the API solubility changes as a function of the PVP/PVAc ratio. Only a limited number of publications were found for PEG, PMMA and HPMC and therefore no statement considering these polymers can be made. In conclusion, a comparison of the available data set and models in literature on the API solubility prediction in polymeric matrices has been made. Using the example of COP we have shown that the data now available may be utilized in developing fast computational models to predict the solubility in polymers. In summary, this data review should assist researchers in choosing a prediction method suited for their studies and the data set presented here should facilitate training newly developed solubility prediction models.

4.9 Acknowledgement

The authors would like to thank Rachel C. Evans greatly for reviewing the manuscript. During the conduction of this research, Andreas Gryczke was employed by BASF SE (Ludwigshafen am Rhein, 67063, Germany). This research did not receive any specific grant from funding agencies in the public, commercial, or not-for-profit sectors.

4.10 References

[1] H. Liu, L.S. Taylor, K.J. Edgar, The role of polymers in oral bioavailability enhancement; a review, Polymer. (2015). doi:10.1016/j.polymer.2015.09.026.

[2] Y. He, C. Ho, Amorphous Solid Dispersions: Utilization and Challenges in Drug Discovery and Development, J. Pharm. Sci. 104 (2015) 3237–3258. doi:10.1002/jps.24541.

[3] S. Janssens, G. Van den Mooter, Review: physical chemistry of solid dispersions, J. Pharm. Pharmacol. 61 (2009) 1571–1586. doi:10.1211/jpp/61.12.0001.

[4] N. Ogawa, T. Hiramatsu, R. Suzuki, R. Okamoto, K. Shibagaki, K. Fujita, C. Takahashi, Y. Kawashima, H. Yamamoto, Improvement in the water solubility of drugs with a solid dispersion system by spray drying and hot-melt extrusion with using the amphiphilic polyvinyl caprolactam-polyvinyl acetate-polyethylene glycol graft copolymer and d -mannitol, Eur. J. Pharm. Sci. 111 (2018) 205–214. doi:10.1016/j.ejps.2017.09.014.

[5] J.A. Baird, L.S. Taylor, Evaluation of amorphous solid dispersion properties using thermal analysis techniques, Adv. Drug Deliv. Rev. 64 (2012) 396–421. doi:10.1016/j.addr.2011.07.009.

[6] B.C. Hancock, M. Parks, What is the true solubility advantage for amorphous pharmaceuticals?, Pharm. Res. 17 (2000) 397–404.

[7] S.B. Murdande, M.J. Pikal, R.M. Shanker, R.H. Bogner, Solubility Advantage of Amorphous Pharmaceuticals: II. Application of Quantitative Thermodynamic Relationships for Prediction of Solubility Enhancement in Structurally Diverse Insoluble Pharmaceuticals, Pharm. Res. 27 (2010) 2704–2714. doi:10.1007/s11095-010-0269-5.

[8] S. Huang, C. Mao, R.O. Williams, C.-Y. Yang, Solubility Advantage (and Disadvantage) of Pharmaceutical Amorphous Solid Dispersions, J. Pharm. Sci. 105 (2016) 3549–3561. doi:10.1016/j.xphs.2016.08.017.

[9] S. Baghel, H. Cathcart, N.J. O'Reilly, Polymeric Amorphous Solid Dispersions: A Review of Amorphization, Crystallization, Stabilization, Solid-State Characterization, and Aqueous Solubilization of Biopharmaceutical Classification System Class II Drugs, J. Pharm. Sci. 105 (2016) 2527–2544. doi:10.1016/j.xphs.2015.10.008.

[10] J. Gupta, C. Nunes, S. Vyas, S. Jonnalagadda, Prediction of Solubility Parameters and Miscibility of Pharmaceutical Compounds by Molecular Dynamics Simulations, J. Phys. Chem. B. 115 (2011) 2014–2023. doi:10.1021/jp108540n.

[11] M. Vasanthavada, W.-Q. (Tony) Tong, Y. Joshi, M.S. Kislalioglu, Phase Behavior of Amorphous Molecular Dispersions II: Role of Hydrogen Bonding in Solid Solubility and Phase Separation Kinetics, Pharm. Res. 22 (2005) 440–448. doi:10.1007/s11095-004-1882-y.

[12] F. Qian, J. Huang, M.A. Hussain, Drug-polymer solubility and miscibility: Stability consideration and practical challenges in amorphous solid dispersion development, J. Pharm. Sci. (2010) n/a-n/a. doi:10.1002/jps.22074.

[13] K. Wlodarski, W. Sawicki, A. Kozyra, L. Tajber, Physical stability of solid dispersions with respect to thermodynamic solubility of tadalafil in PVP-VA, Eur. J. Pharm. Biopharm. 96 (2015) 237–246. doi:10.1016/j.ejpb.2015.07.026.

[14] P. Piccinni, Y. Tian, A. McNaughton, J. Fraser, S. Brown, D.S. Jones, S. Li, G.P. Andrews, Solubility parameter-based screening methods for early-stage formulation development of itraconazole amorphous solid dispersions, J. Pharm. Pharmacol. 68 (2016) 705–720. doi:10.1111/jphp.12491.

[15] F. Meng, V. Dave, H. Chauhan, Qualitative and quantitative methods to determine miscibility in amorphous drug–polymer systems, Eur. J. Pharm. Sci. 77 (2015) 106–111. doi:10.1016/j.ejps.2015.05.018.

[16] B. Tian, X. Wang, Y. Zhang, K. Zhang, Y. Zhang, X. Tang, Theoretical Prediction of a Phase Diagram for Solid Dispersions, Pharm. Res. (2014). doi:10.1007/s11095-014-1500-6.

[17] A. Paudel, J. Van Humbeeck, G. Van den Mooter, Theoretical and Experimental Investigation on the Solid Solubility and Miscibility of Naproxen in Poly(vinylpyrrolidone), Mol. Pharm. 7 (2010) 1133–1148. doi:10.1021/mp100013p.

[18] Y. Zhao, P. Inbar, H.P. Chokshi, A.W. Malick, D.S. Choi, Prediction of the thermal phase diagram of amorphous solid dispersions by flory-huggins theory, J. Pharm. Sci. 100 (2011) 3196–3207. doi:10.1002/jps.22541.

[19] J. Tao, Y. Sun, G.G.Z. Zhang, L. Yu, Solubility of Small-Molecule Crystals in Polymers: d-Mannitol in PVP, Indomethacin in PVP/VA, and Nifedipine in PVP/VA, Pharm. Res. 26 (2009) 855–864. doi:10.1007/s11095-008-9784-z.

[20] Y. Sun, J. Tao, G.G.Z. Zhang, L. Yu, Solubilities of crystalline drugs in polymers: An improved analytical method and comparison of solubilities of indomethacin and nifedipine in PVP, PVP/VA, and PVAc, J. Pharm. Sci. (2010) n/a-n/a. doi:10.1002/jps.22251.

[21] S.O. Kyerematen, M. Pudlas, G.H. Woehrle, A Fast and Reliable Empirical Approach for Estimating Solubility of Crystalline Drugs in Polymers for Hot Melt Extrusion Formulations, J. Pharm. Sci. 103 (2014) 2847–2858. doi:10.1002/jps.23941.

[22] A. Mahieu, J.-F. Willart, E. Dudognon, F. Danède, M. Descamps, A New Protocol To Determine the Solubility of Drugs into Polymer Matrixes, Mol. Pharm. 10 (2013) 560–566. doi:10.1021/mp3002254.

[23] E.S. Bochmann, D. Neumann, A. Gryczke, K.G. Wagner, Micro-scale prediction method for API-solubility in polymeric matrices and process model for forming amorphous solid dispersion by hot-melt extrusion, Eur. J. Pharm. Biopharm. 107 (2016) 40–48. doi:10.1016/j.ejpb.2016.06.015.

[24] R.A. Bellantone, P. Patel, H. Sandhu, D.S. Choi, D. Singhal, H. Chokshi, A.W. Malick, N. Shah, A method to predict the equilibrium solubility of drugs in solid polymers near room temperature using thermal analysis, J. Pharm. Sci. 101 (2012) 4549–4558. doi:10.1002/jps.23319.

[25] J. Alin, N. Setiawan, M. Defrese, J. DiNunzio, H. Lau, L. Lupton, H. Xi, Y. Su, H. Nie, N. Hesse, L.S. Taylor, P.J. Marsac, A novel approach for measuring room temperature enthalpy of mixing and associated solubility estimation of a drug in a polymer matrix, Polymer. 135 (2018) 50–60. doi:10.1016/j.polymer.2017.11.056.

[26] Z. Yang, K. Nollenberger, J. Albers, S. Qi, Molecular Implications of Drug–Polymer Solubility in Understanding the Destabilization of Solid Dispersions by Milling, Mol. Pharm. 11 (2014) 2453–2465. doi:10.1021/mp500205c.

[27] P.J. Marsac, T. Li, L.S. Taylor, Estimation of Drug–Polymer Miscibility and Solubility in Amorphous Solid Dispersions Using Experimentally Determined Interaction Parameters, Pharm. Res. 26 (2009) 139–151. doi:10.1007/s11095-008-9721-1.

[28] P.J. Marsac, H. Konno, L.S. Taylor, A Comparison of the Physical Stability of Amorphous Felodipine and Nifedipine Systems, Pharm. Res. 23 (2006) 2306–2316. doi:10.1007/s11095-006-9047-9.

[29] S. Kim, P.A. Thiessen, E.E. Bolton, J. Chen, G. Fu, A. Gindulyte, L. Han, J. He, S. He, B.A. Shoemaker, J. Wang, B. Yu, J. Zhang, S.H. Bryant, PubChem Substance

and Compound databases, Nucleic Acids Res. 44 (2016) D1202–D1213. doi:10.1093/nar/gkv951.

[30] W. Brostow, R. Chiu, I.M. Kalogeras, A. Vassilikou-Dova, Prediction of glass transition temperatures: Binary blends and copolymers, Mater. Lett. 62 (2008) 3152–3155. doi:10.1016/j.matlet.2008.02.008.

[31] P.R. Couchman, F.E. Karasz, A classical thermodynamic discussion of the effect of composition on glass-transition temperatures, Macromolecules. 11 (1978) 117–119.

[32] R Core Team, R: A Language and Environment for Statistical Computing, R Foundation for Statistical Computing, Vienna, Austria, 2018. https://www.R-project.org/.

[33] Molecular Operating Environment (MOE), Chemical Computing Group ULC, 1010 Sherbooke St. West, Suite #910, Montreal, QC, Canada, H3A 2R7, 2018.

[34] J. Friedman, T. Hastie, R. Tibshirani, Regularization Paths for Generalized Linear Models via Coordinate Descent, J. Stat. Softw. 33 (2010) 1–22.

[35] T. Helleputte, LiblineaR: Linear Predictive Models Based on the LIBLINEAR C/C++ Library, 2017.

[36] R.-E. Fan, K.-W. Chang, C.-J. Hsieh, X.-R. Wang, C.-J. Lin, LIBLINEAR: A Library for Large Linear Classification, J Mach Learn Res. 9 (2008) 1871–1874.

[37] M.K.C. from J. Wing, S. Weston, A. Williams, C. Keefer, A. Engelhardt, T. Cooper, Z. Mayer, B. Kenkel, the R.C. Team, M. Benesty, R. Lescarbeau, A. Ziem, L. Scrucca, Y. Tang, C. Candan, T. Hunt, caret: Classification and Regression Training, 2018. https://CRAN.R-project.org/package=caret.

[38] I. Guyon, J. Weston, S. Barnhill, V. Vapnik, Gene Selection for Cancer Classification using Support Vector Machines, Mach. Learn. 46 (2002) 389–422. doi:10.1023/A:1012487302797.

[39] P.J. Marsac, S.L. Shamblin, L.S. Taylor, Theoretical and Practical Approaches for Prediction of Drug–Polymer Miscibility and Solubility, Pharm. Res. 23 (2006) 2417–2426. doi:10.1007/s11095-006-9063-9.

[40] P.J. Flory, Principles of polymer chemistry, 19. print, Cornell Univ. Press, Ithaca, NY, 2006.

[41] S. Thakral, N.K. Thakral, Prediction of drug-polymer miscibility through the use of solubility parameter based flory-huggins interaction parameter and the experimental

validation: PEG as model polymer, J. Pharm. Sci. 102 (2013) 2254–2263. doi:10.1002/jps.23583.

[42] J. Djuris, I. Nikolakakis, S. Ibric, Z. Djuric, K. Kachrimanis, Preparation of carbamazepine–Soluplus® solid dispersions by hot-melt extrusion, and prediction of drug–polymer miscibility by thermodynamic model fitting, Eur. J. Pharm. Biopharm. 84 (2013) 228–237. doi:10.1016/j.ejpb.2012.12.018.

[43] C. Donnelly, Y. Tian, C. Potter, D.S. Jones, G.P. Andrews, Probing the Effects of Experimental Conditions on the Character of Drug-Polymer Phase Diagrams Constructed Using Flory-Huggins Theory, Pharm. Res. 32 (2015) 167–179. doi:10.1007/s11095-014-1453-9.

[44] A. Prudic, Y. Ji, G. Sadowski, Thermodynamic Phase Behavior of API/Polymer Solid Dispersions, Mol. Pharm. 11 (2014) 2294–2304. doi:10.1021/mp400729x.

[45] M. Yang, P. Wang, H. Suwardie, C. Gogos, Determination of acetaminophen's solubility in poly(ethylene oxide) by rheological, thermal and microscopic methods, Int. J. Pharm. 403 (2011) 83–89. doi:10.1016/j.ijpharm.2010.10.026.

[46] A. Prudic, T. Kleetz, M. Korf, Y. Ji, G. Sadowski, Influence of Copolymer Composition on the Phase Behavior of Solid Dispersions, Mol. Pharm. 11 (2014) 4189–4198. doi:10.1021/mp500412d.

[47] K. Lehmkemper, S.O. Kyerematen, O. Heinzerling, M. Degenhardt, G. Sadowski, Long-Term Physical Stability of PVP- and PVPVA-Amorphous Solid Dispersions, Mol. Pharm. 14 (2017) 157–171. doi:10.1021/acs.molpharmaceut.6b00763.

[48] C. Luebbert, F. Huxoll, G. Sadowski, Amorphous-Amorphous Phase Separation in API/Polymer Formulations, Molecules. 22 (2017) 296. doi:10.3390/molecules22020296.

[49] M. Gordon, J.S. Taylor, Ideal Copolymers and the second-order transitions of synthetic rubbers. I. Non-crystalline Copolymers, J. Appl. Chem. 2, September 1952 (1952).

[50] M.B. Rask, M.M. Knopp, N.E. Olesen, R. Holm, T. Rades, Influence of PVP/VA copolymer composition on drug–polymer solubility, Eur. J. Pharm. Sci. 85 (2016) 10–17. doi:10.1016/j.ejps.2016.01.026.

[51] M.B. Rask, M.M. Knopp, N.E. Olesen, R. Holm, T. Rades, Comparison of two DSC-based methods to predict drug-polymer solubility, Int. J. Pharm. 540 (2018) 98–105. doi:10.1016/j.ijpharm.2018.02.002.

[52] C. Luebbert, G. Sadowski, Moisture-induced phase separation and recrystallization in amorphous solid dispersions, Int. J. Pharm. 532 (2017) 635–646. doi:10.1016/j.ijpharm.2017.08.121.

[53] M.M. Knopp, L. Tajber, Y. Tian, N.E. Olesen, D.S. Jones, A. Kozyra, K. Löbmann, K. Paluch, C.M. Brennan, R. Holm, A.M. Healy, G.P. Andrews, T. Rades, Comparative Study of Different Methods for the Prediction of Drug–Polymer Solubility, Mol. Pharm. 12 (2015) 3408–3419. doi:10.1021/acs.molpharmaceut.5b00423.

[54] M.M. Knopp, N. Gannon, I. Porsch, M.B. Rask, N.E. Olesen, P. Langguth, R. Holm, T. Rades, A Promising New Method to Estimate Drug-Polymer Solubility at Room Temperature, J. Pharm. Sci. 105 (2016) 2621–2624. doi:10.1016/j.xphs.2016.02.017.

[55] K. Lehmkemper, S.O. Kyerematen, O. Heinzerling, M. Degenhardt, G. Sadowski, Impact of Polymer Type and Relative Humidity on the Long-Term Physical Stability of Amorphous Solid Dispersions, Mol. Pharm. 14 (2017) 4374–4386. doi:10.1021/acs.molpharmaceut.7b00492.

[56] K. Kothari, V. Ragoonanan, R. Suryanarayanan, The Role of Drug–Polymer Hydrogen Bonding Interactions on the Molecular Mobility and Physical Stability of Nifedipine Solid Dispersions, Mol. Pharm. 12 (2015) 162–170. doi:10.1021/mp5005146.

[57] T. Matsumoto, G. Zografi, Physical Properties of Solid Molecular Dispersions of Indemethacin with Poly(vinylpyrrolidone) and Poly(vinylpyrrolidone-co-vinylacetate) in Relation to Indomethacin Crystallization, Pharm. Res. 16 (1999) 1722–1728.

[58] K. Bansal, U.S. Baghel, S. Thakral, Construction and Validation of Binary Phase Diagram for Amorphous Solid Dispersion Using Flory–Huggins Theory, AAPS PharmSciTech. (2015). doi:10.1208/s12249-015-0343-8.

[59] S. Hengsawas Surasarang, J.M. Keen, S. Huang, F. Zhang, J.W. McGinity, R.O. Williams, Hot melt extrusion versus spray drying: hot melt extrusion degrades albendazole, Drug Dev. Ind. Pharm. 43 (2017) 797–811. doi:10.1080/03639045.2016.1220577.

[60] M.B. Rask, M.M. Knopp, N.E. Olesen, R. Holm, T. Rades, Influence of PVP/VA copolymer composition on drug–polymer solubility, Eur. J. Pharm. Sci. 85 (2016) 10–17. doi:10.1016/j.ejps.2016.01.026.

[61] S. Verma, V.S. Rudraraju, A Systematic Approach to Design and Prepare Solid Dispersions of Poorly Water-Soluble Drug, AAPS PharmSciTech. 15 (2014) 641–657. doi:10.1208/s12249-014-0093-z.

[62] S. Baghel, H. Cathcart, N.J. O'Reilly, Theoretical and experimental investigation of drug-polymer interaction and miscibility and its impact on drug supersaturation in aqueous medium, Eur. J. Pharm. Biopharm. 107 (2016) 16–31. doi:10.1016/j.ejpb.2016.06.024.

[63] F. Meng, A. Trivino, D. Prasad, H. Chauhan, Investigation and correlation of drug polymer miscibility and molecular interactions by various approaches for the preparation of amorphous solid dispersions, Eur. J. Pharm. Sci. 71 (2015) 12–24. doi:10.1016/j.ejps.2015.02.003.

[64] Y. Tian, D.S. Jones, G.P. Andrews, An Investigation into the Role of Polymeric Carriers on Crystal Growth within Amorphous Solid Dispersion Systems, Mol. Pharm. 12 (2015) 1180–1192. doi:10.1021/mp500702s.

[65] C. Luebbert, G. Sadowski, Moisture-induced phase separation and recrystallization in amorphous solid dispersions, Int. J. Pharm. 532 (2017) 635–646. doi:10.1016/j.ijpharm.2017.08.121.

[66] S. Li, Y. Tian, D.S. Jones, G.P. Andrews, Optimising Drug Solubilisation in Amorphous Polymer Dispersions: Rational Selection of Hot-melt Extrusion Processing Parameters, AAPS PharmSciTech. 17 (2016) 200–213. doi:10.1208/s12249-015-0450-6.

[67] A. Forster, J. Hempenstall, I. Tucker, T. Rades, Selection of excipients for melt extrusion with two poorly water-soluble drugs by solubility parameter calculation and thermal analysis, Int. J. Pharm. 226 (2001) 147–161.

[68] M.M. Knopp, N.E. Olesen, P. Holm, P. Langguth, R. Holm, T. Rades, Influence of Polymer Molecular Weight on Drug-Polymer Solubility: A Comparison between Experimentally Determined Solubility in PVP and Prediction Derived from Solubility in Monomer, J. Pharm. Sci. 104 (2015) 2905–2912. doi:10.1002/jps.24410.

[69] X. Wang, A. Michoel, G. Van den Mooter, Study of the phase behavior of polyethylene glycol 6000–itraconazole solid dispersions using DSC, Int. J. Pharm. 272 (2004) 181–187. doi:10.1016/j.ijpharm.2003.11.026.

[70] Y. Chen, S. Wang, S. Wang, C. Liu, C. Su, M. Hageman, M. Hussain, R. Haskell, K. Stefanski, F. Qian, Initial Drug Dissolution from Amorphous Solid Dispersions Controlled by Polymer Dissolution and Drug-Polymer Interaction, Pharm. Res. 33 (2016) 2445–2458. doi:10.1007/s11095-016-1969-2.
[71] M.A. Altamimi, S.H. Neau, Use of the Flory–Huggins theory to predict the solubility of nifedipine and sulfamethoxazole in the triblock, graft copolymer Soluplus, Drug Dev. Ind. Pharm. 42 (2016) 446–455. doi:10.3109/03639045.2015.1075033.
[72] V. Caron, Y. Hu, L. Tajber, A. Erxleben, O.I. Corrigan, P. McArdle, A.M. Healy, Amorphous Solid Dispersions of Sulfonamide/Soluplus® and Sulfonamide/PVP Prepared by Ball Milling, AAPS PharmSciTech. 14 (2013) 464–474. doi:10.1208/s12249-013-9931-7.
[73] R. Dukeck, P. Sieger, P. Karmwar, Investigation and correlation of physical stability, dissolution behaviour and interaction parameter of amorphous solid dispersions of telmisartan: A drug development perspective, Eur. J. Pharm. Sci. 49 (2013) 723–731. doi:10.1016/j.ejps.2013.05.003.
[74] G. Van den Mooter, P. Augustijns, N. Blaton, R. Kinget, Physico-chemical characterization of solid dispersions of temazepam with polyethylene glycol 6000 and PVP K30, Int. J. Pharm. 164 (1998) 67–80.

4.11 Appendix A: Empirical model of solubility in COP

A.1. Data used

To predict if the solubility at 100°C is at least 0.2 (w/w), we used R, a freely available language and environment for statistical computing and graphics [1]. Molecular descriptors of the compounds in Table 1 were computed with MOE [2]. These data were imported into our program using ChemmineR [3] and enriched with data from our experiments as well as those found in the PubChem database [4].

A.2. Initial model building using LASSO

To obtain an initial estimate of the number of descriptors necessary to separate soluble and insoluble compounds, we performed regularized logistic regression using the package glmnet [5]. We used the LASSO regularization, which basically adds a penalty

term |β1| to the log likelihood function used in regular logistic regression. Simply put, LASSO sets the coefficients of features that contribute most to the error of the model to zero. Thus, LASSO regression may be used for feature selection.

A.3. Optimal number of features

Then, to obtain an estimate of the error for new (unseen) data as a function of the number of features employed we performed nested leave-one out crossvalidation (LOOCV). The outer loop was used to predict the binary outcome (soluble at 100 °C: yes/no), while the inner loop was used to train the hyperparameter of the regularized logistic regression model. Prior to training a model, the features were standardized such that the mean and standard deviation of all features in the training set were zero and one, respectively. The features of the left-out compound were standardized using the values of the training set. Regularized regression modelling was performed using the LiblineaR package [6]. Balanced accuracy was used for the selection of the hyperparameter and to assess the predictive accuracy and was computed using the package caret [7].

By leaving out one compound, a first model was trained using the 146 features for the remaining 20 compounds (outer loop). The optimal value for the hyperparameter of this model was identified by leave-one out crossvalidation and a given sequence of values for the hyperparameter (inner loop). The solubility of the left-out compound was predicted, and the result was stored for later use. The least-ranking feature was removed, and the process was repeated until only a single feature remained (recursive feature elimination). The whole process was performed for each compound in turn.

By plotting the predictive accuracy as a function of the number of features used we may estimate the optimal number of features. We restricted the plot to the number of features selected by the LASSO approach and observed the predictive accuracy leveling off when using 8 features.

A.4. Final feature selection

The final set of 8 features was selected by recursive feature elimination as above. However, all compounds were used for building the nested models.

A.5. References

[1] R Core Team, R: A Language and Environment for Statistical Computing, R Foundation for Statistical Computing, Vienna, Austria, 2018. https://www.R-project.org/.

[2] Molecular Operating Environment (MOE), Chemical Computing Group ULC, 1010 Sherbooke St. West, Suite #910, Montreal, QC, Canada, H3A 2R7, 2018.

[3] Y. Cao, A. Charisi, L.-C. Cheng, T. Jiang, T. Girke, ChemmineR: a compound mining framework for R, Bioinformatics. 24 (2008) 1733–1734. doi:10.1093/bioinformatics/btn307.

[4] S. Kim, P.A. Thiessen, E.E. Bolton, J. Chen, G. Fu, A. Gindulyte, L. Han, J. He, S. He, B.A. Shoemaker, J. Wang, B. Yu, J. Zhang, S.H. Bryant, PubChem Substance and Compound databases, Nucleic Acids Res. 44 (2016) D1202–D1213. doi:10.1093/nar/gkv951.

[5] J. Friedman, T. Hastie, R. Tibshirani, Regularization Paths for Generalized Linear Models via Coordinate Descent, J. Stat. Softw. 33 (2010) 1–22.

[6] T. Helleputte, LiblineaR: Linear Predictive Models Based on the LIBLINEAR C/C++ Library, 2017.

[7] M.K.C. from J. Wing, S. Weston, A. Williams, C. Keefer, A. Engelhardt, T. Cooper, Z. Mayer, B. Kenkel, the R.C. Team, M. Benesty, R. Lescarbeau, A. Ziem, L. Scrucca, Y. Tang, C. Candan, T. Hunt, caret: Classification and Regression Training, 2018. https://CRAN.R-project.org/package=caret.

4.12 Appendix B: detailed compilation of physicochemical characteristics of APIs and sugar derivates under investigation

API	MW [g/mol]	Tm [°C]	H(fus) [J/g]	Tg [°C]	ΔCp at Tg [J/(g*K)]	Tm/Tg [-]	True density (g/cm^3)
Aceclofenac	354,2	149,3	144,3	15,0	-	10,0	1,5
Acetaminophen	151,2	170,5	193,5	23,3	0,6	7,3	1,2
Albendazole	265,3	197,7	145,57	61,2	0,2	3,2	1,4
Bisacodyl	361,4	133,6	101,35	16,1	0,4	8,3	1,3
Carbamazepine	236,3	175,1	43,4	52,7	0,4	3,3	1,3
		190,2	92,4			3,6	
Celecoxib	381,4	160,9	95,8	56,8	0,4	2,8	1,5
Chloramphenicol	323,1	150,0	92,91	29,5	0,5	5,1	1,5
Cilostazol	369,5	158,6	124,9	31,2	0,5	5,1	1,3
Cinnarizine	368,5	118,3	102,2	8,6	0,6	13,8	1,1
Clozapine	326,8	182,1	59,7	59,7	0,4	3,1	1,3
Curcumin	368,4	176,0	113,46	69,0	0,5	2,6	0,9
Dipyridamole	504,6	167,1	55,3	38,2	0,7	4,4	1,3
Felodipine	384,3	144,2	78,4	45,0	0,3	3,2	1,4
Gliclazide	323,4	170,5	124,6	39,6	0,5	4,3	1,2
Griseofulvin	352,8	218,3	113,9	88,9	0,3	2,5	1,5
Ibuprofen	206,3	75,3	105,5	-44,4	0,4	-1,7	1,1
Ibuprofen sodium	228,3	200,1	72,24	-	-	-	1,2
Indomethacin	357,8	160,1	87,7	44,4	0,3	3,6	1,4
Itraconazole	705,6	165,8	74,2	57,7	0,4	2,9	1,4
Ketoconazole	531,4	148,1	101,81	42,9	0,3	3,5	1,3
Lacidipine	455,6	182,1	110,3	43,7	-	4,2	-
Lamotrigine	256,1	215,8	136,15	93,3	0,5	2,3	1,6
Loratadine	382,9	134,6	72,1	34,9	0,3	3,9	1,3
Mannitol	182,2	166,1	328,7	12,6	-	13,2	1,5
Naproxen	230,3	156,1	124,4	6,7	0,3	23,3	1,3
Nifedipine	346,3	172,2	98,2	44,3	0,3	3,9	1,4
Posaconazole	700,8	167,7	63,9	59,8	0,4	2,8	1,3
Praziquantel	312,4	138,3	95,2	35,9	0,4	3,9	1,2
Probucol	516,8	126,3	64,6	25,6	0,5	4,9	1,1
Ritonavir	720,9	121,8	90,2	48,6	0,5	2,5	1,3
Sucrose	342,3	189,3	132,8	66,1	0,6	2,9	1,4
Sulfadiazine	250,3	259,9	159,41	not measurable		-	1,5
Sulfadimidine	278,3	196,7	129,35	74,0	0,5	2,7	1,3
Sulfamerazine	264,3	237,1	138,86	62,0	0,8	3,8	1,4
Sulfamethoxazole	253,3	169,9	113,3	15,9	-	10,7	1,4
Sulfathiazole	255,3	201,7	112,42	58,0	0,4	3,5	1,5
Tadalafil	389,4	302,3	120,29	149,9	-	2,0	-
Telmisartan	514,6	268,3	108,7	129,5	0,4	2,1	1,3
Temazepam	300,7	159,4	90,9	66,1	0,3	2,4	-
Verapamil-HCl	491,1	142,3	112,2	55,2	0,5	2,6	1,3

API	molar volume [cm^3/mol]	H-donors [-]	H-acceptors [-]	Ionization potential [eV]	logP [-]	logS [-]
Aceclofenac		2	5			-5,2
Acetaminophen	187,9	2	2	9,50	1,42	-1,6
Albendazole	953,5	2	4	9,87	3,32	-4,1
Bisacodyl	244,0	0	5	10,05	1,86	-5,5
Carbamazepine	314,9	1	1	9,08	4,15	-3,2
Celecoxib	294,2	1	7	7,70	5,30	-4,9
Chloramphenicol	227,60	3	5	7,88	1,82	-2,8
Cilostazol	344,3	1	5	10,70	3,60	-4,1
Cinnarizine	749,8	0	2	8,87	4,98	-5,3
Clozapine	514,8	1	4	10,87	1,48	-3,2
Curcumin		2	6			-4,8
Dipyridamole	887,9	4	12	8,11	0,11	-2,7
Felodipine	347,4	1	5	10,82	4,29	-4,7
Gliclazide	300,0	2	4	9,18	3,43	-3,2
Griseofulvin	13,6	0	6	11,59	2,81	-3,8
Ibuprofen	222,3	1	2	8,55	3,07	-3,5
Ibuprofen sodium		0	2			
Indomethacin	1008,1	1	4	8,31	3,93	-5,2
Itraconazole	697,2	0	9	10,00	5,71	-4,9
Ketoconazole	587,7	0	6	9,93	4,21	-4,8
Lacidipine		1	7			-5,3
Lamotrigine	292,6	2	5	11,14	3,17	-2,7
Loratadine	445,9	0	3	10,00	4,83	-4,5
Mannitol	218,2	6	6	10,21	999,00	0,1
Naproxen	394,1	1	3	7,71	3,04	-3,6
Nifedipine	288,9	1	7	9,06	3,03	-4,3
Posaconazole	703,1	1	11	8,15	4,70	-4,8
Praziquantel	496,6	0	2	8,06	2,41	-2,9
Probucol	477,8	2	4	9,13	9,91	-7,1
Ritonavir	2085,8	4	9	10,00	7,08	-5,8
Sucrose	238,3	8	11	7,89	1,59	0,4
Sulfadiazine	225,0	2	6	10,00	2,59	-2,6
Sulfadimidine	292,0	2	6	10,00	3,21	-3,1
Sulfamerazine		2	6			-2,9
Sulfamethoxazole	217,65	2	6	9,33	3,10	-2,7
Sulfathiazole		2	6			-2,4
Tadalafil	480,5	1	4	7,35	2,09	-3,2
Telmisartan	546,1	1	4	7,95	7,26	-5,2
Temazepam	414,9	1	3	10,50	1,97	-3,8
Verapamil-HCl	571,3	1	6	6,39	5,09	-5,1

API	refractive index [-]	dipole moment [Debye]	Specific references
Aceclofenac			Tm, Tg, ρ, H(fus) [51]
Acetaminophen	1,33	2,7	Tg, ΔCp, ρ, H(fus) [46]; Tm [40]
Albendazole	1,55	9,9	
Bisacodyl	1,85	3,1	
Carbamazepine	1,40	2,9	
Celecoxib	1,45	2,0	
Chloramphenicol	1,57	2,7	Tg, ΔCp, ρ, [46]
Cilostazol	1,28	2,7	
Cinnarizine	1,40	1,2	Tm, H(fus) [16]; Tg, ρ [55]; ΔCp [A. Alhalaweh, A. Alzghoul, D. Mahlin, C.A.S. Bergström, Physical stability of drugs after storage above and below the glass transition temperature: Relationship to glass-forming ability, International Journal of Pharmaceutics. 495 (2015) 312–317. doi:10.1016/j.ijpharm.2015.08.101.]
Clozapine	1,17	2,0	
Curcumin			Tm, Tg, H(fus), ΔCp, ρ [56]
Dipyridamole	1,36	1,7	
Felodipine	1,39	2,7	
Gliclazide	1,41	2,7	
Griseofulvin	99,00	2,7	
Ibuprofen	1,56	2,4	
Ibuprofen sodium			Tm, H(fus),ρ [R. Censi, V. Martena, E. Hoti, L. Malaj, P. Di Martino, Sodium ibuprofen dihydrate and anhydrous: Study of the dehydration and hydration mechanisms, Journal of Thermal Analysis and Calorimetry. 111 (2013) 2009–2018. doi:10.1007/s10973-012-2194-9.]
Indomethacin	1,53	2,7	
Itraconazole	1,32	2,0	
Ketoconazole	1,24	2,7	Tm, H(fus), ρ [27]
Lacidipine			Tm, H(fus), Tg [60]
Lamotrigine	1,41	1,4	
Loratadine	1,34	2,7	
Mannitol	1,29	2,8	Tm, H(fus), Tg [60]
Naproxen	1,61	2,7	
Nifedipine	1,55	2,0	
Posaconazole	1,32	2,0	
Praziquantel	1,27	2,3	
Probucol	1,39	3,9	
Ritonavir	1,48	2,7	
Sucrose	1,24	3,9	Tm, H(fus) [60]; ρ [27]
Sulfadiazine	1,59	1,2	Tm, H(fus), Tg, ΔCp, ρ [65]
Sulfadimidine	1,51	1,2	Tm, H(fus), Tg, ΔCp, ρ [65]
Sulfamerazine			Tm, H(fus), Tg, ΔCp, ρ [65]
Sulfamethoxazole	1,43	1,6	Tm, H(fus), Tg, ρ [64]
Sulfathiazole			Tm, H(fus), Tg, ΔCp, ρ [65]
Tadalafil	1,12	2,7	Tm, Tg [13]; H(fus) [J.-S. Choi, J.-S. Park, Design of PVP/VA S-630 based tadalafil solid dispersion to enhance the dissolution rate, European Journal of Pharmaceutical Sciences. 97 (2017) 269–276. doi:10.1016/j.ejps.2016.11.030.]
Telmisartan	1,65	2,7	
Temazepam	1,28	3,0	Tm, H(fus), Tg [67]; ΔCp [G. Van den Mooter, P. Augustijns, R. Kinget, Stability prediction of amorphous benzodiazepines by calculation of the mean relaxation time constant using the Williams–Watts decay function, European Journal of Pharmaceutics and Biopharmaceutics. 48 (1999) 43–48. doi:10.1016/S0939-6411(99)00013-2.]
Verapamil-HCl	1,22	1,2	

General references	
Molecular weight	PubChem database [S. Kim, P.A. Thiessen, E.E. Bolton, J. Chen, G. Fu, A. Gindulyte, L. Han, J. He, S. He, B.A. Shoemaker, J. Wang, B. Yu, J. Zhang, S.H. Bryant, PubChem Substance and Compound databases, Nucleic Acids Research. 44 (2016) D1202–D1213. doi:10.1093/nar/gkv951.]
H-acceptors	PubChem database [S. Kim, P.A. Thiessen, E.E. Bolton, J. Chen, G. Fu, A. Gindulyte, L. Han, J. He, S. He, B.A. Shoemaker, J. Wang, B. Yu, J. Zhang, S.H. Bryant, PubChem Substance and Compound databases, Nucleic Acids Research. 44 (2016) D1202–D1213. doi:10.1093/nar/gkv951.]
H-donors	PubChem database [S. Kim, P.A. Thiessen, E.E. Bolton, J. Chen, G. Fu, A. Gindulyte, L. Han, J. He, S. He, B.A. Shoemaker, J. Wang, B. Yu, J. Zhang, S.H. Bryant, PubChem Substance and Compound databases, Nucleic Acids Research. 44 (2016) D1202–D1213. doi:10.1093/nar/gkv951.]
Ionization potential	Estimated with MOPAC6
logP	estimated with ObenBabel 2.4.0
logS	Drugbank.ca database, estimated with ALOGPS [D.S. Wishart, Y.D. Feunang, A.C. Guo, E.J. Lo, A. Marcu, J.R. Grant, T. Sajed, D. Johnson, C. Li, Z. Sayeeda, N. Assempour, I. Iynkkaran, Y. Liu, A. Maciejewski, N. Gale, A. Wilson, L. Chin, R. Cummings, D. Le, A. Pon, C. Knox, M. Wilson, DrugBank 5.0: a major update to the DrugBank database for 2018, Nucleic Acids Research. 46 (2018) D1074–D1082. doi:10.1093/nar/gkx1037.]
refractive index	Estimated with method adopted from van Krevelen and Vogel
dipole moment	Estimated with MOPAC6

5 Predicting melt rheology for hot-melt extrusion by means of a simple Tg-measurement

Esther S. Bochmann [1,a]; Elgin E. Üstüner [1,a,b]; Andreas Gryczke [b]; Karl G. Wagner [a]

[1]shared first author

[a] Department of Pharmaceutical Technology and Biopharmaceutics, University of Bonn, Bonn, Germany

[b] Global Technical Marketing Solubilization, BASF SE, Ludwigshafen, Germany

This part was published as

E.S. Bochmann, E.E. Üstüner, A. Gryczke, K.G. Wagner, Predicting melt rheology for hot-melt extrusion by means of a simple T_g-measurement, European Journal of Pharmaceutics and Biopharmaceutics. 119 (2017) 47–55. doi:10.1016/j.ejpb.2017.05.010.

5.1 Graphical abstract

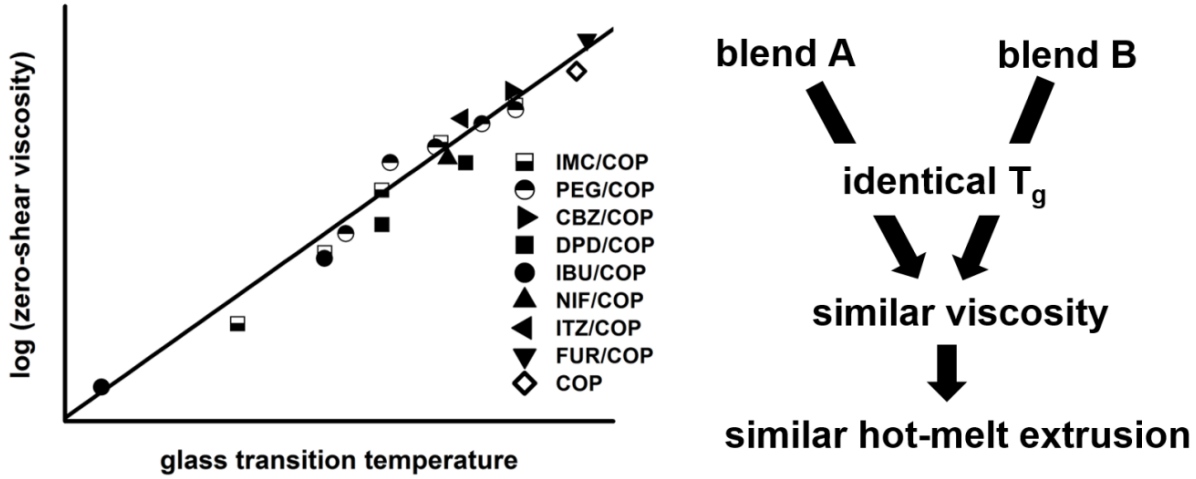

5.2 Abstract

The feasibility of predicting melt rheology by using the glass transition temperature (T_g) of a desired amorphous solid dispersion (ASD) for hot-melt extrusion (HME) and other melt-based processes is presented. Three groups of three different active pharmaceutical ingredients (APIs) or plasticizer/copovidone mixtures, with identical glass transition in rheological testing, were used. Their rheological behavior as a function of temperature and frequency were analyzed by means of small amplitude oscillatory shear (SAOS) on an oscillatory rheometer. The zero-shear viscosity (η_0) identified at 150 °C was compared to T_g, measured by differential scanning calorimetry (DSC) and SAOS. A strong correlation between η_0 and T_g was identified, independent of the API or plasticizer used to achieve T_g of the mixture. To evaluate and rate the discrepancy in η_0 of the different mixtures at same T_g, hot-melt extrusion trials were conducted to measure torque and mean residence time. In this paper, carbamazepine, dipyridamole, indomethacin, ibuprofen, polyethylene glycol (PEG 1500) in vinylpyrrolidone-vinyl acetate copolymer (copovidone) as matrix polymer were used.

5.3 Keywords

Hot-melt extrusion, melt rheology, glass transition temperature, amorphous solid dispersion, small amplitude oscillatory shear, prediction model

5.4 Chemical compounds studied in this article

Carbamazepine (PubChem CID: 2554); Dipyridamole (PubChem CID: 3108); Ibuprofen (PubChem CID: 3672); Indomethacin (PubChem CID: 3715); Nifedipine (PubChem CID: 4485); Itraconazole (PubChem CID: 55283); Furosemide (PubChem CID: 3440)

5.5 Introduction

In recent years, hot-melt extrusion (HME) as a solvent free and rational to scale process has been gaining more and more attention, especially for the production of amorphous solid dispersions (ASDs) to increase bioavailability of poorly soluble active pharmaceutical ingredients (APIs) [1]. Despite the given availability of small scale extruders for early formulation development, the material consumption exceeds usually 10 g per batch for small scale extruders comprising a modular screw design. Often the API is expensive and/or its availability limited. Therefore, microscale tests and simulations to minimize the effort for setting-up extrusion trials close to optimal conditions are required. To identify a suitable matrix polymer for forming a thermodynamically stable ASD with a specific API, various prediction methods to determine the solubility of an API in a polymeric matrix have been reported [2–8]. Concerning the extrusion process itself, simulation software attracts more and more attention to estimate good starting conditions for HME trials but, relies heavily on the availability of viscosity data for the formulation of interest [9–11].

Out of the nature of the process, melt rheology of the material to be extruded is useful [12,13] for process design and control and can even be performed in material sparing micro-scale assays. Melt rheology as an expression of applied shear and resulting viscosity influences the temperature profile along screws, energy input or viscous heat dissipation, torque (motor load) and hence the extrusion performance [1,12,14]. The viscosity of obtained extrudates can be changed by screw speed during extrusion (shear rate variation) [15]. Furthermore, viscosity is an important factor for process control and for the minimization of energy input by screw design, screw speed, through-

put or the addition of plasticizer. In general, plasticizer is not recommended as it increases the drug's mobility in the more flexible polymer matrix. Even more, viscosity is an essential input variable for process simulation. Therefore, rheological testing informs the optimal process parameter set-up for HME [16–18]. By using melt rheology prior to extrusion, the effort associated with process development can be minimized and number of trials needed to achieve the desired condition for extrusion can be reduced. For instance, the easy accessible zero-shear viscosity (η_0), which is indicating the viscosity at finite small shear rates, can be used as a polymer screening tool for HME [19]. However, polymer melts exhibit a shear thinning behavior, therefore the zero-shear viscosity does not reflect the rheological properties in HME processes at higher applied shear rates.

Generally, two different types of rheometric systems are available for polymer melts, capillary or oscillatory rheometers [13]. Capillary rheometers have the advantage that they directly investigate the shear rate range close to that generated in the HME process, but their use is limited. First, they require the use of large amounts of material, on the order of > 10 g per measurement, which is cost prohibitive in the early stages of pharmaceutical product development. In addition, due to force and as such pressure limitations of the capillary rheometer to push the material out of the cylinder through the die, lower temperatures were not feasible. The applicable temperature range of the capillary rheometer was hence smaller compared to small amplitude oscillatory shear (SAOS) measurements [20–22]. Another advantage of SAOS rheology is the far lower material consumption (< 1 g) compared to capillary rheology. Furthermore, SAOS enables a viscoelastic characterization of materials which is important in hot-melt extrusion since a plastic deformation is required to obtain a homogeneous extrusion strand.

Unfortunately, melt rheology is still a time-consuming business and trained personal is needed. A full characterization (e.g. in shear rate- and temperature-dependency) of one melt via SAOS can consume three to five working days.

Regarding the viscosity of ASDs, the dissolved API usually acts as a solid state plasticizer in the API-polymer melt if its glass transition temperature (T_g) is lower than the one of the polymer, decreasing the zero-shear viscosity [20,23–25]. This plasticizing

effect can be characterized easily by a decrease in T_g by means of differential scanning calorimetry (DSC). Of course, different API-polymer blends will achieve different T_g and will end up with different melt viscosity, even when API concentration is constant. The question is, whether other aspects, e.g. shear rate- or temperature-dependency of the polymer melt viscosity, do change if the T_g of the API-polymer blend is similar and only the API (i.e. chemical species) is exchanged? Our hypothesis was that a change in T_g would only cause a "constant" shift in shear rate and temperature dependence of the rheological profile of the pure polymer, independent of the API or plasticizer used, due to the T_g being connected to a specific change in the melt viscosity. Therefore, our hypotheses assume that only the mobility of polymeric chain is influenced by the addition of an API or plasticizer but without changing the polymeric chain architecture in general. If our assumption is true, a simple T_g measurement by DSC would provide the necessary additional information concerning the desired API-polymer melt viscosity, given the general melt behavior of the pure polymer is already known. Confirmation of the validity of our hypothesis would lead to a tremendous ease in HME development, since the only information required for extrusion set-up will be 1) the rheological behavior of the pure polymer and 2) the decrease in T_g by the plasticizing effect of an API or plasticizer, independent of its nature.

The purpose of this work was hence to characterize the influence of PEG 1500 and various APIs on the melt rheological behavior of copovidone and to correlate it with the glass transition temperature of the API-polymer blends used. The variation in viscosity profiles and their potential effect on the HME process is evaluated. Only APIs which are completely soluble in the polymer melt have been considered.

In addition, the authors are aware of specific interactions, such as hydrogen bonding, which will influence the viscosity to an unknown and unpredictable extent [26,27]. However, the prediction of shear viscosity via DSC measurement might be suitable to set-up early HME simulation and extrusion trials, saving costs and time.

5.6 Material and methods

5.6.1 Material

Dipyridamole (DPD) was obtained from Sigma-Aldrich Chemical Co. (St. Louis, MO, USA), Indomethacin (IMC) and PEG 1500 (PEG) were purchased from Alfa Aesar (Karlsruhe, Germany). Vinylpyrrolidone-vinyl acetate copolymer (copovidone, Kollidon® VA64, COP), Carbamazepine (CBZ) and Ibuprofen (IBU) were provided by BASF SE (Ludwigshafen, Germany) (Table 5.1). The APIs were chosen due to their different glass transition temperatures (Table 5.1), high (DPD) or low (IBU, IMC) recrystallization tendencies, high (IMC) or low (CBZ) solubilities in COP, and high (PEG) or low (all API) molecular weights.

Table 5.1 *Physicochemical properties of substances under investigation.*

Substance	Molecular weight [g/mol]	Melting point [°C]	Glass transition temperature [°C]
Indomethacin (IMC)	358	160	44
Carbamazepine (CBZ)	236	175	53
Dipyridamole (DPD)	505	167	38
Ibuprofen (IBU)	206	75	-44
PEG 1500 (PEG)	1,500	47	-42
Copovidone (COP)	45,000 - 70,000	-	107

5.6.2 Methods

5.6.2.1 Preparation of physical mixtures

For DSC trials, a MM400 ball mill from Retsch GmbH (Haan, Germany) with 30 Hz and 3x 5 min milling cycles was used. In the case of rheological trials, a batch mill (Tube Mill control, IKA®-Werke GmbH & Co.KG, Staufen, Germany) with 15000 rpm for 10 sec and additional 5 sec after some minutes was employed, except mixtures containing PEG 1500. Those with PEG 1500 were treated with an agate mortar and pestle instead to ensure homogeneous mixing. For extrusion trials, physical mixtures were

prepared by using a Turbula mixer (Willy A. Bachofen AG – Maschinenfabrik, Muttenz, Swiss) for 10 min at 22 rpm.

5.6.2.2 Defining the API or plasticizer weight fraction by rheological trials

The content of API or plasticizer in its copovidone blend was experimentally adjusted to a specific transition temperature ($T_{g,\ Rheo}$) by means of rheological measurements (temperature sweeps, see below). Due to their $T_{g,\ Rheo}$, three groups consisting of three different blends were defined based on which had similar glass transitions to compare their rheological behavior in further experiments (Table 5.2). In this way, defined weight fractions of API or plasticizer were characterized as soluble in copovidone in our previous work [4].

Table 5.2 *Determined weight fractions of API or PEG/COP mixtures used, adjusted to their T_g in SAOS and corresponding T_g in DSC.*

Mixture	**weight fraction [-]**	**T_g identified by *tan(δ)* [°C]**	**T_g identified by DSC [°C]**
COP	**-**	126	107
	Group 1 ($T_{g,\ Rheo}$: ~124 °C; $T_{g,\ DSC}$: ~102 °C)		
IMC/COP	0.050	123	102
PEG/COP	0.014	125	102
CBZ/COP	0.047	125	103
	Group 2 ($T_{g,\ Rheo}$: ~117 °C; $T_{g,\ DSC}$: ~91 °C)		
IMC/COP	0.200	116	91
PEG/COP	0.040	118	92
DPD/COP	0.325	118	91
	Group 3 ($T_{g,\ Rheo}$: ~104 °C; $T_{g,\ DSC}$: ~80 °C)		
IMC/COP	0.450	103	79
PEG/COP	0.085	104	76
IBU/COP	0.105	104	86

5.6.2.3 Rheometry (SAOS)

An oscillatory rheometer (Haake® MARS® III, Thermo Scientific, Karlsruhe, Germany) equipped with a plate-plate geometry (d = 20 mm) was used. All experiments were

conducted at least three times in controlled deformation AutoStrain mode with a gap height of 0.75 mm. Amplitude sweeps conducted at the beginning verified that an amplitude of 5 % was suitable for all rheological tests.

To compare the results of SAOS with DSC experiments later, a transition temperature ($T_{g,\,Rheo}$) was identified by temperature sweeps with an angular frequency of 6.28 rad/s (1 Hz), where the blend was softened and subsequently cooled down (3 K/min) until the peak of loss factor *tan(δ)* (Eq. (5.1)) was exceeded. This local peak (or maximum) of *tan(δ)* determines the point where the material behaves equally elastic and plastic at same time. Below this point, the elastic properties dominate, whereas above this point the polymer melt act more viscous. The inflection point of *tan(δ)* was identified as $T_{g,\,Rheo}$ (Fig 5.1).

$$tan(\delta) = \frac{G''}{G'} \tag{5.1}$$

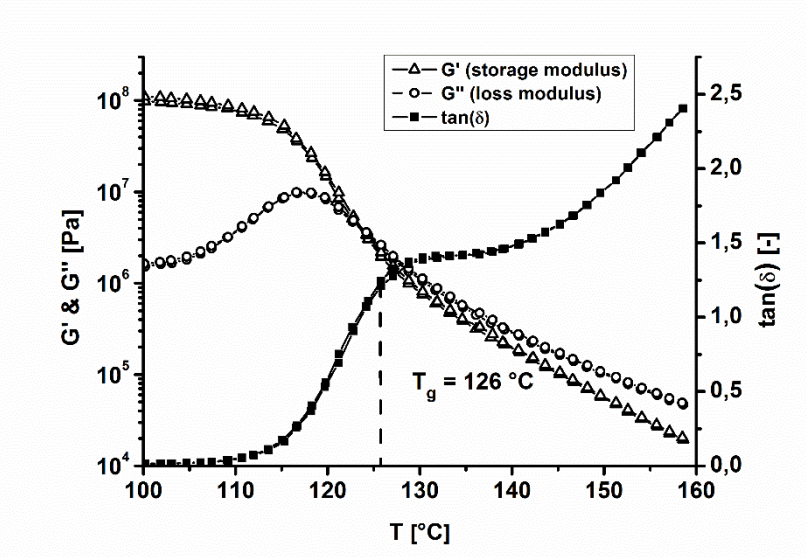

Figure 5.1 *Temperature sweep of copovidone with the local peak of tan(δ) determined as transition temperature as an example.*

Frequency sweeps were conducted from 62.83 rad/s (10 Hz) to 0.63 rad/s (0.1 Hz) in 10 K steps in a suitable temperature range (Fig 5.2a). To identify the temperature range where the specimen was thermorheologically simple during frequency sweeps, the van Gurp-Palmen plot was employed (Fig 5.2b) and identified the application of

time temperature superposition (TTS) as suitable. In TTS, all frequency sweeps were horizontally shifted into one master curve (Fig 5.2c) at a prior set reference temperature.

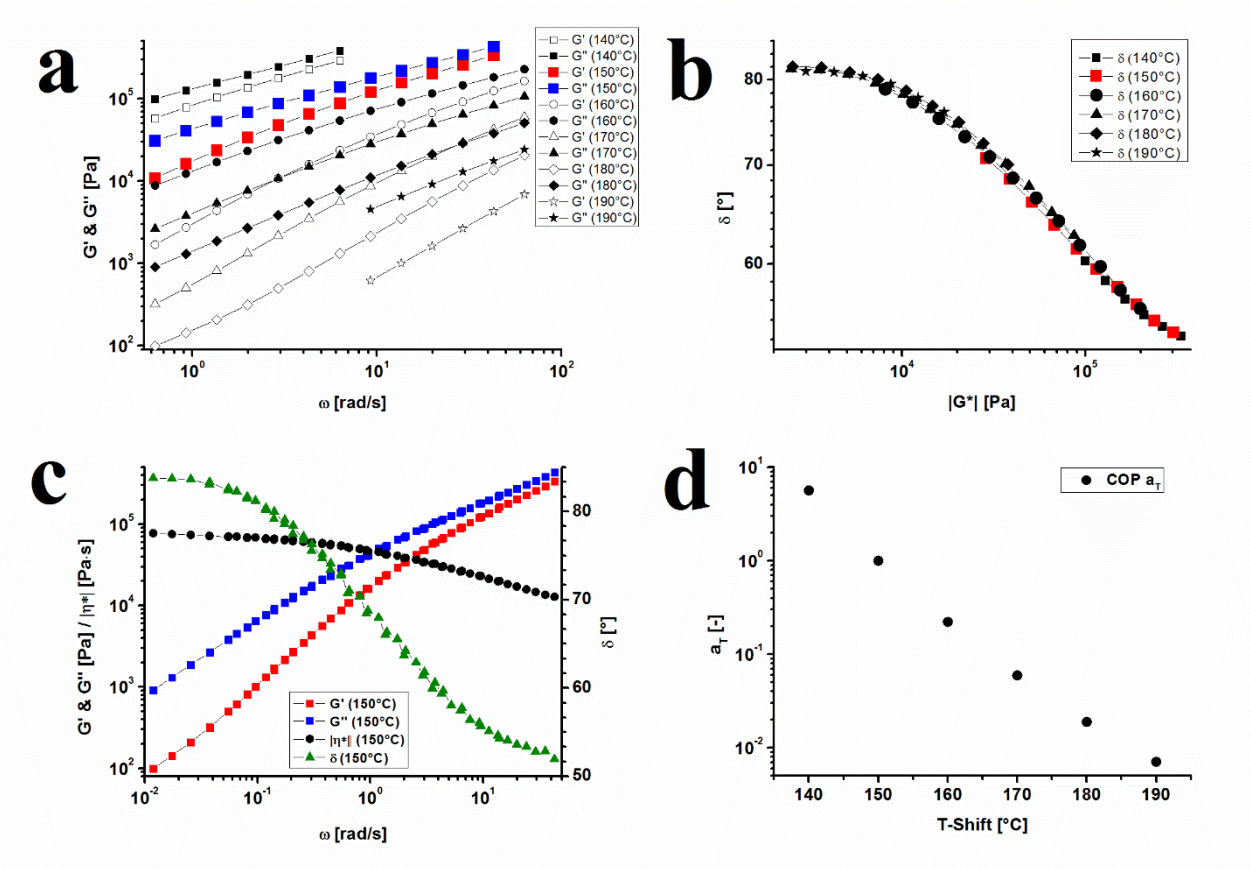

Figure 5.2a-d *Frequency sweeps (a), van Gurp-Palmen plot (b) and resulting master curve (c) with corresponding shift factors a_T (d) of copovidone at 150 °C as an example.*

The viscosity of resulting master curves was fit to the Carreau-Yasuda equation (CY-equation, Eq. (5.2)) [28–31],

$$\eta = \eta_\infty + (\eta_0 - \eta_\infty) \cdot [1 + (\lambda\dot{\gamma})^a]^{(n-1)/a} \tag{5.2}$$

where η_0 and η_∞ are the zero shear and infinite shear viscosity, λ is the characteristic time, n is the Power law index and a is the Yasuda constant. Due to a more accurate curve fitting, η_∞ was set to zero (Eq. (5.3)).

$$\eta = \eta_0 \cdot [1 + (\lambda\dot{\gamma})^a]^{(n-1)/a} \tag{5.3}$$

By applying TTS, shift factors a_T for each frequency sweep in TTS were obtained (Fig 5.2d) and were adapted to Williams-Landel-Ferry fit (WLF-fit, Eq. (5.4)) [28–31],

$$\log(a_T) = \frac{-C_1\,(T-T_0)}{C_2+(T-T_0)} \tag{5.4}$$

where C_1 and C_2 are constants, T is the intended temperature and T_0 is the reference temperature. It describes the temperature dependence of λ (Eq. (5.5)) and η_0 (Eq. (5.6)) of the CY-equation (Eq. (5.2)),

$$a_T = \frac{\eta_T}{\eta_0} \tag{5.5}$$

$$a_T = \frac{\lambda_T}{\lambda_0} \tag{5.6}$$

where subscript T denotes the intended temperature and subscript 0 the reference temperature of the master curve. In conclusion, CY-equation and WLF-fit enable the extrapolation of data by means of angular frequency and temperature within a limited range [32]. All mathematical operations and curve fittings were conducted by using Origin® Pro 8G (OriginLab, Northampton, MA, USA).

In SAOS, unsteady shear conditions are applied, whether the results are comparable to steady shear conditions, e.g. flow through pipes, need be tested. It is assumed, that the viscosity obtained in oscillatory experiments can be converted into a shear-rate-dependent viscosity, this is known as the empirical Cox-Merz rule [33] (general invalid for suspensions, gels and crosslinked materials). In the case of the pure polymer COP, the application of the Cox-Merz rule was tested by high pressure capillary rheometry which identified a similar flow profile as in SAOS (data not shown). Due to upcoming measuring issues (applicable temperature range, plug flow), all other COP-blends were tested in rotation on the rheometer at shear rates up to 10 s^{-1} (data not shown). Due to the viscoelastic properties of the investigated blends, higher shear rates were inapplicable at the rotational rheometer. In the case of pure COP and all COP-blends,

the conducted experiments showed that the Cox-Merz rule could be applied, confirming that tests under unsteady shear conditions are comparable to steady shear conditions.

5.6.2.4 Differential Scanning Calorimetry (DSC)

A DSC 2 (Mettler Toledo, Gießen, Germany) equipped with an auto sampler, nitrogen cooling and nitrogen as purge gas (30 ml/min) was used. The system was calibrated with indium and zinc standards. At least three samples of approximately 5 – 10 mg of each mixture were analyzed, using 40 µl aluminum pans with a pierced lid. Glass transition temperatures ($T_{g,\,DSC}$) and melting temperatures (T_m) were analyzed via heating-cooling-heating cycles of 10 K/min (Tables 5.1 and 5.2).

5.6.2.5 Extrusion trials

For hot-melt extrusion, a co-rotating twin-screw extruder ZE 12 from Three-Tec GmbH (Seon, Switzerland) with a functional length of 25:1 L/D, 12 mm screws, 2 mm die and a maximum torque of 15 N·m was used. The screw configuration consists of 125 mm conveying elements (18 mm and 12 mm pitch), 18 mm kneading element (30°), 18 mm kneading element (60°), 36 mm conveying element (12 mm and 9 mm pitch), 18 mm kneading element (60°), 18 mm kneading element (90°) and 66 mm conveying element (12 mm pitch). The throughput was kept constant at 2.0 g/min and the screw speed was set to 100 rpm to enable a high filling ratio of the extruder. Mean residence times (MRTs) were measured and calculated by using ExtruVis3 of ExtruVis (Riedstadt, Germany). To determine the feed rate during MRT measurements more precisely, the extruded material over a certain time was collected and weighed (Table 5.5). The extrusion temperature was chosen due to the zero-shear viscosity (10,000-1,000 Pa·s) of the blends investigated. This is only a rough estimation of an extrusion temperature set-up to enable the extrusion process by a low viscous melt. Due to the set screw speed and the shear thinning behavior of the blends, an even lower viscosity might be achieved during the extrusion process. The extrusion temperature was defined as 160 °C for T_g-group 1, 150 °C for T_g-group 2 and 140 °C in the case of T_g-group 3 (Tables 5.3 and 5.5).

5.7 Results

5.7.1 Characterization of melt rheological properties

To compare the melt rheological behavior of the API/polymer or plasticizer/polymer blends investigated in this study, the zero-shear viscosity (η_0) obtained by CY-equation at temperatures measured is listed in Table 5.3. An increase in temperature or a reduction in T_g, mixture resulted in the decrease of η_0 values (Fig 5.3a, c and e), whereas a_T seemed to remain constant for all T_g-groups (Fig 5.3b, d and f). In general, if the logarithmical dependence of viscosity is kept in mind, within a T_g-group similar results for η_0 can be obtained. In Figure 5.3, the melt rheological behavior at 150 °C of each blend, including its CY-fit and WLF-fit, is shown in more detail.

Table 5.3 *Comparison of zero-shear viscosity in the measurable temperature range of mixtures investigated.*

Mixture	**Zero-shear viscosity η_0 [Pa·s]**				
	140 °C	**150 °C**	**160 °C**	**170 °C**	**180 °C**
COP	329,203	61,006	14,039	3,843	1,229
Group 1 ($T_{g,\,Rheo}$: ~124 °C; $T_{g,\,DSC}$: ~102 °C)					
IMC/COP 5 %	-	32,521	7,734	2,189	729
PEG/COP 1.38 %	-	30,119	7,551	2,274	-
CBZ/COP 4.7 %	-	42,469	9,395	2,472	786
Group 2 ($T_{g,\,Rheo}$: ~117 °C; $T_{g,\,DSC}$: ~91 °C)					
IMC/COP 20 %	30,408	7,315	2,034	653	234
PEG/COP 4 %	46,028	11,409	3,303	1,113	-
DPD/COP 32.5 %	-	3,660	1,044	352	133
Group 3 ($T_{g,\,Rheo}$: ~104 °C; $T_{g,\,DSC}$: ~80 °C)					
IMC/COP 45 %	2,361	597	187	71	-
PEG/COP 8.5 %	5,711	1,796	649	275	-
IBU/COP 10.5 %	6,947	1,977	648	-	-

In the case of T_g-group 1 ($T_{g,\,Rheo}$= ~124 °C) and in comparison to pure COP, the zero-shear viscosity was reduced from ~60,000 Pa·s to 30,000 - 40,000 Pa·s (Fig 5.3a, b). Based on identical curve magnitude and curve progression of CY-fit and WLF-fit for IMC/COP, PEG/COP and CBZ/COP in T_g-group 1, these mixtures show identical melt

rheology and identical frequency- and temperature-dependent viscosity. This result is in accordance with almost identical T_gs of the individual mixtures.

Regarding T_g-group 2 ($T_{g,\,Rheo}$ = 117 °C), the viscosity was decreased to 3,000-11,000 Pa·s (Fig 5.3c, d), due to an increase in API or plasticizer content and lower glass transition. Compared to T_g-group 1, the individual CY-fits of the melt viscosity showed higher discrepancy in curve magnitude. The higher content of API/plasticizer or the highly-reduced glass transition might have promoted this difference in viscosity. However, almost identical curve progression of the CY-fits and identical a_T and WLF-fits indicated a similar frequency and temperature dependence for IMC/COP, PEG/COP and DPD/COP blend of T_g-group 2.

In T_g-group 3 ($T_{g,\,Rheo}$ = 104 °C), a clear discrepancy in viscosity between IMC/COP (~600 Pa·s) and PEG/COP or IBU/COP (~2,000 Pa·s) was seen (Fig 5.3e, f). IMC lowered the viscosity much more than PEG or IBU and led to a larger difference in viscosity curve magnitude compared to T_g-group 1 and 2. It is unclear whether this was related to the behavior of IMC with its highly specific interactions to COP [34,35], or is generally valid for all APIs with similar weight fractions or plasticizing effects. Nevertheless, almost half by weight of the polymer was replaced by IMC but still the accuracy in temperature and frequency dependence was comparable to T_g-group 1 and 2.

Overall, the temperature dependency of the T_g-groups, described by WLF-fit and a_T, led to similar results and to the conclusion of smaller difference among the individual blends when compared to each other or to pure COP (Fig 5.3 and 5.2d). Regarding the curve progression of CY-fits, almost similar outcomes were obtained, indicating a similar frequency dependence. However, the variability in curve magnitude of CY-fits for a given T_g-group varied as a function of the reduced COP glass transition. Hence, correlation between T_g and η_0 decreased slightly with increasing plasticization. Whether this limitation in correlation influences extrusion experiments, or if it can be neglected, is later discussed in section 5.7.3 and compared to hot-melt extrusion trials.

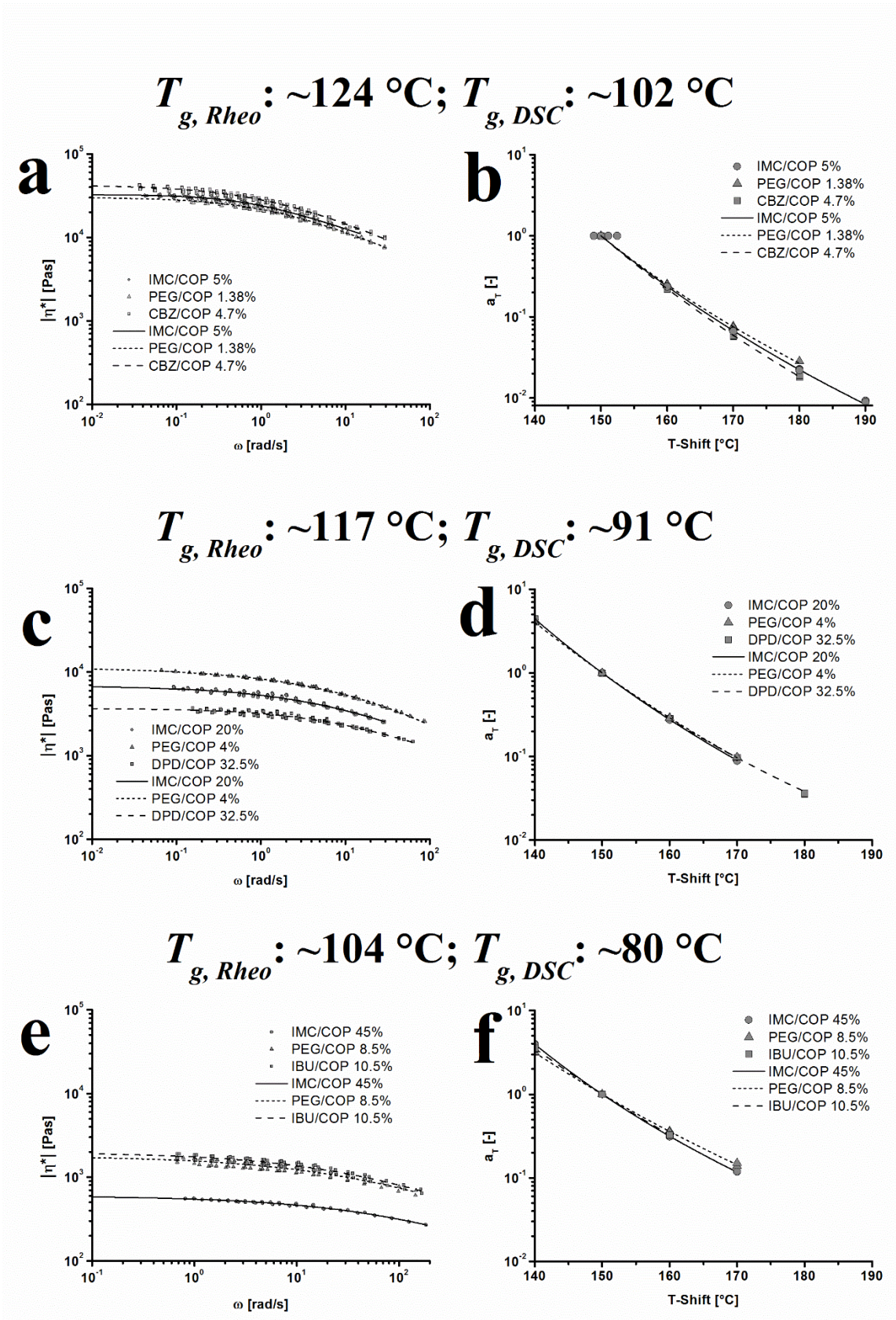

Figure 5.3a-f *Carreau-Yasuda fits and corresponding WLF fits at 150 °C for T_g-group 1 (a, b), T_g-group 2 (c, d) and T_g-group 3 (e, f).*

5.7.2 **Comparison of zero shear viscosity and corresponding glass transition**

To evaluate the relationship between the melt viscosity and the transition temperature of API/ or plasticizer/COP mixtures measured by both DSC and SAOS, T_g and corresponding η_0 at 150 °C of various COP blends are shown in Figure 4. In addition to the measured T_g and η_0 of blends investigated, several other additional APIs and weight fractions of earlier experiments were included to expand the data set and improve subsequent curve fitting. The regression curve fitting was performed for the entire data set (21 data points), again for only IMC (6 data points) and once again for only PEG (8 data points).

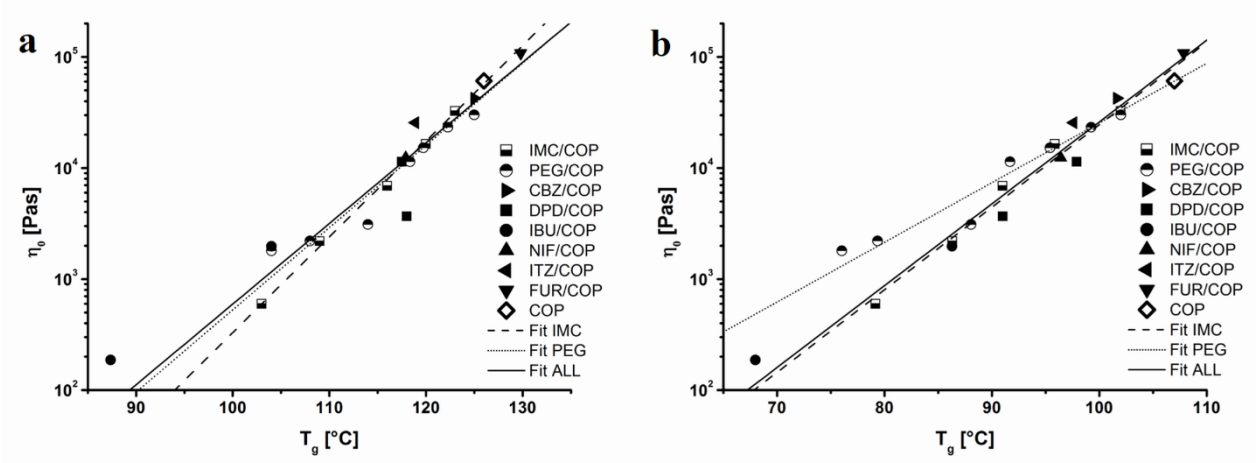

Figure 5.4a-b *Correlation between $T_{g,\,Rheo}$ (a) or $T_{g,\,DSC}$ (b) and corresponding zero-shear viscosity at 150 °C of various API- or plasticizer/COP mixtures, regression curves were performed for IMC/COP, PEG/COP and the entire data set (NIF = nifedipine; ITZ = itraconazole; FUR = furosemide).*

In general, since the measuring techniques by DSC and SAOS are not comparable, the values of $T_{g,\,DSC}$ and $T_{g,\,Rheo}$ differ. First, this is rooted at the different parameters which were used to identify the T_g hence, leading to deviating values in T_g. Secondly in DSC, the T_g is analyzed during a heating ramp, whereas in SAOS $T_{g,\,Rheo}$ was determined during a cooling ramp.

In the case of η_0 to $T_{g,\,Rheo}$, all regression curves showed an adjusted correlation coefficient (r^2) of more than 0.9, indicating a strong dependence of η_0 to T_g and an accurate

mathematical description by a simple exponential fit with two variables only (Eq. (5.7), Table 5.4, Fig 5.4a).

$$\eta_0 = a \cdot e^{(b \cdot T_g)} \tag{5.7}$$

Table 5.4 *Regression curve parameters of zero-shear viscosity and corresponding glass transition for IMC/COP mixtures, PEG/COP mixtures and the whole data set.*

Data	Result of fit [$\eta_0 = a \cdot e^{(b \cdot T_g)}$]		
	a	***b***	**adjusted r^2**
All $T_{g,\ Rheo}$	3.29 E-5	0.167	0.920
All $T_{g,\ DSC}$	1.11 E-3	0.170	0.963
IMC $T_{g,\ Rheo}$	7.89 E-7	0.198	0.997
IMC $T_{g,\ DSC}$	9.05 E-4	0.171	0.977
PEG $T_{g,\ Rheo}$	2.07 E-5	0.171	0.925
PEG $T_{g,\ DSC}$	1.07 E-1	0.124	0.948

In all curve fittings for $T_{g,\ Rheo}$, the variable a tended to zero, whereas the variable b was between 0.17 – 0.20. In the case of IMC/COP, the highest r^2 of 0.997 was achieved, proving the direct dependence of η_0 on T_g, if only one API is regarded. Concerning PEG/COP and its r^2 of 0.925, the lower r^2 might be an effect of the higher molecular weight of PEG, its higher viscosity, and thus higher contribution to the viscosity of the mixture, compared to a small API molecule. Consequently, PEG itself might have an additional specific effect on the rheological behavior beyond plasticizing, causing the slight decrease in regression curve accuracy, although negligible extent. For the entire data set, an accuracy of r^2=0.920 in curve fitting was achieved. This correlation confirms the original assumption that the magnitude of the viscosity is mainly influenced by the T_g and to a lesser extent by specific nature of the API or plasticizer, given a constant polymeric matrix (COP).

Compared to $T_{g,\ Rheo}$, $T_{g,\ DSC}$ versus η_0 and the respective regression curves of PEG and IMC varied more without compromising the adjusted r^2; however, *a* and *b* showed increasing difference (Table 5.4, Fig 5.4b). The variable *a* for IMC was 0.17 and for PEG 0.12. The variable *b* was increased slightly, especially for PEG, but still tended to zero. In particular, the PEG fit deviated with respect to $T_{g,\ Rheo}$ curve fitting. Compared

to SAOS, this may be an effect of pronounced phase separation due to less intensive mixing, without shear stress, in DSC trials. Additional DSC measurements with 15 % PEG in COP already showed two glass transitions, hence a phase separation. Due to the detection limit of DSC, this phase separation might occur already at lower PEG weight fractions and may have caused the difference in regression curve progression. Therefore, two points (7 % and 8.5 %) of PEG data were eliminated to perform the regression curve fitting for the entire data set which is in good accordance with the IMC and $T_{g,\,Rheo}$ results. In conclusion, as was for $T_{g,\,Rheo}$ versus η_0, the dependence of η_0 on $T_{g,\,DSC}$ is obvious and seemed independent of the API or plasticizer used.

5.7.3 **Extrusion trials and mean residence time (MRT) measurements**

The extrusion performance of mixtures in T_g-groups 1-3 are listed in Table 5.5. During hot-melt extrusion, the melt temperature in the die was always 10 K higher than the set barrel temperature of the last barrel sections, leading to a lower viscous melt than originally intended (Tables 5.3 and 5.5).

Table 5.5 *Extrusion performance at 100 rpm and 2 g/min of blends investigated.*

Mixture	$T_{Extrusion}$ [°C]	T_{Sensor} [°C]	Torque [N·m]	Feed rate [g/min]	MRT [s]
COP	170	180.1	6.5	2.3	290
Group 1 ($T_{g,\,Rheo}$: ~124 °C; $T_{g,\,DSC}$: ~102 °C)					
IMC/COP 5 %	160	169.8	6.7	2.1	304
PEG/COP 1.38 %	160	169.8	7.3	1.9	305
CBZ/COP 4.7 %	160	170.0	5.9	1.8	310
Group 2 ($T_{g,\,Rheo}$: ~117 °C; $T_{g,\,DSC}$: ~91 °C)					
IMC/COP 20 %	150	160.3	5.9	2.0	325
PEG/COP 4 %	150	160.2	9.5	1.9	366
DPD/COP 32.5 %	150	159.9	5.2	2.1	323
Group 3 ($T_{g,\,Rheo}$: ~104 °C; $T_{g,\,DSC}$: ~80 °C)					
IMC/COP 45 %	140	148.9	3.9	2.0	336
PEG/COP 8.5 %	140	149.3	8.7	1.8	393
IBU/COP 10.5 %	140	150.2	8.6	2.1	343

In the case of T_g-group 1, the torque varied only 1.4 N·m between the different COP-based blends, indicating an identical behavior during extrusion. The similarity in processing within the T_g-groups was confirmed by both the low difference in torque and in mean residence time (6 s MRT difference). Therefore, no important variation in extrusion was found between IMC/COP, PEG/COP and CBZ/COP of T_g-group 1, which was in good accordance with the melt rheological behavior (Fig 5.3a, b).

Regarding T_g-group 2 and its torque and MRT values, IMC/COP and DPD/COP achieved identical behavior during extrusion. PEG/COP instead resulted in higher torque and higher MRT, which might be an effect of higher viscosity (Fig 5.3c, d). However, the specific behavior of PEG during extrusion seemed more reasonable. The material built up in the extruder and was not conveyed well which resulted in a higher torque and MRT. In conclusion for T_g-group 2, the behavior might be similar in extrusion but in the case of PEG, further investigations are needed to clarify the cause of higher torque and MRT.

For T_g-group 3, the results of melt rheology were reflected in extrusion. PEG/COP and IBU/COP had almost identical torque, whereas IMC achieved a much lower value (Fig 5.3e, f). This could be easily explained by the lower viscosity of IMC/COP compared to PEG/COP and IBU/COP, which might be related to specific interactions between IMC and COP [34,35]. Nevertheless, MRT was almost identical for IMC/COP and IBU/COP. The increase in MRT of PEG/COP might be triggered by the same reason as for PEG/COP of T_g-group 2. During extrusion, the material stuck to the screws, causing an increase in MRT.

In conclusion, similar behavior at extrusion is likely but in light of the specific behavior of PEG and IMC, further investigations with additional API or plasticizer in COP and identical T_g are needed. However, the authors are confident that further investigations will prove similar behavior in extrusion for melts containing material with the identical plasticizing effect.

5.8 Discussion

In general, for predicting melt viscosity and dependent extrusion performance of ASDs, a suitable correlation between $T_{g,\,Rheo}$ and η_0 was identified, independent of API or plasticizer and its molecular weight, recrystallization tendency, weight fraction and plasticizing effect with only few exceptions (Fig 5.4).

Regarding the physical background of the T_g – zero-shear viscosity correlation, the dependency becomes obvious: In general, the molecular mobility of a specimen can be described as a cooperative site exchange process. The extent of this site exchange process depends on the available free volume, known as the free volume theory [36–38]. To enable viscous flow, a molecule must be able to change its position with another, where the new position has to be unoccupied. Consequently, a certain free volume has to be present to enable this site change. If the free volume is increased, site exchanges increase and the irreversible resistance against viscous flow decreases. Hence, the viscosity of a system decreases with increasing free volume in temperature-dependency. Below the T_g, the present free volume is too small to facilitate this cooperative site exchange processes, the molecular mobility of molecular chain segments is decreased, leaving the system frozen in a non-equilibrated state. Consequently, viscosity and glass transition depend on the free volume in the specimen, it is obvious that both parameters are likely to correlate. As plasticizers or API are mainly influencing the extent of free volume, it seems logical that they are changing the viscosity and T_g to a similar extent without compromising their correlation.

Moreover, APIs with strong specific interactions, e.g. hydrogen bonding, such as IMC should be regarded carefully. Specific interactions might affect the resulting melt viscosity, especially at higher API weight fractions, causing a slight deviation from the correlation of T_g to η_0 (Fig 5.3 and 5.4). However, extrusion trials only detected differences in torque, while MRT seemed unaffected. Due to the higher dependence of MRT on temperature independent variables n and a of CY-fit compared to temperature dependent η_0 and λ, similar MRT values can be explained (Fig 5.3) [39]. In conclusion, due to similar rheological behavior as a function of frequency and temperature of the investigated blends (Fig 5.3), strong specific interactions are only affecting torque at

unchanged MRT in HME. Furthermore, specific interactions are only decreasing torque and hence are not limiting the extrusion at the desired temperature. With respect to similar MRT, changes in thermal stress to the extruded material are unlikely. Consequently, the MRT at a given screw configuration can be estimated via the T_g of a required mixture. This enables an easy optimization of MRT, which is needed for thermal instable APIs or for dissolving poorly soluble APIs in a polymeric matrix during HME. However, further investigations are needed to evaluate the impact of the temperature profile along the screws.

In addition, an increase in API or plasticizer weight fraction triggered a slight decrease in correlation of T_g to η_0. In the case of IMC/COP 20 % and DPD/COP 32.5 % and their discrepancy in viscosity at 150 °C (Fig 3c), extrusion trials indicated the variation in viscosity as negligible (Table 5.5).

Nevertheless, material build-up during polymer extrusion due to added API or plasticizer, especially employing substances of low melting point, led to an unpredictable increase in torque and increase in MRT (Table 5.5). This increase might be triggered by material which stuck to the screws, as it was observed for PEG/COP mixtures. An abnormal behavior in extrusion of added material was therefore limiting the prediction of extrusion performance by using T_g and η_0. Furthermore, inhomogeneous specimens during DSC measurements and corresponding change in T_g, as was observed for PEG/COP high weight fractions, was limiting the correlation of η_0 to T_g, DSC but did not compromise the correlation to $T_{g,\,Rheo}$ (Fig 5.4).

Overall, the assumption of a general connection between T_g and a corresponding change in melt viscosity was confirmed, independent of the added API or plasticizer to COP with only few exceptions. A simple T_g measurement by DSC enables an estimate of the melt viscosity of a material, if the general melt behavior of the pure polymer is known. In this way, the effort in gaining an estimate of the melt viscosity information of an API- or plasticizer-polymer mixture can be reduced drastically. However, the mathematical description of such T_g-viscosity correlation is expected to be polymer-dependent and needs to be elucidated or confirmed for every polymeric matrix.

5.9 Conclusion

A correlation between glass transition temperature (T_g) and melt viscosity was confirmed and enables the prediction of amorphous solid dispersion (ASD) extrusion performance. The melt rheological behavior was largely independent of added active pharmaceutical ingredient (API) or plasticizer to copovidone with respect to different molecular weight, recrystallization tendency, weight fraction and plasticizing effect with only few exceptions. Regarding extrusion performance, abnormal behavior of added API or plasticizer and specific interactions between the materials were limiting the prediction. In the case of specific interactions between API and matrix polymer, only torque was reduced but no effect on mean residence time (MRT) was observed. The effort in gaining melt viscosity information of an ASD can be reduced to T_g measurement by differential scanning calorimetry (DSC) and knowledge of the rheological behavior of the pure matrix polymer. In conclusion, material and costs to set-up extrusion trials to the desired conditions can be reduced.

5.10 Acknowledgement

The authors would like to thank Rachel C. Evans greatly for reviewing the manuscript. This research did not receive any specific grant from funding agencies in the public, commercial, or not-for-profit sectors.

5.11 References

[1] S. Shah, S. Maddineni, J. Lu, M.A. Repka, Melt extrusion with poorly soluble drugs, Int. J. Pharm. 453 (2013) 233–252. doi:10.1016/j.ijpharm.2012.11.001.

[2] P.J. Marsac, T. Li, L.S. Taylor, Estimation of Drug–Polymer Miscibility and Solubility in Amorphous Solid Dispersions Using Experimentally Determined Interaction Parameters, Pharm. Res. 26 (2009) 139–151. doi:10.1007/s11095-008-9721-1.

[3] A. Mahieu, J.-F. Willart, E. Dudognon, F. Danède, M. Descamps, A New Protocol To Determine the Solubility of Drugs into Polymer Matrixes, Mol. Pharm. 10 (2013) 560–566. doi:10.1021/mp3002254.

[4] E.S. Bochmann, D. Neumann, A. Gryczke, K.G. Wagner, Micro-scale prediction method for API-solubility in polymeric matrices and process model for forming amorphous solid dispersion by hot-melt extrusion, Eur. J. Pharm. Biopharm. 107 (2016) 40–48. doi:10.1016/j.ejpb.2016.06.015.

[5] Y. Zhao, P. Inbar, H.P. Chokshi, A.W. Malick, D.S. Choi, Prediction of the thermal phase diagram of amorphous solid dispersions by flory-huggins theory, J. Pharm. Sci. 100 (2011) 3196–3207. doi:10.1002/jps.22541.

[6] J. Gupta, C. Nunes, S. Vyas, S. Jonnalagadda, Prediction of Solubility Parameters and Miscibility of Pharmaceutical Compounds by Molecular Dynamics Simulations, J. Phys. Chem. B. 115 (2011) 2014–2023. doi:10.1021/jp108540n.

[7] Y. Sun, J. Tao, G.G.Z. Zhang, L. Yu, Solubilities of crystalline drugs in polymers: An improved analytical method and comparison of solubilities of indomethacin and nifedipine in PVP, PVP/VA, and PVAc, J. Pharm. Sci. (2010) n/a-n/a. doi:10.1002/jps.22251.

[8] S.O. Kyerematen, M. Pudlas, G.H. Woehrle, A Fast and Reliable Empirical Approach for Estimating Solubility of Crystalline Drugs in Polymers for Hot Melt Extrusion Formulations, J. Pharm. Sci. 103 (2014) 2847–2858. doi:10.1002/jps.23941.

[9] A. Eitzlmayr, J. Khinast, G. Hörl, G. Koscher, G. Reynolds, Z. Huang, J. Booth, P. Shering, Experimental characterization and modeling of twin-screw extruder elements for pharmaceutical hot melt extrusion, AIChE J. 59 (2013) 4440–4450. doi:10.1002/aic.14184.

[10] J. Rantanen, J. Khinast, The Future of Pharmaceutical Manufacturing Sciences, J. Pharm. Sci. 104 (2015) 3612–3638. doi:10.1002/jps.24594.

[11] D.E. Zecevic, K.G. Wagner, Rational Development of Solid Dispersions via Hot-Melt Extrusion Using Screening, Material Characterization, and Numeric Simulation Tools, J. Pharm. Sci. 102 (2013) 2297–2310. doi:10.1002/jps.23592.

[12] B. Lang, J.W. McGinity, R.O. Williams, Hot-melt extrusion – basic principles and pharmaceutical applications, Drug Dev. Ind. Pharm. 40 (2014) 1133–1155. doi:10.3109/03639045.2013.838577.

[13] J. Aho, J.P. Boetker, S. Baldursdottir, J. Rantanen, Rheology as a tool for evaluation of melt processability of innovative dosage forms, Int. J. Pharm. 494 (2015) 623–642. doi:10.1016/j.ijpharm.2015.02.009.

[14] J. Thiry, F. Krier, B. Evrard, A review of pharmaceutical extrusion: Critical process parameters and scaling-up, Int. J. Pharm. 479 (2015) 227–240. doi:10.1016/j.ijpharm.2014.12.036.

[15] J. Lyons, P. Blackie, C. Higginbotham, The significance of variation in extrusion speeds and temperatures on a PEO/PCL blend based matrix for oral drug delivery, Int. J. Pharm. 351 (2008) 201–208. doi:10.1016/j.ijpharm.2007.09.041.

[16] S.S. Gupta, T. Parikh, A.K. Meena, N. Mahajan, I. Vitez, A.T.M. Serajuddin, Effect of carbamazepine on viscoelastic properties and hot melt extrudability of Soluplus®, Int. J. Pharm. 478 (2015) 232–239. doi:10.1016/j.ijpharm.2014.11.025.

[17] H. Liu, X. Zhang, H. Suwardie, P. Wang, C.G. Gogos, Miscibility studies of indomethacin and Eudragit® E PO by thermal, rheological, and spectroscopic analysis, J. Pharm. Sci. 101 (2012) 2204–2212. doi:10.1002/jps.23075.

[18] S.M. Maru, M. de Matas, A. Kelly, A. Paradkar, Characterization of thermal and rheological properties of zidovidine, lamivudine and plasticizer blends with ethyl cellulose to assess their suitability for hot melt extrusion, Eur. J. Pharm. Sci. 44 (2011) 471–478. doi:10.1016/j.ejps.2011.09.003.

[19] M.S. Dudhedia, A.M. Agrawal, Rheological study of copovidone and solid dispersion blend used for hot melt extrusion, J. Appl. Polym. Sci. 133 (2016) n/a-n/a. doi:10.1002/app.43278.

[20] H. Suwardie, P. Wang, D.B. Todd, V. Panchal, M. Yang, C.G. Gogos, Rheological study of the mixture of acetaminophen and polyethylene oxide for hot-melt extrusion application, Eur. J. Pharm. Biopharm. 78 (2011) 506–512. doi:10.1016/j.ejpb.2011.03.013.

[21] A. Paradkar, A. Kelly, P. Coates, P. York, Shear and extensional rheology of hydroxypropyl cellulose melt using capillary rheometry, J. Pharm. Biomed. Anal. 49 (2009) 304–310. doi:10.1016/j.jpba.2008.11.014.

[22] S. Syrjälä, J. Aho, Capillary rheometry of polymer melts — Simulation and experiment, Korea-Aust. Rheol. J. 24 (2012) 241–247. doi:10.1007/s13367-012-0029-7.

[23] M. Yang, P. Wang, H. Suwardie, C. Gogos, Determination of acetaminophen's solubility in poly(ethylene oxide) by rheological, thermal and microscopic methods, Int. J. Pharm. 403 (2011) 83–89. doi:10.1016/j.ijpharm.2010.10.026.

[24] D.S. Jones, D.N. Margetson, M.S. McAllister, G.P. Andrews, Characterisation and modelling of the thermorheological properties of pharmaceutical polymers and

their blends using capillary rheometry: Implications for hot melt processing of dosage forms, Int. J. Pharm. 493 (2015) 251–259. doi:10.1016/j.ijpharm.2015.07.024.
[25] J. Aho, M. Edinger, J. Botker, S. Baldursdottir, J. Rantanen, Oscillatory Shear Rheology in Examining the Drug-Polymer Interactions Relevant in Hot Melt Extrusion, J. Pharm. Sci. 105 (2016) 160–167. doi:10.1016/j.xphs.2015.11.029.
[26] A. Shabbir, H. Goldansaz, O. Hassager, E. van Ruymbeke, N.J. Alvarez, Effect of Hydrogen Bonding on Linear and Nonlinear Rheology of Entangled Polymer Melts, Macromolecules. 48 (2015) 5988–5996. doi:10.1021/acs.macromol.5b00757.
[27] C. Osterwinter, C. Schubert, C. Tonhauser, D. Wilms, H. Frey, C. Friedrich, Rheological Consequences of Hydrogen Bonding: Linear Viscoelastic Response of Linear Polyglycerol and Its Permethylated Analogues as a General Model for Hydroxyl-Functional Polymers, Macromolecules. 48 (2015) 119–130. doi:10.1021/ma501674x.
[28] D.W. Clegg, A.A. Collyer, Rheological measurement, Chapman & Hall, London; New York, 1998.
[29] U. Eisele, Introduction to Polymer Physics, Springer Berlin Heidelberg, Berlin, Heidelberg, 1990. http://dx.doi.org/10.1007/978-3-642-74434-1 (accessed November 27, 2015).
[30] D.W. van Krevelen, Properties of polymers: their correlation with chemical structure: their numerical estimation and prediction from additive group contributions, 4th, completely rev. ed ed., Elsevier, Amsterdam, 2009.
[31] R.I. Tanner, Engineering rheology, 2nd ed, Oxford University Press, New York, 2000.
[32] R.K. Jena, X. Chen, C.Y. Yue, Y.C. Lam, Viscosity of COC polymer (TOPAS) near the glass transition temperature: Experimental and modeling, Polym. Test. 29 (2010) 933–938. doi:10.1016/j.polymertesting.2010.08.007.
[33] W.P. Cox, E.H. Merz, Rheology of Polymer Melts—A Correlation of Dynamic and Steady Flow Measurements, in: Committee D-20 (Ed.), Int. Symp. Plast. Test. Stand., ASTM International, 100 Barr Harbor Drive, PO Box C700, West Conshohocken, PA 19428-2959, 1959: pp. 178-178–11. doi:10.1520/STP44206S.
[34] A. Forster, J. Hempenstall, T. Rades, Characterization of glass solutions of poorly water-soluble drugs produced by melt extrusion with hydrophilic amorphous pol-

ymers, J. Pharm. Pharmacol. 53 (2001) 303–315. http://onlinelibrary.wiley.com/doi/10.1211/0022357011775532/abstract (accessed February 2, 2015).

[35] T. Matsumoto, G. Zografi, Physical Properties of Solid Molecular Dispersions of Indomethacin with Poly(vinylpyrrolidone) and Poly(vinylpyrrolidone-co-vinylacetate) in Relation to Indomethacin Crystallization, Pharm. Res. 16 (1999) 1722–1728.

[36] A.K. Doolittle, Studies in Newtonian Flow. II. The Dependence of the Viscosity of Liquids on Free-Space, J. Appl. Phys. 22 (1951) 1471–1475. doi:10.1063/1.1699894.

[37] T.G. Fox, P.J. Flory, Second-Order Transition Temperatures and Related Properties of Polystyrene. I. Influence of Molecular Weight, J. Appl. Phys. 21 (1950) 581–591. doi:10.1063/1.1699711.

[38] M.L. Williams, R.F. Landel, J.D. Ferry, The Temperature Dependence of Relaxation Mechanisms in Amorphous Polymers and Other Glass-forming Liquids, J. Am. Chem. Soc. 77 (1955) 3701–3707. doi:10.1021/ja01619a008.

[39] K. Kohlgrüber, M. Bierdel, Co-rotating twin-screw extruders: fundamentals, technology, and applications, Carl Hanser Publishers ; Hanser Gardner Publications, Munich [Germany] : Cincinnati, Ohio, 2008.

6 Numerical simulation of hot-melt extrusion processes for amorphous solid dispersions using model-based melt viscosity

Esther S. Bochmann [a] Kristina E Steffens [a]; Andreas Gryczke [b]; Karl G. Wagner [a]

[a] Department of Pharmaceutical Technology and Biopharmaceutics, University of Bonn, Bonn, Germany

[b] Global Technical Marketing Solubilization, BASF SE, Ludwigshafen, Germany

This part was published as

E.S. Bochmann, K.E. Steffens, A. Gryczke, K.G. Wagner, Numerical simulation of hot-melt extrusion processes for amorphous solid dispersions using model-based melt viscosity, European Journal of Pharmaceutics and Biopharmaceutics. 124 (2018) 34–42. doi:10.1016/j.ejpb.2017.12.001.

6.1 Graphical abstract

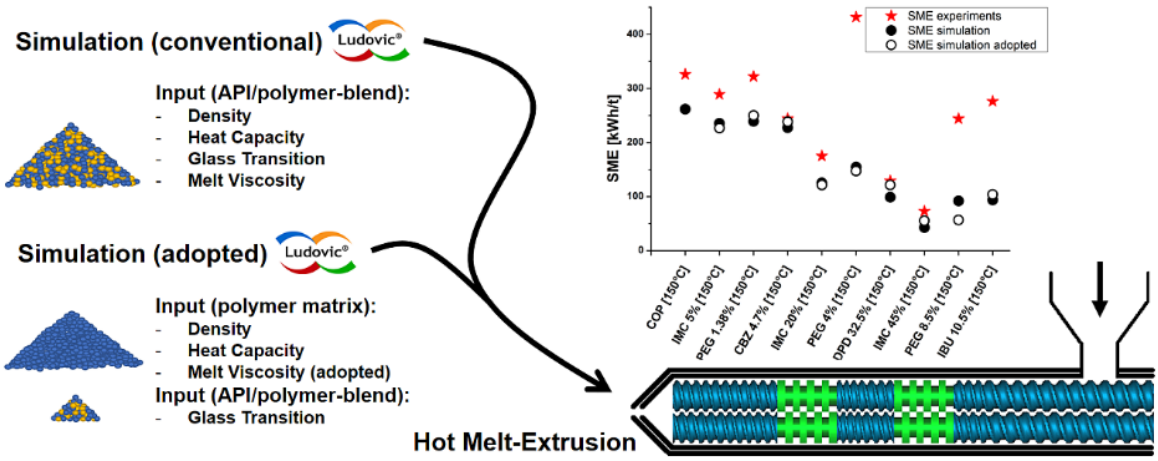

6.2 Abstract

Simulation of HME processes is a valuable tool for increased process understanding and ease of scale-up. However, the experimental determination of all required input parameters is tedious, namely the melt rheology of the amorphous solid dispersion (ASD) in question. Hence, a procedure to simplify the application of hot-melt extrusion (HME) simulation for forming amorphous solid dispersions (ASD) is presented. The commercial 1D simulation software Ludovic® was used to conduct (i) simulations using a full experimental data set of all input variables including melt rheology and (ii) simulations using model-based melt viscosity data based on the ASDs glass transition and the physical properties of polymeric matrix only. Both types of HME computation were further compared to experimental HME results. Variation in physical properties (e.g. heat capacity, density) and several process characteristics of HME (residence time distribution, energy consumption) among the simulations and experiments were evaluated. The model-based melt viscosity was calculated by using the glass transition temperature (T_g) of the investigated blend and the melt viscosity of the polymeric matrix by means of a T_g-viscosity correlation. The results of measured melt viscosity and model-based melt viscosity were similar with only few exceptions, leading to similar HME simulation outcomes. At the end, the experimental effort prior to HME simulation could be minimized and the procedure enables a good starting point for rational development of ASDs by means of HME. As model excipients, vinylpyrrolidone-vinyl acetate

copolymer (COP) in combination with various APIs (carbamazepine, dipyridamole, indomethacin, and ibuprofen) or polyethylene glycol (PEG 1500) as plasticizer were used to form the ASDs.

6.3 Keywords

hot-melt extrusion, melt rheology, glass transition temperature, amorphous solid dispersion, simulation, prediction model

6.4 Chemical compounds studied in this article

Carbamazepine (PubChem CID: 2554); Dipyridamole (PubChem CID: 3108); Ibuprofen (PubChem CID: 3672); Indomethacin (PubChem CID: 3715); Copovidone (PubChem CID: 25086-89-9)

6.5 Introduction

In formulation development, the so-called enabling technology hot-melt extrusion (HME) is often used to overcome the poor solubility of active pharmaceutical ingredients (APIs) by forming amorphous solid dispersions (ASDs). Unfortunately, the extrusion process-based formulation development is often API-consuming and expensive in terms of time and personal [1–4]. To reduce the effort in early development, several methods and techniques to facilitate a rational procedure have been previously reported [5–8].

A very common example is the use of small-scale co-rotating twin-screw extruders prior the production scale [5,9–11]. It reduces the batch size down to as little as 5 g and they are accepted as screening tools for solid dispersion formulations. Unfortunately due to fundamental differences between lab-scale extruders (e.g. 9 mm screw diameter) and larger scale extruders, a rational scale-up is not feasible [8]. To perform process development and scale-up, extruders of 10-12 mm, respectively 24-27 mm screw diameter should be used instead but this increases the batch size to approx. 50 g/h up to 20 kg/h. Furthermore, the scale-up to production scale can be conducted volumetrically or adiabatically [7,8,12,13]. The most crucial process characteristics in

scale-up are the residence time distribution (RTD) and the specific mechanical energy (SME) [12]. Both parameters should be kept constant by adjusting the various other extrusion parameters (e.g. temperature, screw configuration, screw speed and feed rate) during scale-up.

Another way to perform a rational screening of solid dispersion formulations are micro-scale testing methods by using thermo-analytical techniques such as differential scanning calorimetry (DSC) [14–20], melt rheology [21–23], hot-stage microscopy (HSM) [8,9] and many more. For example, differential scanning calorimetry can be used to determine the glass transition temperature (T_g) for later process conditions [8,24] or for the API-solubility characterization within the polymeric matrix. This solubility prediction can be conducted by using the melting point depression method [14–16], dissolution endpoint method [17–19] or by using the API/polymer ratio-dependent glass transition temperature (T_g) [20,25]. Hot-stage microscopy is a very powerful analytical technique to determine the miscibility of compounds and to assess first hints for an applicable temperature range in extrusion [8,9]. Melt rheology is particularly useful in that it can be used to identify possible process conditions [23,26]. The main advantage of all these methods is the small amount of material required to obtain significant knowledge for subsequent hot-melt extrusion processing. In general, they enable the estimation of a feasible extrusion range and they can be very helpful to predict the shelf life of extruded formulations.

An even more theoretical approach is the simulation of HME processes [27–30] and the use of molecular modelling [14,31,32] or solubility parameters [5,8,24] to estimate a good and early starting point prior any experimental consideration. Prediction of glass transition temperature (T_g) [31], API solubility within the polymeric matrix [5,24,33] and detailed computation of extrusion runs represent only a few applications in HME process analytics. In the case of adiabatic scale-up from small-scale to production-scale extrusion, HME simulation can be most appropriate solution to identify adiabatic conditions in small-scale extruders [13]. The high impact of barrel set temperature here is disguising adiabatic conditions, especially for small scale extruders (<= 12 mm) where heat conduction governs energy uptake rather than viscous dissipation. However, ad-

iabatic conditions can be identified by employing HME simulation. At the end, all mentioned approaches and methods, such as mini-scale twin screw extruders, micro-scale testing methods and HME simulation, enable a rational development of ASDs to overcome the poor solubility of modern APIs. This leads to a not only trial-and-error based formulation but a process development in the sense of quality by design.

Regarding the extrusion computation, a major drawback is the need for experimental input data (e.g. melt viscosity) in order to run the simulation properly. In early stage development, several formulations for an API have to be tested, which is time-consuming, especially in the case of rheological measurements. To enable certain “shortcuts” regarding the estimation of melt viscosity by using only the T_g of the formulation has already been reported in our previous work [34]. To continue this work, we applied our model-based estimates of T_g-viscosity correlation to simulate HME processes for forming ASDs.

The objective of our study reported here was the comparison of extrusion experiments with the computations of the commercial 1D simulation software Ludovic®. The software was fed either with measured melt viscosity data of the respective ASD (including API) or with model-based melt viscosity data by using the T_g of the investigated blends. To evaluate the application of our first estimates of the melt viscosity by using only T_g, several process characteristics of HME (e.g. residence time distribution, energy consumptions) and physical properties (e.g. heat capacity, density, melt rheology) of various mixtures has been investigated. The goal was not to replace extrusion experiments but more to enable a good and early starting point for HME trials by using only the T_g of a desired ASD and characteristics of the polymeric matrix in HME simulation. Therefore, a rational development is supported. This leads to a reduction of needed extrusion trials to define the best formulation and process conditions for forming ASDs. As model excipient, vinylpyrrolidone-vinyl acetate copolymer (COP) in combination with various API or PEG as plasticizer were used to form ASDs.

6.6 Material and methods

6.6.1 Material

Dipyridamole (DPD) was obtained from Swapnroop Drugs & Pharmaceuticals (Maharashtra, India) and Indomethacin (IMC) was purchased from Swati Spentose Pvt. Ltd (Mumbai, India). PEG 1500 (PEG) were obtained from Alfa Aesar (Karlsruhe, Germany). Vinylpyrrolidone-vinyl acetate copolymer (copovidone, Kollidon® VA 64, COP), Carbamazepine (CBZ) and Ibuprofen (IBU) were kindly donated by BASF SE (Ludwigshafen, Germany) (Table 6.1). The APIs were chosen due to their various physicochemical characteristics. The API or plasticizer weight fraction was experimentally adjusted to a specific glass transition temperature (T_g) of the blend, as was already reported in our previous work [34].

Table 6.1 *Physicochemical properties of substances under investigation [34].*

Substance	Molecular weight [g/mol]	Melting point [°C]	Glass transition temperature [°C]
Indomethacin (IMC)	358	160	44
Carbamazepine (CBZ)	236	175	53
Dipyridamole (DPD)	505	167	38
Ibuprofen (IBU)	206	75	-44
PEG 1500 (PEG)	1,500	47	-42
Copovidone (COP)	45,000 - 70,000	-	107

6.6.2 Methods

6.6.2.1 Preparation of physical mixtures

For DSC trials, a MM400 ball mill (Retsch GmbH, Haan, Germany) with 30 Hz and 3 x 5 min milling cycles was used. For extrusion trials, physical mixtures were prepared by using a Turbula mixer (Willy A. Bachofen AG – Maschinenfabrik, Muttenz, Swiss) for 10 min at 50 rpm.

6.6.2.2 Helium pycnometer

The true density of powder blends and extrudates were analyzed by using the helium pycnometer AccuPyc 1330 (Micromeritics GmbH, Norcross, USA). During measurements, the chamber was purged with 20 purge cycles and a fill pressure of 136.86 kPa·g. Subsequently, samples were analyzed with a fill pressure of 136.86 kPa·g and an equilibration rate of 0.0345 kPa·g/min. The sample was analyzed in 25 runs or until a standard deviation of 0.01 % was reached. For every material, the procedure was repeated two times.

6.6.2.3 Differential scanning calorimetry (DSC)

A DSC 2 (Mettler Toledo, Gießen, Germany) equipped with an auto sampler, nitrogen cooling and nitrogen as purge gas (30 ml/min) was used. The system was calibrated with n-octane, indium and zinc standards. At least three samples of approximately 10 mg of each mixture were analyzed, using 40 µl aluminum pans with a pierced lid. Heat capacities were measured against a sapphire standard in TOPEM® mode (modulated DSC) with 1 K pulse height, 15-30 s pulse width and an underlying heating rate of 2 K/min. Prior to heat capacity analysis, the samples were annealed at elevated temperatures to promote a homogenous distribution of the API/plasticizer in the polymeric matrix.

6.6.2.4 Extrusion trials and residence time distribution (RTD)

For hot-melt extrusion, a co-rotating twin-screw extruder ZE 12 (Three-Tec GmbH, Seen, Switzerland) with a functional length of 25:1 L/D, 12 mm screws, 2 mm die and a maximum torque of 15 N·m was used. The screw configuration is shown in Fig 6.1.

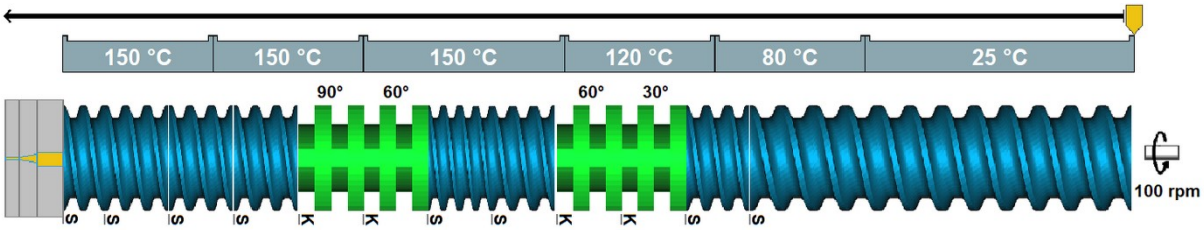

Figure 6.1 *Extruder and screw configuration used (S = conveying element; K = kneading element).*

The throughput was kept constant at 2.0 g/min and the screw speed was set to 100 rpm to enable a high filling ratio of the extruder. Mean residence times (MRTs) were measured with iron oxide (Sicovit® Red 30 E 172, BASF SE, Ludwigshafen, Germany) and calculated by using ExtruVis3 (ExtruVis, Riedstadt, Germany). To determine the feed rate during MRT measurements more precisely, the extruded material was collected and weighed over time. Afterwards, the feed rate was adjusted to a range of 2.0 ± 5 % g/min. The extrusion barrel temperature was set to 150 °C. Furthermore, extrusion data of our previous work were also considered for extrusion simulation in this work [34]. The specific mechanical energy (SME) of extrusion experiments was calculated by using following equation (Eq. (6.1)),

$$SME = \frac{2\pi \cdot n \cdot \tau}{\dot{m} \cdot 60} \tag{6.1}$$

where n is the screw speed [rpm] and $\dot{m}$ characterizes the feed rate [kg/h]. The variable τ determines the maximum torque per shaft [N·m] where the torque of idling speed (1.2 N·m) has been subtracted.

6.6.2.5 Simulation software Ludovic®

The simulation software Ludovic® V6.0.1 PharmaEdition (Sciences Computers Consultants, Saint Etienne, France) was used for computing the flow conditions of hot-melt extrusion processes. It is a one-dimensional approach for flow modelling and allows the calculation of various parameters along the screw profile (e.g. temperature, pressure, shear rate, residence time, global energy distributions, etc.). The model assumes non-isothermal flow conditions and an instantaneous melting prior to the first restrictive

screw element. Due to the unknown filling ratio of a starve-fed extruder, the computation starts at the die and proceeds backwards in an iterative procedure until the final product temperature is achieved [35].

6.7 Results

6.7.1 Physical properties of investigated blends and pure COP

To evaluate the difference in physical properties of the investigated blends, true density and heat capacity of physical mixtures and extrudates were analyzed and compared to pure COP (Table 6.2).

Table 6.2 *Glass transition temperature, true density and heat capacity of COP-blends investigated.*

Mixture	T_g [°C]	ρ [kg/m^3] powder	ρ [kg/m^3] extrudate	C_p [J/(g·K)] at 25 °C	C_p [J/(g·K)] at 150 °C
COP	107	1,178	1,191	1.013	1.720
	Group 1 (T_g: ~102 °C)				
IMC 5 %	102	1,190	1,198	0.966	1.730
PEG 1.38 %	102	1,179	1,191	1.138	1.877
CBZ 4.7 %	103	1,197	1,197	1.020	1.782
	Group 2 (T_g: ~91 °C)				
IMC 20 %	91	1,216	1,221	1.067	1.867
PEG 4 %	92	1,200	1,191	0.851	1.439
DPD 32.5 %	91	1,226	1,211	0.964	1.651
	Group 3 (T_g: ~80 °C)				
IMC 45 %	79	1,249	1,250	0.930	1.616
PEG 8.5 %	76	1,195	1,195	0.863	1.570
IBU 10.5 %	86	1,173	1,178	0.840	1.400

Regarding pure COP, the true density increased slightly from powder at 1,178 kg/m^3 to its extrudate with 1,191 kg/m^3. In comparison, the densities of physical mixtures and extrudates of all COP-blends were similar to pure COP, respectively. The highest deviation of 6 % from pure COP was found for IMC/COP 45 %, which was likely triggered

by the highest API content in this investigation. In the case of the temperature-dependent heat capacity, an increase for COP from 1.013 J/(g·K) at 25 °C to 1.720 J/(g·K) at 150 °C was obtained. An increase in heat capacity as a function of temperature was also observed for COP blends but in most cases with an overall reduced value compared to pure COP. Especially the blends of T_g-group 3, which had the lowest glass transitions, decreased up to approx. 20 %.

Although density and heat capacity are required input parameters for the Ludovic® simulation software, extrusion simulation is mostly effected by extrusion set-up (e.g. throughput, screw speed and screw configuration) or melt viscosity. Small differences in further physical properties between the pure polymeric matrix and ASD thereof might be less important. Therefore, the difference in heat capacity and true density of pure COP to its COP-blends might be negligible for simulation. Consequently, the use of physical properties of pure COP instead of probably unknown data of desired COP blends was sufficient to simulate extrusion and to estimate a good starting point for later extrusion experiments.

6.7.2 **Comparison of energy consumption during extrusion and conventional extrusion simulation with measured melt viscosity**

To determine the variation in energy consumption, conventional simulation by the software Ludovic® and the specific mechanical energy (SME) derived by extrusion experiments were compared (Fig. 6.2).

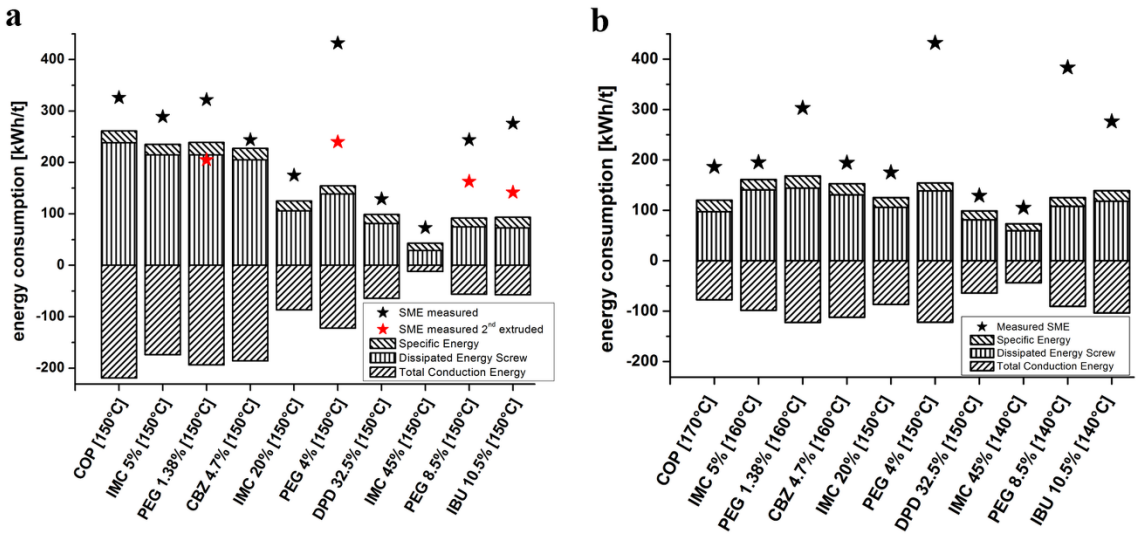

Figure 6.2a-b *Energy consumption of simulated and experimental extrusion runs at a fixed temperature (150 °C) (a) and temperature gradient (140 – 170 °C) (b). Bar charts represent the simulated energy consumption, whereas the stars are indicating the experimental SME.*

In the case of the conventional simulation, physical properties and melt viscosity of the desired blend were used. In simulation, the sum of specific energy, dissipated energy of screw/die and melting energy constitutes the SME. Due to the used 12 mm small-scale extruder, obtained data for the die attributed dissipated energy were negligible (data not shown) and were not further employed. In the case of melting energy, the heat of fusion of the APIs were not considered in simulation because Ludovic® offers only one entry field for melting/softening temperature. In our case, the T_gs of investigated blends were entered, which did not possess any heat of fusion. For simulation and extrusion, two temperature regimes were investigated: extrusion at 150 °C as a fixed temperature and a variable temperature profile (140 °C to 170 °C) where the melt viscosity of COP and COP-blends during extrusion were similar.

Concerning the specific energy derived by simulation, the variation between the individual blends of all T_g-groups (ASDs of identical T_g) were negligible. The specific energy indicated the energy dedicated to heat up the material from ambient temperature to its melting point or glass transition temperature. This suggested that the variation in physical properties of the blends (see section 6.7.1) was not influencing the simulation

results to a major extent (up to 8 %). Only in the case of 45 % IMC-COP blend, a variation of 20 % was found, which was triggered by the high API-content in combination with the respective low viscosity melt and the low viscous dissipation energy thereof. Thus, in the case of simulation trials, the variation in physical properties might be neglected. Consequently, the data of pure COP instead of the data of each individual blend for simulation purposes was feasible for further simulation trials.

Since the screw related dissipated energy and the total conduction energy were melt viscosity-dependent, a deviation between the individual blends and between the two temperature regimes was expected. The screw related dissipated energy characterized the energy which is generated by screw rotation through viscous dissipation effects and the conduction energy determined the energy generated by barrel regulation-induced heat flux. During simulation at extrusion temperature 150 °C, the dissipated energy and the total conduction energy were the highest for pure COP and were continuously alleviated with decreasing T_g from T_g-group 1 to T_g-group 3 (Fig 6.2a). This behavior can be easily explained by a decrease in melt viscosity as a function of glass transition temperature. Since the variation in melt viscosity was the lowest for T_g-group 1, the variation in energy consumption between IMC 5 %, PEG 1.38 % and CBZ 4.7 % was as expected low, too [34]. In comparison to T_g-group 1, due to higher deviation of melt viscosity among T_g-group 2 (IMC 20 %, PEG 4 % and DPD 32.5 %), the deviation in energy consumption likewise increased. Regarding the energy consumptions of T_g-group 3 in simulation, values for IMC 45 % were much lower than for PEG 8.5 % and for IBU 10.5 %, respectively. This reflected the behavior in melt viscosity perfectly. IMC 45 % exhibited a much lower melt viscosity than PEG 8.5 % and IBU 10.5 %. In Fig 6.3b, the extrusion temperatures enabled a similar melt viscosity of all investigated blends and pure COP, which led to roughly similar energy consumptions in simulation, compared to extrusion temperature at 150 °C [34].

Comparing simulation results to extrusion experiments, likely due to loss of energy between the gearbox of the extruder and the screws or further friction, the SME of extrusion experiments were always higher than calculated by Ludovic®. In the case of pure COP and IMC, CBZ or DPD containing blends, the experimental SME did not

differ more than approx. 50 kWh/t from the simulated value. However, blends containing PEG or IBU achieved a much higher SME in extrusion trials than in simulation. Especially the SME of PEG 4 % was more than doubled. This deviation in SME might be rooted in the low melting point of IBU and PEG (Table 6.1), which were even lower than the T_g of their COP blends (Table 6.2). Consequently, IBU and PEG would melt prior the softening of COP during extrusion and producing a sticky suspension in the first zones of the extruder. To take the effect of a low melting point into account, the point of melting in the simulation was shifted from zone 3 (120 °C) (initial data not shown) to the beginning of zone 2 (80 °C) (Fig 6.2). Furthermore, due to the early melting of IBU and PEG, a phase segregation in the first extruder zones was likely. Molten IBU and PEG may have sunken to the bottom of the extruder barrel and a concentration gradient was produced, which subsequently might cause a melt viscosity gradient during extrusion. To investigate whether phase segregation effects occurred, blends containing IBU and PEG were extruded twice at 150 °C to evaluate the variation of SME between both extrusion experiments (Fig 6.2a). In the second extrusion run, milled extrudates of the first run were fed into the extruder. Feeding this homogeneous material suppressed phase segregation effects and a lower SME was obtained. At the end, the SME of the second extrusion runs were more consistent to the simulated values by Ludovic® than the SMEs of the first extrusion runs and the highest variation of 85 kWh/t was found for PEG 4 %, confirming the phase segregation hypothesis. The increase in SME for low melting substances (IBU, PEG) and the still existing difference between experimental and calculated SME can be further explained as follows: In principle, if low melting substances are present, the material will melt prior to the softening of the polymer and it will produce a low viscous melt as already stated. The remaining polymer particles tend to “swim” in this melt, because the large difference between the melt viscosity of API and polymer inhibited a sufficient dispersion by the extruder. Furthermore, with respect to the low viscous melt, an increase in temperature by shearing in the kneading blocks is prohibited and softening of the polymer particles is prolonged and shifted to the following conveying zone. Due to absence of high shear stress and resulting temperature increase in this conveying zone, the highly viscous state of the blend and softening of the polymer particles is further prolonged. At the end, an increase in torque and SME is obtained, as it was observed for PEG and IBU containing COP blends [36].

In summary, Ludovic® could simulate extrusion trials with exceptions. Since the software is not able to consider any phase segregation effects and further specific behavior of blends with low melting point substances (IBU and PEG), the experimental SME might be higher than calculated by Ludovic®. However, except few limitations the software reliably estimates extrusion trials. Thus, Ludovic® can be used to validate, whether the model-based melt viscosity, derived from our T_g-viscosity correlation, is leading to the same outcome as measured melt viscosity would do. This procedure would enable a computation with less effort for estimating a good starting point for extrusion trials in early drug development.

6.7.3 **Estimation of viscosity data and their application for extrusion simulation**

In the Ludovic® simulation software, the melt viscosity has to be defined as a function of shear rate and temperature. In this study, we used the Carreau-Yasuda equation for the shear rate-dependency and the William-Landel-Ferry fit for the temperature-dependency [37–40]. To estimate the melt viscosity by using only the T_g of an ASD and the melt viscosity of pure COP, we applied the following procedure:

In our recent work, we proposed a correlation between T_g and zero-shear viscosity which was described by (Eq. (6.2)),

$$\eta_0 = a \cdot e^{b \cdot T_g} \tag{6.2}$$

where η_0 is the zero-shear viscosity at a set reference temperature, *a* and *b* are variables [34]. The reference temperature is the temperature where the melt viscosity was derived from to estimate *a* and *b* (Fig 6.3).

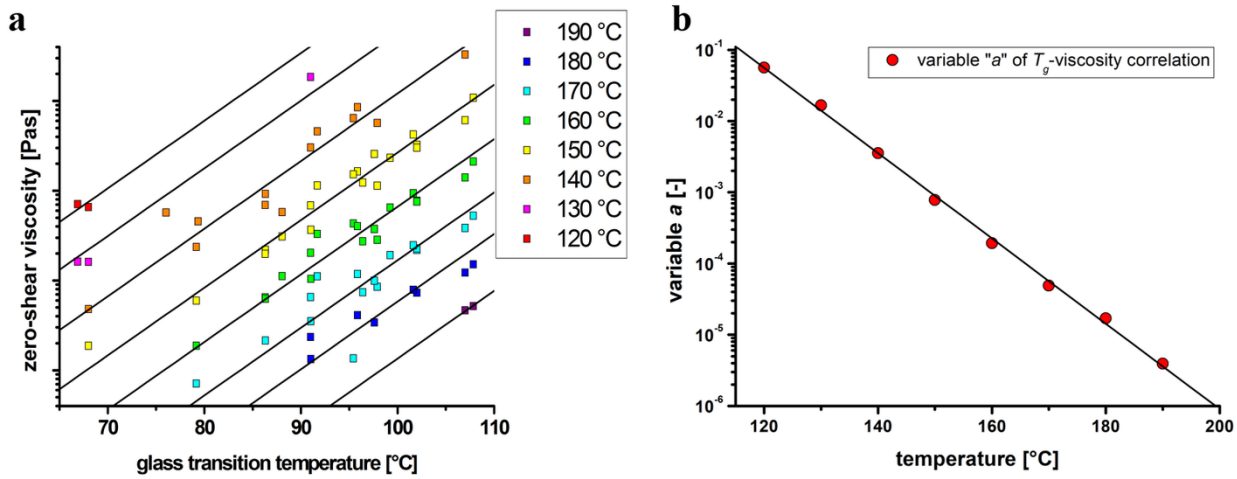

Figure 6.3a-b *Correlation between glass transition temperature and zero-shear viscosity (a) and the temperature dependency of a (b).*

Further investigations indicated that variable *b* was constant as a function of temperature whereas variable *a* had a logarithmic temperature-dependency (Fig 6.3b). Therefore, extrapolation was conducted by setting b as constant and only *a* was separately adjusted for each temperature (Fig 6.3). This T_g-viscosity correlation was applied to calculate η_0 of the investigated blends to use it for the Carreau-Yasuda equation. A reduced version of the Carreau-Yasuda equation was employed to describe the shear rate-dependent flow (Eq. (6.3)),

$$\eta = \eta_0 \cdot [1 + (\lambda\dot{\gamma})^a]^{(n-1)/a} \tag{6.3}$$

where *n* and *a* are constants and *λ* is a temperature-dependent relaxation time [37,38]. For the later procedure, *n* and *a* were taken from pure COP to estimate the melt viscosity of a desired blend. In the case of *λ* and due its temperature- and T_g-dependency, it was adjusted by (Eq. (6.4)),

$$a_T = \frac{\eta_{0,blend}}{\eta_{0,COP}} \quad \text{and} \quad a_T = \frac{\lambda_{blend}}{\lambda_{COP}} \tag{6.4}$$

where the index “COP” denotes the data of pure COP at a set reference temperature and index “blend” the desired blend with known T_g.

Furthermore, the William-Landel-Ferry fit (WLF-fit, Eq. (6.5)) was employed to describe the temperature-dependency of melt viscosity,

$$\log(a_T) = \frac{-C_1\,(T-T_0)}{C_2+(T-T_0)} \tag{6.5}$$

where C_1 and C_2 are empirical constants, T_0 is the reference temperature and T is the desired temperature [39,40]. In our further procedure, C_1 and C_2 were taken from pure COP data at a set reference temperature. In summary to estimate the melt viscosity of a desired blend with the help of the Carreau-Yasuda and WLF-fit, η_0 and λ were adjusted to the desired blend by using its T_g, whereas all other parameters were taken from pure COP data at the same reference temperature.

In Figure 6.4, model-based and measured melt viscosity of the investigated blends were shown. In the case of model-based melt viscosity, IMC 5 % and PEG 1.38 % had identical glass transition temperatures thus the same model-based melt viscosity curve was obtained, the same happened for IMC 20 % and DPD 32.5 %. In the case of T_g-group 1, the melt viscosity data were almost identical.

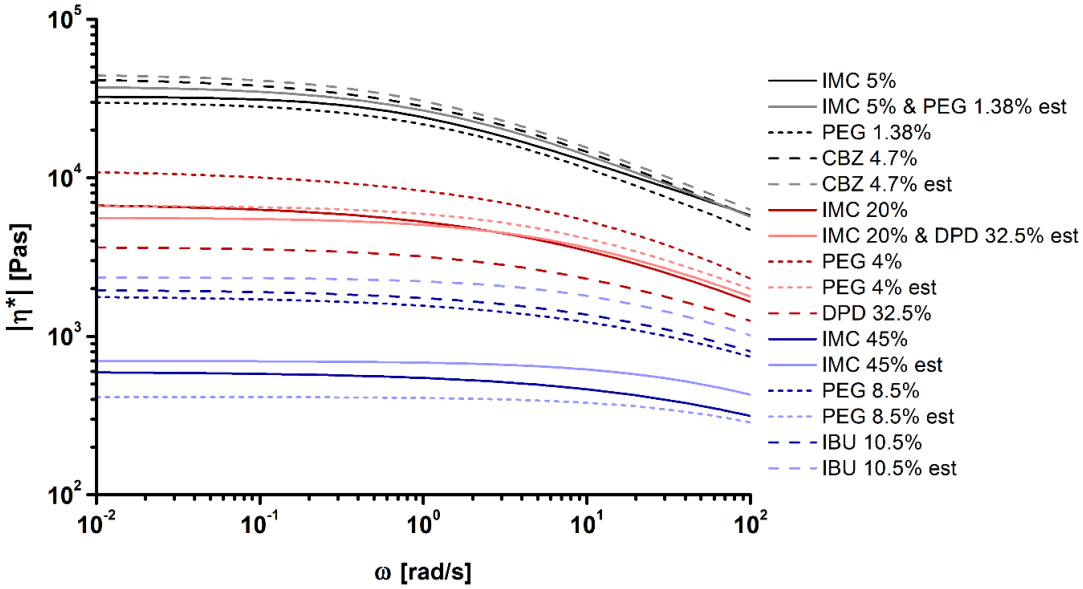

Figure 6.4 *Comparison of Carreau-Yasuda fits from experimental (dark colour) and estimated viscosity (pale colour) at 150 °C, T_g-group 1 in black, T_g-group 2 in red and T_g-group 3 in blue.*

With increasing API-content and decreasing T_g, the difference between the model-based melt viscosity and measured viscosity increased from T_g-group 1 to T_g-group 3. The highest variation was found for PEG 8.5 % where the model-based melt viscosity (η_0 = 415 Pa·s) was much lower than the measured melt viscosity (η_0 = 1,796 Pa·s). This behavior might be triggered by inhomogeneities in the PEG-COP mixture during DSC measurements, as we already described in our recent work [34]. Therefore, this variation is more due to measuring issues in DSC than to a limitation in our correlation. Concerning the two temperature regimes, no substantial difference in data accuracy between them could be found.

To investigate, whether the difference in model-based and measured melt viscosity is mainly influencing the simulation of extrusion trials, measured SME in extrusion trials, conventional simulation and simulation by using a model-based melt viscosity and COP physical properties, were compared (Fig 6.5).

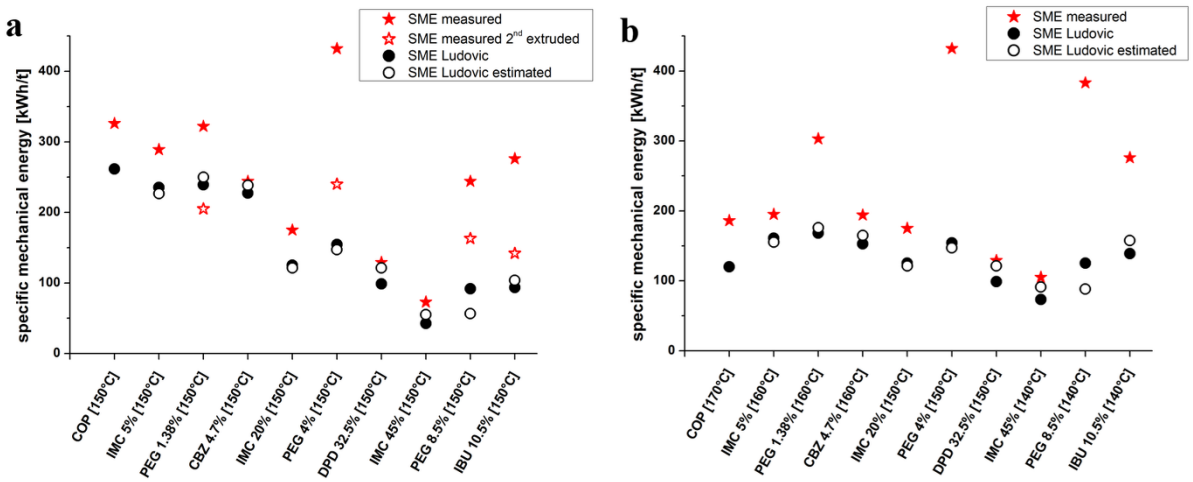

Figure 6.5a-b *Comparison of specific mechanical energy (SME) evaluated by extrusion experiments, extrusion simulation with measured and estimated viscosity at a fixed temperature (150 °C) (a) and temperature gradient (140 – 170 °C) (b).*

In all cases, the model-based simulation was similar to the conventional simulation. Due to measuring issues during T_g determination by means of DSC, PEG 8.5 % had the highest deviation of 38 % between model-based and conventional simulation by Ludovic®. In most cases, the simulated SMEs by using model-based melt viscosity

deviated not more than approx. 10 % from the conventional simulation with measured melt viscosity of the blend. However, due to the high API content of IMC 45 % and DPD 32.5 %, the SME varied of approx. 25 % from the conventional simulation. At the end, the simulation of IMC 45 % and DPD 32.5 % with model-based viscosity superimposed more with the experimental SME, compared to the conventional simulation but this might be coincidental.

In conclusion, an estimation of melt viscosity for amorphous solid dispersion to predict the energy consumption of later extrusion trials by using the simulation software Ludovic® was feasible. Accordingly, our proposed procedure can be used prior any extrusion run in early stage development. It reduces the effort of physicochemical characterization of each formulation that should be investigated. However, as a proof of concept, the evaluation of APIs in COP and ASD thereof, which were not considered to establish the T_g-viscosity correlation in the first place, is still ongoing work.

6.7.4 **Comparison of residence time distribution**

Residence time distribution (RTD) was compared between the experimental data, conventional simulation and simulation by using model-based melt viscosity. The time of onset (t_{Onset}), peak (t_{Peak}), mean (t_{Mean}) and offset (t_{Offset}), where 95 % of the API/Tracer was washed out, were investigated. Both temperature regimes were evaluated but no variation in data could be found (data not shown). Therefore, only RTD measurements and computation at 150 °C are presented (Table 6.3).

Table 6.3 *Residence time distributions at 150 °C of extrusion experiments and computation by Ludovic® using either experimental characteristics of the COP-blend, or estimated viscosity and physical properties of pure COP.*

RTD parameter [s]	COP	T_g-group 1 (T_g: ~102 °C)			T_g-group 2 (T_g: ~91 °C)			T_g-group 3 (T_g: ~80 °C)		
		IMC 5%	PEG 1.38%	CBZ 4.7%	IMC 20%	PEG 4%	DPD 32.5%	IMC 45%	PEG 8.5%	IBU 10.5%
Measured residence time distribution										
t_{Onset}	116	110	129	114	147	137	139	136	162	159
(± SD)	*(± 12)*	*(± 5)*	*(± 9)*	*(± 13)*	*(± 20)*	*(± 17)*	*(± 22)*	*(± 5)*	*(± 19)*	*(± 36)*
t_{Peak}	246	260	289	258	280	301	299	293	328	319
(± SD)	*(± 28)*	*(± 18)*	*(± 25)*	*(± 17)*	*(± 8)*	*(± 3)*	*(± 11)*	*(± 22)*	*(± 7)*	*(± 21)*
t_{Mean}	**297**	**315**	**339**	**310**	**327**	**354**	**331**	**361**	**376**	**383**
(± SD)	***(± 31)***	***(± 7)***	***(± 21)***	***(± 8)***	***(± 2)***	***(± 4)***	***(± 26)***	***(± 6)***	***(± 5)***	***(± 4)***
t_{Offest} **(95%)**	472	497	529	477	488	522	501	557	578	578
(± SD)	*(± 50)*	*(± 1)*	*(± 69)*	*(± 23)*	*(± 5)*	*(± 2)*	*(± 58)*	*(± 11)*	*(± 9)*	*(± 31)*
Simulated residence time distribution with measured viscosity										
t_{Onset}	153	154	157	154	164	157	152	172	165	159
(± SD)	*(± 23)*	*(± 13)*	*(± 17)*	*(± 6)*	*(± 7)*	*(± 7)*	*(± 6)*	*(± 8)*	*(± 7)*	*(± 12)*
t_{Peak}	262	264	267	263	282	268	260	296	282	269
(± SD)	*(± 40)*	*(± 23)*	*(± 33)*	*(± 10)*	*(± 13)*	*(± 10)*	*(± 11)*	*(± 13)*	*(± 14)*	*(± 24)*
t_{Mean}	**350**	**354**	**356**	**352**	**377**	**358**	**347**	**397**	**376**	**360**
(± SD)	***(± 54)***	***(± 32)***	***(± 44)***	***(± 15)***	***(± 18)***	***(± 15)***	***(± 15)***	***(± 18)***	***(± 18)***	***(± 32)***
t_{Offest} **(95%)**	606	613	614	610	655	617	602	690	651	622
(± SD)	*(± 96)*	*(± 57)*	*(± 78)*	*(± 26)*	*(± 32)*	*(± 26)*	*(± 27)*	*(± 32)*	*(± 31)*	*(± 57)*
Simulated residence time distribution with estimated viscosity, physical properties of pure COP										
t_{Onset}	-	154	161	153	161	157	149	172	165	159
(± SD)		*(± 13)*	*(± 11)*	*(± 6)*	*(± 7)*	*(± 6)*	*(± 6)*	*(± 8)*	*(± 7)*	*(± 12)*
t_{Peak}	-	263	275	261	276	257	256	269	282	269
(± SD)		*(± 24)*	*(± 22)*	*(± 10)*	*(± 13)*	*(± 11)*	*(± 11)*	*(±13)*	*(± 14)*	*(± 24)*
t_{Mean}	-	**352**	**366**	**350**	**369**	**356**	**342**	**397**	**376**	**360**
(± SD)		***(± 32)***	***(± 28)***	***(± 15)***	***(± 17)***	***(± 15)***	***(± 15)***	***(± 18)***	***(± 18)***	***(± 32)***
t_{Offest} **(95%)**	-	610	632	607	641	615	592	690	651	622
(± SD)		*(± 57)*	*(± 50)*	*(± 26)*	*(± 31)*	*(± 27)*	*(± 27)*	*(± 32)*	*(± 31)*	*(± 57)*

In the case of experimental RTD, the lowest mean residence time (MRT) of 297 s was observed for COP. The MRT further increased from T_g-group 1 (approx. 320 s) to T_g-group 2 (approx. 340 s) and T_g-group 3 (approx. 370 s). In the case of IMC, CBZ, and DPD-containing blends, the increase in RTD corresponded to an increase in API content (MRT: CBZ 4.7 % < IMC 5 % < IMC 20 % < DPD 32.5 % < IMC 45 %). CBZ 4.7 % with the lowest API content exhibited the lowest MRT of 310 s and IMC 45 %, with the highest API content, achieved the highest MRT of 361 s. The increased MRT at high API content might be a reason of the higher API particle fraction. When the API content is increased, API particles were longer present as in low API-content blends, since the process of API-dissolution within the polymer is prolonged. If a considerable fraction of API particles is present, the material tends to plug flow (likely due to insufficient tackiness to extruder barrel wall) which decreased the forward transport in the extruder. Therefore, an increasing API or particle fraction was increasing the RTD, respectively.

In the case of COP blends containing low melting point substances (IBU, PEG), the RTD further increased, compared to the other COP-blends. The MRT increased from PEG 1.38 % (MRT: 339 s) to IBU 10.5 % (MRT: 383 s), again as a function of API content (MRT: PEG 1.38 % < PEG 4 % < PEG 8.5 % < IBU 10.5 %). In general, an extruder is performing like a spindle pump but in an ineffective way. Therefore, adhesion between the specimen and barrel is needed to transport material forward. In case of low melting point substances, this transport is decreased as a reason of a low viscous melt prior the softening of the COP particles. This reduced forward transport explains the higher RTD compared to the other COP-blends. Additionally, the COP-blends containing PEG and IBU were extruded twice at 150 °C to evaluate if the same behavior, as in SME measurements, was present. In all cases, no differences in RTD between the first and the second extrusion run was observed (data not shown).

However, the highest influence on RTD in our experiments had the feed rate and the filling fluctuation of the volumetric feeder used, respectively. Furthermore, the RTD measurement at a small-scale extruder are always uncertain compared to measurements at larger scale extruders. In general, RTD is mainly influenced by throughput and screw speed and less by temperature and melt viscosity [41,42].

Regarding the HME experiments and conventional simulation, the RTD was in good accordance to each other. However, t_{Onset} and the mean residence time (MRT, t_{mean}) were up to 60 s higher computed than measured. The highest deviation of MRT between experimental and computed MRT was found for pure COP with 18 %. Especially in simulation, the MRT seemed constant between the different T_g-groups. The highest MRT was found for IMC 45 %, which might be triggered by a low T_g and melt viscosity. Additionally, no tendency in the slight t_{Peak} variation was found. Furthermore, t_{Offset} differed between experimental data (472 s – 578 s) and conventional simulation (602 s – 690 s). Since the RTD is measured in HME by using iron oxide and a camera, the camera might not be able to detect very low concentration of tracer, which led to a decrease in t_{Offset}. In summary, although there was some deviation between simulated and measured RTD, the validation of the accuracy in simulation, when model-based melt viscosity etc. were used instead of measured properties, might be sufficient.

In the case of simulation using model-based melt viscosity and physicochemical properties of COP, the RTD superimposed with the conventional simulation. The deviation in data did not exceed 3 % thus using model-based values in simulation did not influence the RTD calculation. Consequently, the use of model-based values in terms of HME simulation for the production of ASD was not influencing the computation of RTD. However, differences (up to 60 s) between computed and real-time measurements were present which might be related to the volumetric feeder (variance in feed rate) used or due to limitations in computation.

6.8 Discussion

In most cases Ludovic®, as an easy one-dimensional model to simulate hot-melt extrusion with low computation time, the simulation was consistent with HME experiments. The higher SME derived from HME trials compared to the simulation was likely triggered by energy loss between the gearbox and the rotating screws (Fig 6.2). Therefore, this behavior might be related to the specific 12 mm extruder used and less to the simulation software itself. It is expected to be more accurate when using another extruder, especially larger size extruders with better torque transmission and instrumentation spread over the entire process length of the extruder (multiple temperature and

pressure readings). In general, deviations between experimental and simulated SMEs are multifactorial. It might be related to the torque transmission, but also due to a vague extruder temperature measurement, changes in viscosity during extrusion (due to API melting and/or degradation) or issues during simulation (simplifications). For evaluating the various factor susceptibility on overall simulation accuracy, additional experiments and subsequent simulations at various scale and extrusion setup are needed. Especially, the simulation failed and calculated a much lower energy consumption than present when low melting point substances were regarded (Fig 6.2a). By extruding PEG and IBU containing COP-blends twice, the reason for this gap between computed and measured SME was identified as phase segregation effects during HME experiments. Furthermore, the softening of the polymer was prolonged and shifted from the kneading block to the conveying zone, further increasing the SME. However, to validate the use of model-based melt viscosity instead of measured melt viscosity for simulation purposes, Ludovic® was feasible.

Conventional simulation and simulation by using only the glass transition temperature to estimate the melt viscosity of a blend, led to similar outcomes. Therefore, a similar accuracy in hot-melt extrusion simulation was achieved, compared to the conventional simulation. Furthermore, using the physical properties of COP (e.g. true density and heat capacity) instead of a desired blend was feasible without any exceptions (Table 6.2, Fig 6.2). Using model-based melt viscosity data by taking the constants of Carreau-Yasuda equation (e.g. n, a) and WLF-fit (e.g. C_1, C_2) of pure COP and adjusting λ and η_0 to the T_g of a desired blend, led to an accurate estimation in most cases (Fig 6.3, 6.4). In contrast, an imprecise estimation of melt viscosity, for example due to a high drug content, would subsequently lead to a more and more vague HME simulation, as it was seen for IMC 45 % and DPD 32.5 % (Fig 6.5). Furthermore, the accurate estimation of melt viscosity depended heavily on a valid T_g-measurement by means of DSC. It was seen for PEG 8.5 %, biased T_gs by inhomogeneity during DSC measurement likely caused an inaccurate estimate of melt viscosity and furthermore an imprecise HME simulation.

In the case of residence time distribution, an increase as a function of API/plasticizer content was observed (Table 6.3). Due to the higher fraction of API/plasticizer particles, plug flow was increased. Thus, the forward transport in the extruder was decreased and the RTD prolonged. The presence of low melting point substances within the blend further prolonged the MRT, due to a decreased forward transport induced by a low viscous melt prior the softening of COP. Regarding the difference between conventional simulated and experimental RTD, a variation of up to 18 % in MRT was observed. This might be related to the volumetric feeder and/or small-scale extruder used or due to limitations in computation. However, the deviation of conventional simulation and simulation using model-based melt viscosity was negligible. Therefore, using model-based melt viscosity and the properties of the pure polymeric matrix to calculate RTD is sufficient.

To conclude, simulation with model-based melt viscosity data provided similar results than conventional computation for both: energy consumption or residence time distribution. Therefore, our method enables the “shortcut” of experimental data to a simple T_g measurement of a desired formulation and the characterization of the polymer matrix only. This simplifies the use of hot-melt extrusion simulation at an early stage of development where several formulations need to be tested. It supports a rational development and it leads to reduction of needed extrusion trials to define the best formulation and process conditions to form ASD.

6.9 Conclusion

A method to “shortcut” experimental data for the use in hot-melt extrusion simulation (1D simulation software Ludovic®) was established and validated. Several process characteristics of HME (e.g. residence time distribution, energy consumptions) and physical properties (e.g. heat capacity, density, melt rheology) of the investigated mixtures has been considered. The use of model-based melt viscosity by using only the glass transition temperature of the blend, led to similar simulation outcomes as with measured melt viscosity, if a critical API content was not exceeded (approx. 30 %). By using model-based melt viscosity data and further physical properties (e.g. true density, heat capacity, melt viscosity) of the pure polymeric matrix, the experimental effort

prior to HME simulation was minimized. However, the accuracy of conventional simulation needs to be improved and influencing factors, which increase deviations between experiment and simulation, has to be determined in more detail. In conclusion, our procedure enables the estimation of a good starting point for HME trials. This supports a rational development for forming amorphous solid dispersions and it leads to a reduction of extrusion trials needed to define the best formulation and process conditions in HME.

6.10 Acknowledgement

The authors would like to thank our partner Sciences Computers Consultants (Saint Etienne, France), especially Philippe David, Giang Trinh and Laurent Ratte for their scientific support and always having an open ear and last but not least for sponsoring the software license. The collaboration with Sciences Computers Consultants includes the improvement of the simulation software and the development of new add-on tools and libraries. Furthermore, we would like to thank Rachel C. Evans greatly for reviewing the manuscript and Kevin Kayser for his experimental assistance. This research did not receive any specific grant from funding agencies in the public, commercial, or not-for-profit sectors other than the above mentioned free use of the software license for Ludovic®.

6.11 References

[1] H. Patil, R.V. Tiwari, M.A. Repka, Hot-Melt Extrusion: from Theory to Application in Pharmaceutical Formulation, AAPS PharmSciTech. 17 (2016) 20–42. doi:10.1208/s12249-015-0360-7.

[2] R.V. Tiwari, H. Patil, M.A. Repka, Contribution of hot-melt extrusion technology to advance drug delivery in the 21st century, Expert Opin. Drug Deliv. 13 (2016) 451–464. doi:10.1517/17425247.2016.1126246.

[3] J.S. LaFountaine, J.W. McGinity, R.O. Williams, Challenges and Strategies in Thermal Processing of Amorphous Solid Dispersions: A Review, AAPS PharmSciTech. (2015). doi:10.1208/s12249-015-0393-y.

[4] A. Newman, G. Knipp, G. Zografi, Assessing the performance of amorphous solid dispersions, J. Pharm. Sci. 101 (2012) 1355–1377. doi:10.1002/jps.23031.

[5] P. Piccinni, Y. Tian, A. McNaughton, J. Fraser, S. Brown, D.S. Jones, S. Li, G.P. Andrews, Solubility parameter-based screening methods for early-stage formulation development of itraconazole amorphous solid dispersions, J. Pharm. Pharmacol. 68 (2016) 705–720. doi:10.1111/jphp.12491.

[6] Y. He, C. Ho, Amorphous Solid Dispersions: Utilization and Challenges in Drug Discovery and Development, J. Pharm. Sci. 104 (2015) 3237–3258. doi:10.1002/jps.24541.

[7] B. Lang, J.W. McGinity, R.O. Williams, Hot-melt extrusion – basic principles and pharmaceutical applications, Drug Dev. Ind. Pharm. 40 (2014) 1133–1155. doi:10.3109/03639045.2013.838577.

[8] A.M. Agrawal, M.S. Dudhedia, E. Zimny, Hot Melt Extrusion: Development of an Amorphous Solid Dispersion for an Insoluble Drug from Mini-scale to Clinical Scale, AAPS PharmSciTech. 17 (2016) 133–147. doi:10.1208/s12249-015-0425-7.

[9] D.E. Zecevic, K.G. Wagner, Rational Development of Solid Dispersions via Hot-Melt Extrusion Using Screening, Material Characterization, and Numeric Simulation Tools, J. Pharm. Sci. 102 (2013) 2297–2310. doi:10.1002/jps.23592.

[10] T. Sakai, M. Thommes, Investigation into mixing capability and solid dispersion preparation using the DSM Xplore Pharma Micro Extruder: Small-scale HME, J. Pharm. Pharmacol. 66 (2014) 218–231. doi:10.1111/jphp.12085.

[11] S. Guns, V. Mathot, J.A. Martens, G. Van den Mooter, Upscaling of the hot-melt extrusion process: Comparison between laboratory scale and pilot scale production of solid dispersions with miconazole and Kollicoat® IR, Eur. J. Pharm. Biopharm. 81 (2012) 674–682. doi:10.1016/j.ejpb.2012.03.020.

[12] J. Thiry, F. Krier, B. Evrard, A review of pharmaceutical extrusion: Critical process parameters and scaling-up, Int. J. Pharm. 479 (2015) 227–240. doi:10.1016/j.ijpharm.2014.12.036.

[13] D.E. Zecevic, Solid dispersion via hot melt extrusion - formulation and process aspects, Dissertation, Eberhard Karls Universität, 2014.

[14] J. Gupta, C. Nunes, S. Vyas, S. Jonnalagadda, Prediction of Solubility Parameters and Miscibility of Pharmaceutical Compounds by Molecular Dynamics Simulations, J. Phys. Chem. B. 115 (2011) 2014–2023. doi:10.1021/jp108540n.

[15] A. Paudel, J. Van Humbeeck, G. Van den Mooter, Theoretical and Experimental Investigation on the Solid Solubility and Miscibility of Naproxen in Poly(vinylpyrrolidone), Mol. Pharm. 7 (2010) 1133–1148. doi:10.1021/mp100013p.

[16] Y. Zhao, P. Inbar, H.P. Chokshi, A.W. Malick, D.S. Choi, Prediction of the thermal phase diagram of amorphous solid dispersions by flory-huggins theory, J. Pharm. Sci. 100 (2011) 3196–3207. doi:10.1002/jps.22541.

[17] S.O. Kyerematen, M. Pudlas, G.H. Woehrle, A Fast and Reliable Empirical Approach for Estimating Solubility of Crystalline Drugs in Polymers for Hot Melt Extrusion Formulations, J. Pharm. Sci. 103 (2014) 2847–2858. doi:10.1002/jps.23941.

[18] Y. Sun, J. Tao, G.G.Z. Zhang, L. Yu, Solubilities of crystalline drugs in polymers: An improved analytical method and comparison of solubilities of indomethacin and nifedipine in PVP, PVP/VA, and PVAc, J. Pharm. Sci. (2010) n/a-n/a. doi:10.1002/jps.22251.

[19] J. Tao, Y. Sun, G.G.Z. Zhang, L. Yu, Solubility of Small-Molecule Crystals in Polymers: d-Mannitol in PVP, Indomethacin in PVP/VA, and Nifedipine in PVP/VA, Pharm. Res. 26 (2009) 855–864. doi:10.1007/s11095-008-9784-z.

[20] E.S. Bochmann, D. Neumann, A. Gryczke, K.G. Wagner, Micro-scale prediction method for API-solubility in polymeric matrices and process model for forming amorphous solid dispersion by hot-melt extrusion, Eur. J. Pharm. Biopharm. 107 (2016) 40–48. doi:10.1016/j.ejpb.2016.06.015.

[21] M.S. Dudhedia, A.M. Agrawal, Rheological study of copovidone and solid dispersion blend used for hot melt extrusion, J. Appl. Polym. Sci. 133 (2016) n/a-n/a. doi:10.1002/app.43278.

[22] J. Aho, M. Edinger, J. Botker, S. Baldursdottir, J. Rantanen, Oscillatory Shear Rheology in Examining the Drug-Polymer Interactions Relevant in Hot Melt Extrusion, J. Pharm. Sci. 105 (2016) 160–167. doi:10.1016/j.xphs.2015.11.029.

[23] F. Yang, Y. Su, J. Zhang, J. DiNunzio, A. Leone, C. Huang, C.D. Brown, Rheology Guided Rational Selection of Processing Temperature To Prepare Copovidone–Nifedipine Amorphous Solid Dispersions via Hot Melt Extrusion (HME), Mol. Pharm. 13 (2016) 3494–3505. doi:10.1021/acs.molpharmaceut.6b00516.

[24] S.-Y. Chan, S. Qi, D.Q.M. Craig, An investigation into the influence of drug–polymer interactions on the miscibility, processability and structure of polyvinylpyrrolidone-based hot melt extrusion formulations, Int. J. Pharm. 496 (2015) 95–106. doi:10.1016/j.ijpharm.2015.09.063.

[25] A. Mahieu, J.-F. Willart, E. Dudognon, F. Danède, M. Descamps, A New Protocol To Determine the Solubility of Drugs into Polymer Matrixes, Mol. Pharm. 10 (2013) 560–566. doi:10.1021/mp3002254.

[26] J. Aho, J.P. Boetker, S. Baldursdottir, J. Rantanen, Rheology as a tool for evaluation of melt processability of innovative dosage forms, Int. J. Pharm. 494 (2015) 623–642. doi:10.1016/j.ijpharm.2015.02.009.

[27] J. Grimard, L. Dewasme, A. Vande Wouwer, A Review of Dynamic Models of Hot-Melt Extrusion, Processes. 4 (2016) 19. doi:10.3390/pr4020019.

[28] J. Rantanen, J. Khinast, The Future of Pharmaceutical Manufacturing Sciences, J. Pharm. Sci. 104 (2015) 3612–3638. doi:10.1002/jps.24594.

[29] A. Durin, P. De Micheli, H.-C. Nguyen, C. David, R. Valette, B. Vergnes, Comparison between 1D and 3D Approaches for Twin-Screw Extrusion Simulation, Int. Polym. Process. 29 (2014) 641–648.

[30] A. Gaspar-Cunha, J.A. Covas, B. Vergnes, Defining the configuration of co-rotating twin-screw extruders with multiobjective evolutionary algorithms, Polym. Eng. Sci. 45 (2005) 1159–1173. doi:10.1002/pen.20391.

[31] M. Maus, K.G. Wagner, A. Kornherr, G. Zifferer, Molecular dynamics simulations for drug dosage form development: thermal and solubility characteristics for hot-melt extrusion, Mol. Simul. 34 (2008) 1197–1207. doi:10.1080/08927020802411695.

[32] A. Prudic, Y. Ji, G. Sadowski, Thermodynamic Phase Behavior of API/Polymer Solid Dispersions, Mol. Pharm. 11 (2014) 2294–2304. doi:10.1021/mp400729x.

[33] F. Meng, V. Dave, H. Chauhan, Qualitative and quantitative methods to determine miscibility in amorphous drug–polymer systems, Eur. J. Pharm. Sci. 77 (2015) 106–111. doi:10.1016/j.ejps.2015.05.018.

[34] E.S. Bochmann, E.E. Üstüner, A. Gryczke, K.G. Wagner, Predicting melt rheology for hot-melt extrusion by means of a simple Tg -measurement, Eur. J. Pharm. Biopharm. 119 (2017) 47–55. doi:10.1016/j.ejpb.2017.05.010.

[35] B. Vergnes, G.D. Valle, L. Delamare, A global computer software for polymer flows in corotating twin screw extruders, Polym. Eng. Sci. 38 (1998) 1781–1792.

[36] K. Kohlgrüber, M. Bierdel, Co-rotating twin-screw extruders: fundamentals, technology, and applications, Carl Hanser Publishers ; Hanser Gardner Publications, Munich [Germany] : Cincinnati, Ohio, 2008.

[37] Yasuda, Kenji, Investigation of the analogies between viscometric and linear viscoelastic properties of polystyrene fluids, Ph.D. thesis, Massachusetts Inst. of Technology, 1979.

[38] P.J. Carreau, Rheological Equations from Molecular Network Theories, Trans. Soc. Rheol. 16 (1972) 99–127. doi:10.1122/1.549276.

[39] A.K. Doolittle, Studies in Newtonian Flow. II. The Dependence of the Viscosity of Liquids on Free-Space, J. Appl. Phys. 22 (1951) 1471–1475. doi:10.1063/1.1699894.

[40] M.L. Williams, R.F. Landel, J.D. Ferry, The Temperature Dependence of Relaxation Mechanisms in Amorphous Polymers and Other Glass-forming Liquids, J. Am. Chem. Soc. 77 (1955) 3701–3707. doi:10.1021/ja01619a008.

[41] M.A. Repka, N. Langley, J. DiNunzio, eds., Melt Extrusion, Springer New York, New York, NY, 2013. http://link.springer.com/10.1007/978-1-4614-8432-5 (accessed September 24, 2015).

[42] P.G. Lafleur, Polymer extrusion, ISTE Ltd/John Wiley and Sons Inc, Hoboken, NJ, 2014.

7 Validation of model-based melt viscosity in hot-melt extrusion numerical simulation

Esther S. Bochmann [a]; Andreas Gryczke [b]; Karl G. Wagner [a]

[a] Department of Pharmaceutical Technology and Biopharmaceutics, University of Bonn, Bonn, Germany

[b] AbbVie Deutschland GmbH & Co. KG, Ludwigshafen am Rhein, Germany

This part was published as

E.S. Bochmann, A. Gryczke, K.G. Wagner, Validation of Model-Based Melt Viscosity in Hot-Melt Extrusion Numerical Simulation, Pharmaceutics. 10(3) (2018) 132. doi.org/10.3390/pharmaceutics10030132.

7.1 Graphical abstract

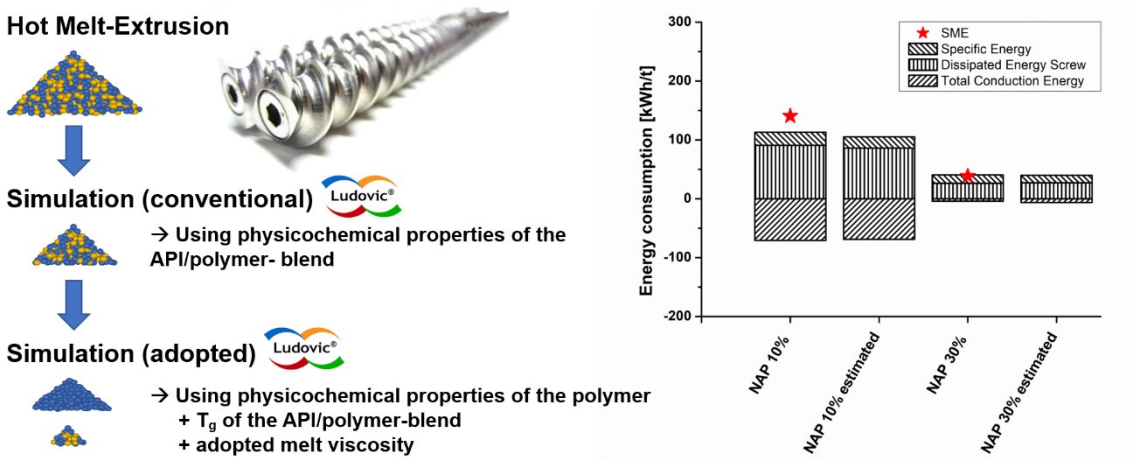

7.2 Abstract

A validation for the use of model-based melt viscosity in hot-melt extrusion numerical simulations was presented. Here, the melt viscosity of an amorphous solid dispersion (ASD) was calculated by using its glass transition temperature (T_g) and the rheological flow profile of the pure polymeric matrix. All further required physical properties were taken from the pure polymer. For forming the ASDs, four active pharmaceutical ingredients (APIs), that had not been considered in first place to establish the correlation between T_g and melt viscosity were examined. The ASDs were characterized in terms of density, specific heat capacity, melt rheology, API solubility in the polymeric matrix, and deviation from the Couchman–Karasz fit to, identify the influencing factors of the accuracy of the simulation using model-based melt viscosity. Furthermore, the energy consumption of the hot-melt extrusion (HME) experiments, conventional simulation, and simulation using model-based melt viscosity were compared. It was shown, with few exceptions, that the use of model-based melt viscosity in terms of the HME simulation did not reduce the accuracy of the computation outcome. The commercial one-dimensional (1D) simulation software Ludovic® was used to conduct all of the numerical computation. As model excipients, vinylpyrrolidone-vinyl acetate copolymer (COP) in combination with four APIs (celecoxib, loratadine, naproxen, and praziquantel) were investigated to form the ASDs.

7.3 Keywords

hot-melt extrusion, melt rheology, glass transition temperature, amorphous solid dispersion, simulation, prediction model

7.4 Chemical compounds studied in this article

Celecoxib (PubChem CID: 2662); Loratadine (PubChem CID: 3957); Naproxen (PubChem CID: 156391); Praziquantel (PubChem CID: 4891); Copovidone (PubChem CID: 25086-89-9)

7.5 Introduction

Nowadays, one of the major challenges in pharmaceutical small molecule formulation development is the increasing number of poorly soluble active pharmaceutical ingredients (APIs) and the respective poor bioavailability. To enhance the solubility of these APIs, the formation and stabilization of amorphous solid dispersions (ASDs) is commonly used. For manufacturing ASDs, hot-melt extrusion (HME), as a continuous and solvent-free process, was often reported [1–6]. Unfortunately, HME is a time and API-consuming procedure, especially in early ASD formulation development, as the various process parameters, such as screw speed, throughput, screw configuration, and temperature profile lead to a complex multivariable process, which is challenging to optimize or scale-up [7–9].

Simulation has been found to be a valid and useful tool to ease HME optimization, scale-up, and to improve the comprehension of the processes itself in order to reduce the remaining API crystallinity and degradation [7,9–12]. By using simulation, the temperature, pressure, and shear profiles along the screws are computed and the process window for HME can be defined [13]. However, the main drawback of HME simulation is the need for experimental product input data to conduct computation. In some cases, these data are not easy to access, especially in terms of melt rheology and thermosensitive APIs. Furthermore, the use of simulation for early formulation screening is limited, as the physicochemical characteristics would need to be laboriously measured

for every formulation under consideration. As simulation is an inevitable tool to evaluate a potential adiabatic scale-up from small- to large-scale extruders, the above-mentioned drawbacks of HME simulation need to be solved [9].

Several challenges in performing the HME simulation were already addressed by several researchers. In the case of screw configuration optimization, different algorithms and process modellings have been used to define the best operating conditions for an extrusion process [12,14]. Investigations into improve the understanding of the extruder performance in mixing capability, mixing elements, and kneading blocks as a function of the staggering angle were evaluated [15]. It was shown that distributive mixing is more related to the staggering angle than to the disc width, and that mixing elements did not performed significantly better than normal conveying elements. Furthermore, the pressure-dependent wall slippage at the barrel and screw surface as well as the modelling fillers in the HME process have been investigated, which is especially important for the extrusion simulation with melt suspensions [16,17]. Investigations on the simulation of residence time distributions (RTD) revealed that the specific throughput, a ratio of throughput over screw speed, is one of the key process parameters in order to control RTD and to determine the flow conditions during extrusion [18,19].

In our recent work, we proposed a procedure to model the melt viscosity of an ASD by using only its glass transition temperature (T_g) and the rheological flow profile of the pure polymeric matrix [20]. It simplifies the application of the HME simulation by reducing the required physicochemical characterization of the ASD. Therefore, the experimental effort was decreased without compromising the accuracy of the computation, which has been proven by comparing the simulation using model-based melt viscosity, conventional simulation, and the data of experimental trials [21]. However, all of the investigated APIs so far were already used to establish the T_g-melt viscosity correlation in the first place, and thus a validation with new APIs is needed.

Therefore, the purpose of this work was to ease the HME simulation by providing evidence for the T_g-melt viscosity correlation. Four APIs (celecoxib, loratadine, naproxen, and praziquantel), which were not used to establish the T_g-melt viscosity correlation in

the first place, were used to form model ASDs of various T_g. As the applied process simulation is not able to predict the physical stability of the ASDs, this paper focuses on the process simulation only. The physical stability of the ASDs would need to be evaluated by other models, as proposed by various authors [22–25]. The ASDs were further characterized in terms of density, specific heat capacity, melt rheology, API solubility in the polymeric matrix, and deviation from the Couchman–Karasz fit. The influence of these factors to the accuracy of the simulation using model-based melt viscosity was evaluated, whereas the density, specific heat capacity, and melt rheology are the input parameter for the simulation itself. The commercial one-dimensional (1D) simulation software, Ludovic® (Sciences Computers Consultants, Saint Etienne, France), was used to conduct the conventional HME simulation and simulation by using model-based melt viscosity and further physicochemical characteristics of the pure polymeric matrix only. Both simulation procedures were compared to the extrusion trials by means of energy consumptions.

7.6 Material and methods

7.6.1 **Material**

Praziquantel (PZQ) was obtained from Divis Laboratories Ltd. (Telangana, India), loratadine (LOR) was purchased from Sris Pharmaceutials (Telangana, India), naproxen (NAP) was received from Sigma Aldrich (St. Louis, MO, USA), and celecoxib (CXB) was obtained from Cadila Pharmaceuticals Ltd. (Ahmedabad, India). Vinylpyrrolidone-vinyl acetate copolymer (copovidone, Kollidon® VA 64, COP) was kindly donated by BASF SE (Ludwigshafen, Germany) (Table 7.1). All of the investigated APIs belong to BCS (Biopharmaceutics classification system) Class II and were thermally stable over the applied temperature range. None of the selected APIs were used to establish the T_g-melt viscosity correlation in the first place, and thus served for model validation [20,21].

Table 7.1 *Physicochemical properties of substances used. The molecular weight was taken from PubChem Substance and Compound databases [26], all other parameters were experimentally determined.*

Substance	Molecular weight [g/mol]	Melting point [°C]	Glass transition temperature [°C]	Heat capacity step at T_g [J/g·K]
Celecoxib (CXB)	381.4	160.9	56.8	0.39
Loratadine (LOR)	382.9	134.6	34.9	0.30
Naproxen (NAP)	230.3	156.1	6.7[1]	0.23
Praziquantel (PZQ)	312.4	138.3	35.9	0.37
Copovidone (COP)	45,000 - 70,000	-	107	0.40

[1]*measured with 10% COP weight fraction because of the active pharmaceutical ingredients (APIs) recrystallization tendency.*

7.6.2 **Methods**

7.6.2.1 Helium pycnometry

The true density of the powder blends and extrudates were measured using the helium pycnometer AccuPyc 1330 (Micromeritics GmbH, Norcross, GA, USA) with 20 purge cycles at a fill pressure of 136.86 kPag. The samples were analyzed in 25 runs or until a standard deviation of 0.01% was reached, using a fill pressure of 136.86 kPag and an equilibration rate of 0.0345 kPag/min. The procedure was repeated two times for every material. The true density of the powder blends and extrudates were used as the input parameters for the HME simulation software, Ludovic®.

7.6.2.2 Differential scanning calorimetry (DSC)

In order to identify the heat capacities and glass transition temperatures of the investigated blends, a DSC 2 (Mettler Toledo, Gießen, Germany) was used. It was equipped with an auto sampler, nitrogen cooling, and nitrogen as purge gas (30 ml/min), and the system was calibrated with n-octane, indium and zinc standards. In the case of the T_g-determination as a function of the API weight fraction, at least three samples for each mixture, of approximately 10 mg, were analyzed in 40 µl aluminum pans with a pierced lid. The T_g-determination was conducted after the annealing of the sample in order to define the solubility of the API in the polymeric melt. Please see section 7.6.2.3 for a more detailed description of the DSC method.

The heat capacities were measured using a sapphire standard in TOPEM® mode (modulated DSC) with 1 K pulse height, 15–30 s pulse width, and an underlying heating rate of 2 K/min. For every blend, three samples of approximately 10 mg were weighed in 40 µl aluminum pans with pierced lids. All of the pans used, including the reference and the pan with the sapphire standard, did not differ more than 0.1 mg in weight from each other. All of the samples were annealed at elevated temperatures for a homogenous API-distribution during the subsequent heat capacity measurement. Every blend for DSC was prepared by using a MM400 ball mill (Retsch GmbH, Haan, Germany) with 30 Hz and 3x 5 min milling cycles.

7.6.2.3 Solubility determination via DSC

To determine the API solubility in vinylpyrrolidone-vinyl acetate copolymer (COP), a protocol of our previous work was used [23]. It determines the solubility of the APIs indirectly, using the glass transition temperature (T_g). The method itself consists of an annealing step and a subsequent T_g analysis of the annealed sample, as well as a further T_g analysis of a completely molten and amorphous sample at elevated temperatures ($T > T_m$).

In more detail, every sample was annealed at a temperature approximately 60 °C above the predicted T_g, blend by the Couchman–Karasz fit, so as to enable a viscous system that promotes an equilibrated state of the solubilized API at the annealing temperature ($T_{Annealing}$). Subsequently, the sample is cooled and heated again by 10 K/min to determine the T_g of this annealed sample. The mentioned heating step ended 10 K above the melting point of the API to obtain a completely amorphous system, which is further analyzed by a cooling–heating cycle with 10 K/min to evaluate the T_g of this amorphous system.

This procedure is conducted by using different API/polymer weight fractions. At the end, the first determined T_g serves as an indicator of the soluble API fraction at $T_{Annealing}$, while the second T_g was used for the characterization of the weight fraction-dependent curve progression of T_g by employing the Brostow Chiu Kalogeras Vassilikou-Dova fit (BCKV-fit, Equation 7.1),

$$T_g = w_1 T_{g,1} + (1 - w_1) T_{g,2} + w_1(1 - w_1)[a_0 + a_1(2w_1 - 1) + a_2(2w_1 - 1)^2] \quad (7.1)$$

where a_0, a_1 and a_2 are variables [27]. The polynomial form of the BCKV-fit enables the consideration of positive and negative deviation from the Couchman-Karasz fit (CK-fit, Equations 7.2-3). It is therefore appropriate for the identification of the solubilized API fraction in the annealed samples, by employing the API weight fraction-dependent curve progression of glass transition temperature.

$$T_g = \frac{w_1 T_{g,1} + k_{CK}(1-w_1) T_{g,2}}{w_1 + k_{CK}(1-w_1)} \quad \text{with} \quad \Delta T_g = T_{g,2} - T_{g,1} \quad (7.2)$$

$$k_{CK} = \frac{\Delta C_{p,2}}{\Delta C_{p,1}} \quad (7.3)$$

In the Couchman-Karasz equation, w is the weight fraction, k_{CK} is the Couchman-Karasz constant C_p the heat capacity step at T_g and the sub-scripts 1 and 2 refer to the API and polymer, respectively [28].

To predict an API solubility phase diagram, the soluble API fraction at a respective temperature was fitted using Equation 7.4,

$$T_{Annealing} = y_0 + A \cdot exp^{R_0 \cdot x} \quad (7.4)$$

where x is the soluble API fraction at the respective temperature, A and R_0 are fitting constants, and y_0 corresponds to the API melting point, but was set as a variable. In general, solubility is referred to as an extrapolation of the dissolved API at 25 °C. Thus, the solubility curve represents the condition at which a crystalline API is solubilized by the polymeric matrix, forming a one phase amorphous solid dispersion.

The obtained solubility curve was confirmed by x-ray powder diffraction (XRPD) measurements, which were in good accordance to the DSC findings (data not shown). In most cases, the XRPD results showed a slightly lower solubility of approximately 5% the API in the polymeric melt than in DSC, as XRPD is more sensitive to crystalline residuals than DSC.

7.6.2.4 Small-amplitude oscillatory shear (SAOS) measurements

The rheometer Haake® MARS® III of Thermo Scientific (Karlsruhe, Germany), equipped with a 20 mm plate-plate geometry was used. For all of the experiments, the gap height was set to 0.75 mm and the amplitude to 5.0%, which was determined as suitable by an amplitude sweep. The measurements were further conducted using the controlled deformation AutoStrain mode, in which the deflection is adjusted to a given amplitude range after every sine wave of deformation. Frequency sweeps were applied in the range of 10 Hz to 0.1 Hz in 10 K steps. The obtained frequency sweeps, in which the specimen was thermorheologically simple, were further employed to create a master curve by means of time temperature superposition (TTS). Consequently, every single frequency sweep is horizontally shifted into one master curve at a set reference temperature. The obtained melt viscosity flow profile was fit to a reduced Carreau-Yasuda equation (CY-equation, Equation 7.5),

$$\eta = \eta_0 \cdot [1 + (\lambda\dot{\gamma})^a]^{(n-1)/a} \tag{7.5}$$

where n and a are constants, λ is a temperature-dependent relaxation time, and η_0 is the zero-shear viscosity [29,30]. The shift factors, a_T, derived from TTS, were employed in the William-Landel-Ferry fit (WLF fit, Equation 7.6) to characterize the temperature-dependent behavior of the blend's melt viscosity.

$$\log(a_T) = \frac{-C_1\,(T-T_0)}{C_2+(T-T_0)} \tag{7.6}$$

C_1 and C_2 are empirical constants, T_0 is the reference temperature, and T is the desired temperature [31,32].

7.6.2.5 Procedure to generate the model-based melt viscosity

In our recent work, we proposed a correlation between T_g and zero-shear viscosity η_0 of an amorphous solid dispersion and its use in HME simulation [20,21]. At a set reference temperature, the rheological flow profile of pure COP with its variables in the CY-fit and WLF-fit served as a starting point for the model-based viscosity calculation. The parameters n and a of the COP CY-fit and the variables in WLF-fit were considered as

constants. The zero-shear viscosity, η_0, was adjusted via the T_g of the investigated blends, using our proposed T_g-melt viscosity correlation (Equation 7.7),

$$\eta_0 = a \cdot e^{b \cdot T_g} \tag{7.7}$$

where *a* and *b* are the empirically determined variables [20]. In the case of *a*, a temperature-dependency was obtained, but *b* remained constant over the investigated temperature range. To adjust λ of CY-fit as well, the ratio between $\eta_{0,COP}$ and $\eta_{0,blend}$ was calculated by Equation 7.8,

$$a_{T,T_g} = \frac{\eta_{0,blend}}{\eta_{0,COP}} \quad \text{and} \quad a_{T,T_g} = \frac{\lambda_{blend}}{\lambda_{COP}} \tag{7.8}$$

and was applied to λ_{COP} to identify λ_{blend}.

7.6.2.6 Computation of extrusion experiments by using the software Ludovic®

The simulation software Ludovic® V6.0.1 PharmaEdition (Sciences Computers Consultants, Saint Etienne, France) for hot-melt extrusion was employed. As a one-dimensional approach, it computes the non-isothermal flow conditions in the extrusion processes and calculates various parameters along the screw profile (e.g., global energy distributions, temperature, pressure, shear rate, residence time, etc.). At the first restrictive screw element, an instantaneous melting of the material is assumed. The computation begins at the die and proceeds backwards in an iterative way, until a final product temperature is reached. This procedure is needed, as the extruder is starve-fed with an unknown filling ratio [33–35]. In the case of conventional simulation, the physical properties and melt viscosity of the desired API/COP-blend were used. In the adopted simulation, the physical properties of the pure COP and model-based melt viscosity were employed instead [21]. Both of the simulation assumptions use the identical simulation algorithm, but the product related input parameter for simulation varies, leading to a reduced experimental effort in the case of the adopted simulation.

In more detail, the following product related input parameters need to be measured prior conventional simulation: heat capacity (solid and liquid state), density (solid and liquid state), thermal conductivity, glass transition temperature, and the melt viscosity

of the formulation. For the thermal conductivity, an approximation of 0.18 W·(m·K)-1 is made for all of the simulations. To decrease the experimental effort in our adopted simulation approach, the following approximation of the product related input parameters were made: heat capacity and density were used from pure COP, and the glass transition temperature of the required API-polymer blend needs to be measured. The melt viscosity is estimated using the $T_{g,\,blend}$ and the rheological profile of COP (please see section 7.6.2.5).

7.6.2.7 Hot-melt extrusion experiments

For performing the hot-melt extrusion experiments, a co-rotating twin-screw extruder ZE 12 (Three-Tec GmbH, Seon, Switzerland) was employed. It had a functional length of 25:1 L/D, 12 mm screws, 2 mm die, a maximum torque of 15 N·m and a fixed screw configuration, which is depicted in Figure 7.1. The screw speed was set to 100 rpm and the throughput was kept constant at 2.0 g/min using a volumetric feeding system. The specific mechanical energy (SME) during extrusion was determined by employing Equation 7.9,

$$SME = \frac{2\pi \cdot n \cdot \tau}{\dot{m} \cdot 60} \tag{7.9}$$

where n is the screw speed [rpm], $\dot{m}$ characterizes the feed rate [kg/h] and τ is the maximum torque per shaft [Nm] with a subtracted idling speed (1.2 Nm). Every physical mixture of 60 g for HME experiments was prepared using a Turbula mixer (Willy A. Bachofen AG – Maschinenfabrik, Muttenz, Swiss) for 10 min at 50 rpm.

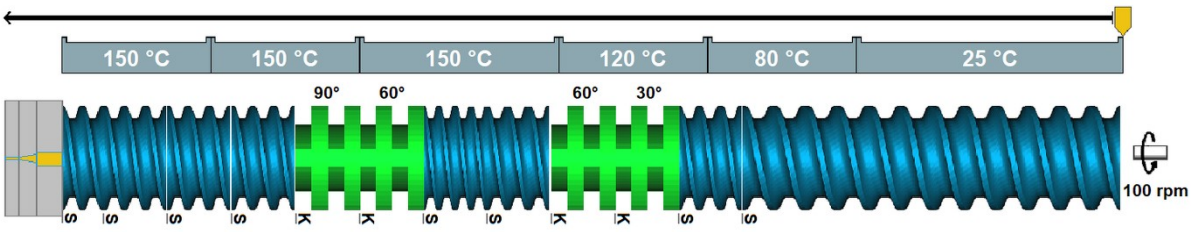

Figure 7.1 *Extruder and screw configuration used with conveying elements (9, 12 and 18 mm pitch) (blue) and kneading elements (30°,60° and 90° staggering angle) (green). Reproduced with permission from the authors of [21], Elsevier B.V., 2017.*

The amorphous state of the obtained extrudates directly after extrusion were confirmed by polarized light microscopy with and without λ-filter (data not shown).

7.7 Results

7.7.1 API solubility in the polymeric matrix and the deviation from Couchman-Karasz fit

In general, the solubility of an API in a polymeric matrix depends on the extent of specific interactions between both materials (e.g., hydrogen bonding). To evaluate whether these specific interactions were influencing the respective melt viscosity of a mixture, phase diagrams for every API in COP were generated (Fig 7.2a-d).

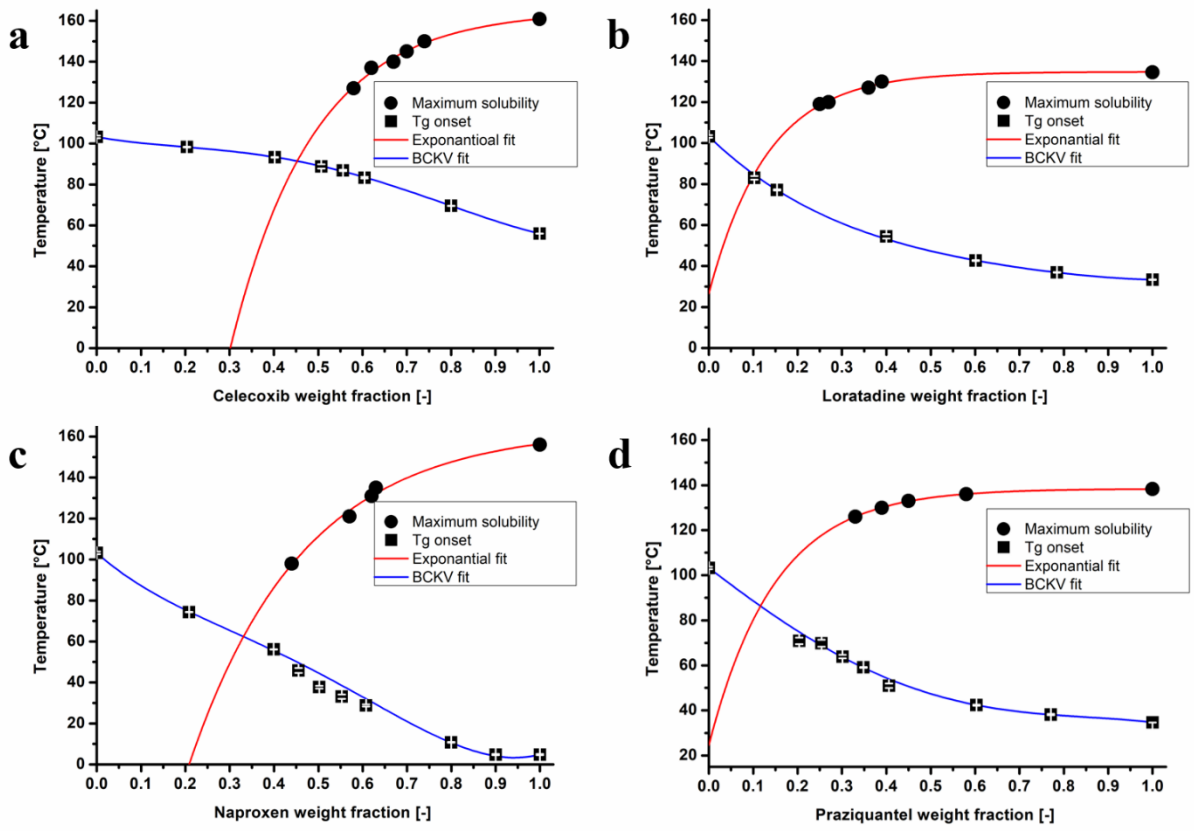

Figure 7.2a-d *Phase diagrams of celecoxib (a), loratadine (b), naproxen (c) and praziquantel (d) in copovidone.*

Celecoxib achieved the highest solubility of 33% in copovidone at 25 °C (Fig. 7.2a). and a slightly lower solubility of 25% in COP was found for naproxen (Fig 7.2c). Regarding loratadine and praziquantel, these APIs were insoluble in copovidone at an

ambient temperature and therefore specific interactions between API and COP were assumed as negligible (Fig 7.2b and 2d). All of the conducted BCKV-fits in this publication featured a high goodness of fit (0.99> adjusted r^2). In the case of exponential fit, a slightly lower but more than appropriate accuracy was found (0.98≥ adjusted r^2).

To evaluate, whether a deviation from the Couchman-Karasz fit (CK-fit, Equations 7.2-3) is influencing the accuracy of the model-based melt viscosity calculation, all of the CK-fits in comparison to the BCKV-fits (Equation 7.1) and the measured T_gs of the API/COP blends in different weight fractions, are shown in Figure 7.3a-d.

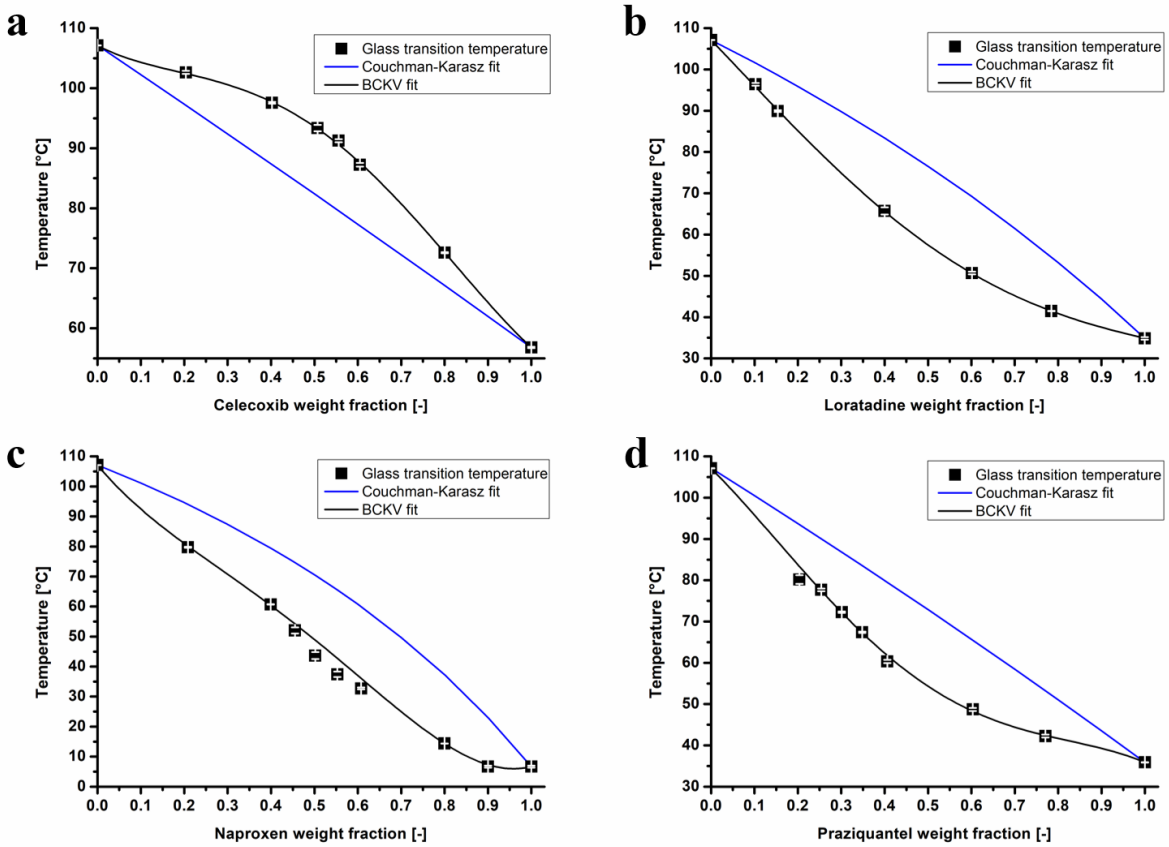

Figure 7.3a-d *Determined glass transition temperatures* (■)*, Couchman-Karasz (CK) and Brostow Chiu Kalogeras Vassilikou-Dova (BCKV) fits of celecoxib (a), loratadine (b), naproxen (c) and praziquantel (d) in different weight fractions in copovidone.*

Celecoxib was the only API that had a positive deviation of up to 8 °C from the CK-fit. For naproxen, a negative deviation of approximately 16 °C was obtained. A similar

negative discrepancy between the CK-fit and BCKV fit of 13 and 14 °C was found for loratadine and praziquantel in COP, respectively. In general, it is reported that a deviation from the CK-fit is connected to the solubility of the API in the polymeric matrix [36]. If no deviation from the CK-fit is found, the API is assumed to be insoluble. As all of the investigated APIs deviated from the CK-fit, this connection between the deviations of the measured T_gs to the CK fit and the solubility of the API in the polymer was not observed.

7.7.2 **Evaluation of potential physical property changes**

To investigate the influence of API and its weight fraction on the physical properties of the respective API/COP blend, the true density (ρ) and specific heat capacity (c_p) of the physical mixtures and extrudates were measured, listed in Table 7.2. In the case of pure COP, the true density increased slightly from powder (1,178 kg/m3) to the extruded material (1,191 kg/m3) [21]. In comparison to the physical mixtures of the COP-blends, the true density was similar to pure COP with a negligible increase of up to 4% ($\rho \leq$ 1,230 kg/m3). Furthermore, the extrudates of all COP blends showed an identical increase of up to 4% in true density ($\rho \leq$ 1,237 kg/m3).

Table 7.2 *Glass transition temperature identified by Brostow Chiu Kalogeras Vassilikou-Dova (BCKV) fit, true density and heat capacity of the COP-blends investigated.*

Mixture	T_g [°C]	ρ [kg/m^3] powder	ρ [kg/m^3] extrudate	C_p [J/(g·K)] at 25 °C	C_p [J/(g·K)] at 150 °C
COP	107	1178	1191	1.013	1.720
CXB 10 %	104	1230	1208	1.142	1.819
CXB 30 %	101	1279	1237	1.011	1.878
LOR 10 %	96	1215	1202	1.143	2.003
LOR 30 %	75	1200	1204	1.097	1.864
NAP 10 %	92	1190	1202	1.182	1.963
NAP 30%	71	1217	1209	1.117	1.883
PZQ 10 %	96	1220	1200	1.165	1.899
PZQ 30%	72	1200	1209	1.104	1.862

In the case of the specific heat capacity, a temperature-dependent increase for the pure COP from 1.013 J/(g·K) at 25 °C to 1.720 J/(g·K) at 150 °C was observed [21]. Regarding the API/COP physical mixtures, an increase in specific heat capacity of up

to 14% (c_p ≤ 1.182 J/(g·K)) at 25 °C and at 150 °C (c_p ≤ 2.003 J/(g·K)) was found, respectively.

The only slight deviation of the true density and specific heat capacity of COP-blends from the pure COP data were in good accordance to the findings in our recent work [21]. We already showed that a small deviation in both of the parameters did not affect the later use of pure COP data instead of the COP-blends data, as required by the input parameters for the Ludovic® simulation software. Furthermore, the accuracy of the computation outcomes for the 12 mm twin-screw extruder used was not reduced. Therefore, the small differences in the density and specific heat capacity of the ASDs compared with the pure polymeric matrix were assumed as negligible. In the case of the model-based simulation, the data of the pure COP instead of the COP-blend values were further investigated.

7.7.3 **Comparison of SAOS measurements and model-based melt viscosity calculation**

The measured melt viscosity and the model-based melt viscosity as a function of angular frequency at 150 °C is shown in Figure 7.4a-d. In general, the model-based melt viscosity of the 10% API/COP-blends were in better accordance with the measured data than the respective 30% API/COP-blends. The best agreement was found for NAP10%, for which both of the viscosity curves were superimposed ($\eta_{0,measured}$= 7198 Pa·s to $\eta_{0,estimated}$= 7141 Pa·s) (Figure 7.4c). Among all of the 10% API-blends, the highest deviation between the viscosities was found for CXB10% ($\eta_{0,measured}$= 40,791 Pa·s to $\eta_{0,estimated}$= 56,292 Pa·s) (Figure 7.4a). In the case of the 30% API/COP-blends, the discrepancy between the measured and model-based melt viscosity increased for both CXB30% ($\eta_{0,measured}$= 9381 Pa·s to $\eta_{0,estimated}$= 29,114 Pa·s) and LOR30% ($\eta_{0,measured}$= 1488 Pa·s to $\eta_{0,estimated}$= 343 Pa·s) (Figure 7.4a-b). However, NAP30% showed a deviation between the model-based melt viscosity to the measured data ($\eta_{0,measured}$= 259 Pa·s to $\eta_{0,estimated}$= 165 Pa·s). In conclusion, the accuracy of the melt viscosity estimation via the blend's T_g was a function of the API weight fraction. The border for estimating the melt viscosity with a sufficient accuracy seemed to be between a 10-30% API weight fraction, dependent on the API solubility. APIs soluble

at 25 °C within COP (e.g. celecoxib) might be underestimated, whereas the insoluble APIs (e.g. loratadine) might be overestimated.

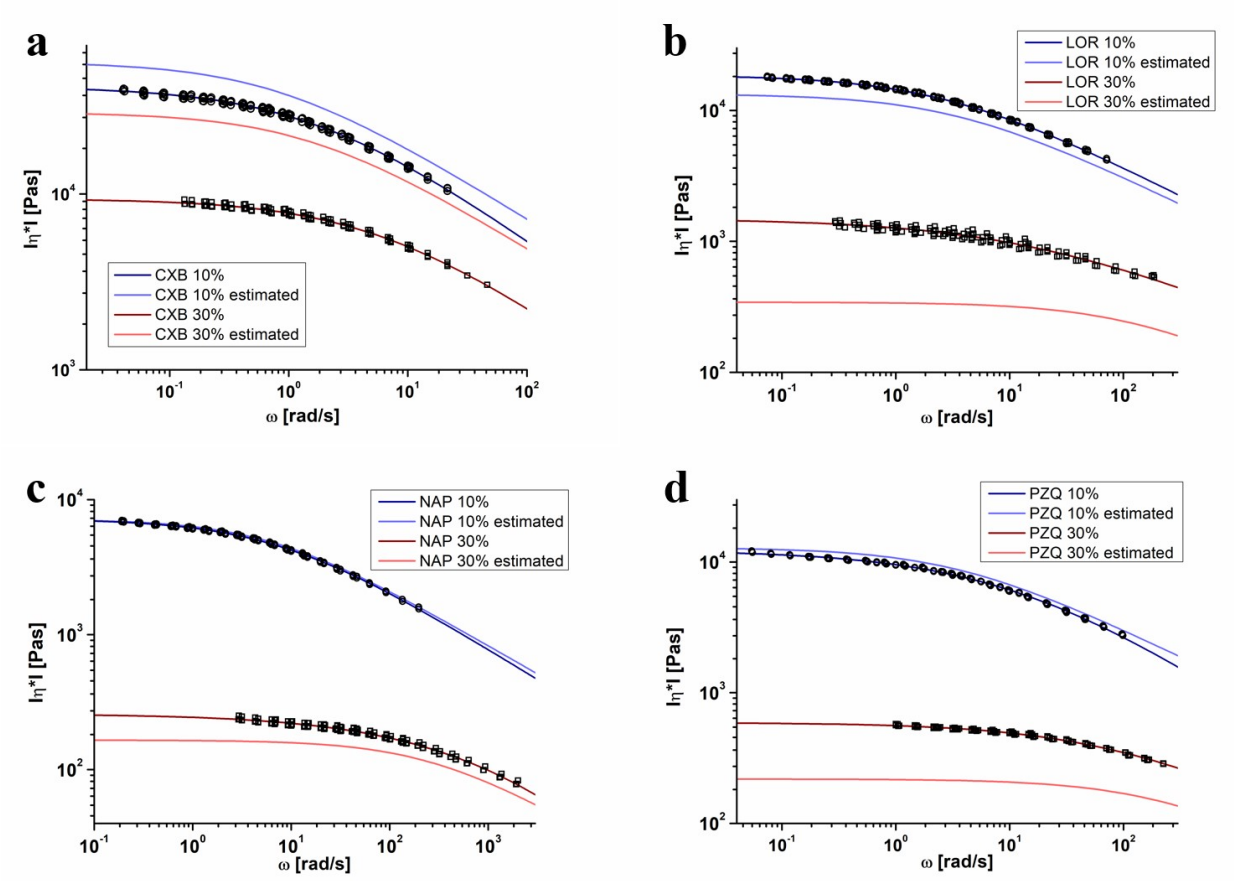

Figure 7.4a-d *Comparison of estimated melt viscosity and small amplitude oscillatory shear (SAOS) experiments at 150 °C for celecoxib (a), loratadine (b), naproxen (c) and praziquantel (d) in copovidone.*

7.7.4 Energy consumption in HME experiments, conventional simulation and simulation using model-based melt viscosity

The specific mechanical energy (SME) determined from HME experiments was compared to the energy consumptions obtained from the conventional simulation and the simplified simulation aided by using model-based melt viscosity at extrusion temperature of 150 °C (Figure 7.5a-d). In the HME simulation, SME is the sum of the specific energy, dissipated energy and melting energy [37]. In our case, the melting energy remained unconsidered in the simulation, because the Ludovic® model does not include a melting/softening temperature input for the API heat of fusion. Instead, in the

relevant input parameter in Ludovic®, the melting temperature was filled with the glass transition temperature of the API/COP-blend.

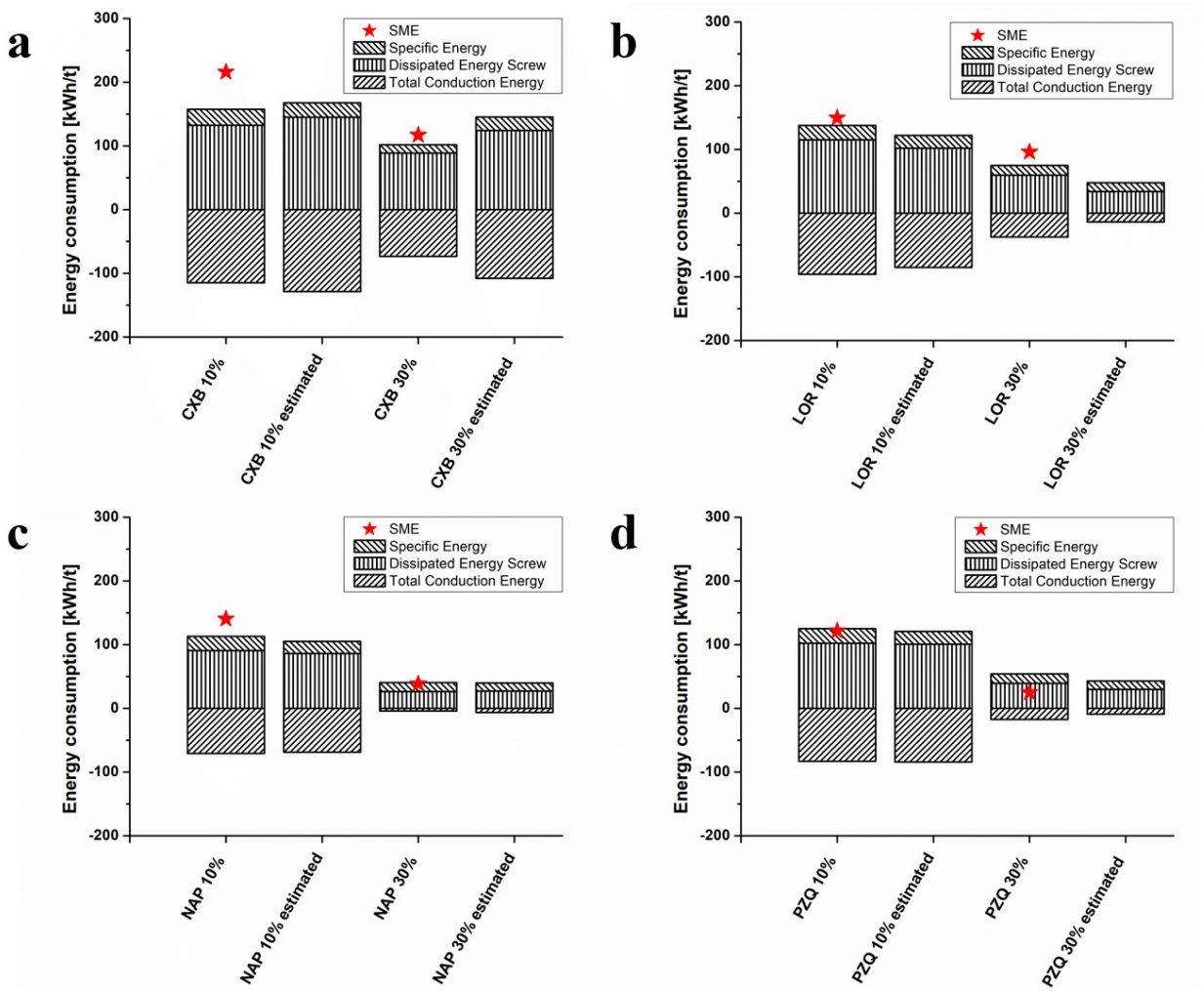

Figure 7.5a-d *Energy consumption in hot-melt extrusion (HME) experiments, conventional simulation, and simulation using model-based melt viscosity at 150 °C extrusion temperature for celecoxib (a), loratadine (b), naproxen (c) and praziquantel (d) in copovidone.6*

When all of the results are considered, because of the dependence of the dissipated energy on the melt viscosity, the dissipated energy decreased with both the lower viscosity and higher API content. The conduction energy, which determined the energy generated by barrel regulation-induced heat flux, also decreased in a similar manner.

Because of the plasticizing effect of the APIs and the respective decreased melt viscosity and glass transition temperature, all of the 10% API/COP blends achieved a higher SME than the corresponding 30% API/COP blend.

In the conventional simulation and HME experiments, similar SME results were obtained. Because of the 12 mm twin-screw extruder and the volumetric feeding system that were used, a variation in the feed rate might cause the slightly higher SME to be detected in the extrusion trials compared with the computed SMEs. For highly viscous melts, a loss of energy between the gearbox of the extruder and the screws or further friction was likely, which further led to discrepancies between the measured and simulated values. Furthermore, the determined torque for calculating the SME was measured by energy power and might have uncertainties for our small-scale extruder. In the case of the 10% API/COP-blends, the highest deviation between the measured and conventional simulated SMEs were seen for CXB10% (58 kWh/t) and NAP10% (27 kWh/t) (Fig 7.5a, c). The SMEs of LOR10% and PZQ10% nearly superimposed instead (Figure 7.5b and 7.5d). A similar variance in the data between the measured and conventional simulated SMEs was found for the 30% API/COP-blends. The SMEs of NAP30% were superimposed, whereas the highest deviation in data was found for PZQ30% (29 kWh/t) (Figure 7.5c and 7.5d).

In the case of the model-based simulation, the computation outcomes were in good accordance with the conventional simulation (<20% deviation), except CXB30% and LOR30%. In the case of the loratadine containing samples, a higher discrepancy between the model-based and conventional SME was found. As a result of the high API-content, the model-based computation for LOR30% differed from the conventional one and failed to calculate the correct SME. The same findings were observed for the celecoxib-containing blends. The SME of CXB10% was simulated similarly by both approaches, but in terms of CXB30%, the model-based simulation failed. However, the SMEs of the naproxen- and praziquantel-containing blends deviated not more than approximately 10 kWh/t from the results of the conventional simulation. For PZQ30%, the model-based simulation fits better than the conventional one to the HME experiments, which might be coincidental. Therefore, the use of the model-based melt viscosity in the simulation led to a similar outcome as a conventional HME simulation, as

long as a critical API weight fraction is not reached (approximately ≥30%) in the desired amorphous solid dispersion. Otherwise, the probability of an inadequate SME computation might increase.

7.8 Discussion

In the case of the solubility in copovidone of the four investigated APIs, celecoxib and naproxen were soluble, whereas loratadine and praziquantel were insoluble at room temperature. Regarding the deviations from the Couchman–Karasz model, celecoxib in copovidone was the only API that achieved a positive deviation from the CK-fit. For loratadine, naproxen, and praziquantel, a negative deviation from the CK-fit was observed. The assumption that a deviation from the Couchman–Karasz fit is connected to the solubility of the API in the polymeric matrix was not confirmed by our solubility findings. All of the APIs had a variation from the CK-fit, but only naproxen and celecoxib were actually soluble in copovidone. Especially regarding the 10% API/COP blends, the influence of the deviation from the CK model to our adopted HME simulation using model-based melt viscosity, cannot be confirmed. In the case of the 30% API/COP blends, only celecoxib might show a decreased simulation accuracy, related to the positive deviation from the CK model. However, the failed CXB 30% adopted simulation seems more connected to the high solubility of celecoxib in COP than to the deviation from the CK-fit.

Regarding the estimation of the rheological flow profiles of the investigated API/COP blends and the computed energy consumptions in the simulation thereof, the SMEs of the 10% API/COP blends corresponded to the experimental findings and to the conventional HME simulation. Accordingly, a 10% API weight fraction did not influence the accuracy of the resulted HME simulation, using the mainly estimated product input parameter. It leads to the conclusion that a formulation with a 10% API weight fraction can be generally be predicted by our adopted HME simulation, independent of the API’s nature.

In the case of the 30% API content, the melt viscosity calculation and HME simulation for naproxen and praziquantel were consistent with the experimental data. The simulation of SME for celecoxib and loratadine failed, which was a result of the inadequate calculated model-based melt viscosities. The rank order from the overestimated to underestimated melt viscosity data compared to experimental results is CXB ▸ NAP ▸ PZQ ▸ LOR. This order corresponds perfectly to the solubility order in COP of CXB (33%, 25 °C) ▸ NAP (25%, 25 °C) ▸ PZQ (insoluble at 25 °C) ▸ LOR (insoluble at 27 °C). Therefore, at high API weight fractions, the solubility and the respective specific interactions between the API and the polymeric matrix might become prominent and influence the viscosity by decreasing it. In our recent work, the influence of specific interactions on the melt viscosity was already found for indomethacin, which is highly soluble in copovidone (approximately 36% at ambient temperature) [21,23]. Regarding the model-based melt viscosity, it seems that not only the glass transition temperature is important for such calculation, but also the amount of specific interactions (e.g., solubility) should be considered. If an API is less soluble or insoluble in the polymeric matrix of the formulation, our adopted HME simulation is applicable. For highly soluble APIs at high API weight fractions, the uncertainty of the HME simulation using the model-based melt viscosity is increasing and should be carefully regarded. The adopted simulation approach might fail because of the influence of specific interaction between the API and polymer, reducing the melt viscosity to an unpredictable extent.

Furthermore, the original data set for our T_g-melt viscosity correlation was mainly comprising soluble APIs in the range of naproxen and less insoluble APIs. Therefore, our original data set might have triggered this uncertainty in the model-based melt viscosity calculation independent of the API solubility in COP. An improvement of the melt viscosity calculation would be the consideration of the influence of API solubility on the melt viscosity. This is still ongoing work, as the presented data set is not appropriate to allow for this consideration. Additionally, the overestimation of the CXB 30% melt viscosity might be further triggered by the rarely occurred positive deviation from CK-fit.

In general, the use of model-based melt viscosity for amorphous solid dispersions in the hot-melt extrusion simulation is feasible to compute energy consumptions thereof,

using the Ludovic® software. The experimental short-cut in the HME simulation is functional; however, the assumptions have to be improved to enable the calculation at higher API weight fractions. In accordance with our purpose to simplify the use of HME computation in early stage development and to reduce the effort needed, we were able to prove the good suitability of our model. Therefore, this procedure would enable an enhanced and fast estimate of a good starting point for extrusion trials in early drug development for amorphous solid dispersions.

7.9 Conclusion

A hot-melt extrusion numerical simulation using a model-based melt viscosity and further physical properties of the pure polymeric matrix led to accurate computation outcomes, as did the conventional simulation, with only few exceptions. All of the HME simulations, conducted using the commercial 1D simulation software Ludovic®, were confirmed by the energy consumptions of the HME experiments. It was shown that even APIs, which were not considered to establish the T_g-melt viscosity correlation for amorphous solid dispersions in the first place, were impeccably simulated. However, the formulations with a high API weight fraction (≥30% *w/w*) should be regarded cautiously, as a decrease in computation accuracy is likely. This decrease in accuracy was likely triggered by the influence of specific interactions as a result of the solubility of the APIs, which were not considered in establishing the T_g-melt viscosity correlation. In conclusion, reducing the experimental effort prior to the HME simulation using a model-based melt viscosity for simulation purposes, was proven as a valuable API-independent method to simplify the HME process optimization in the early formulation development for forming amorphous solid dispersions.

7.10 Author contributions

Conceptualization, K.G.W.; Methodology, E.S.B; Validation, E.S.B. and A.G.; Investigation, E.S.B.; Resources, K.G.W. and A.G.; Writing-Original Draft Preparation, E.S.B.; Writing-Review & Editing, K.G.W. and A.G.; Supervision, K.G.W.; Project Administration, K.G.W..

7.11 Funding

This research received no external funding, except the free use of the software license for Ludovic®.

7.12 Acknowledgement

The authors would like to thank BASF SE, primarily Thorsten Cech und Florian Bang for providing measuring time on their rheometer. Further warm thanks to Sciences Computers Consultants (Saint Etienne, France), especially Philippe David, Giang Trinh, Laurent Ratte and Pauline Alvares for their scientific support and always having an open ear and last but not least for sponsoring the software license. Additionally, we would like to thank Rachel C. Evans greatly for reviewing the manuscript. During the conduction of this research, Andreas Gryczke was employed by BASF SE (Ludwigshafen am Rhein, 67063, Germany).

7.13 Conflicts of Interest

The authors declare no conflict of interest. The founding sponsors had no role in the design of the study; in the collection, analyses or interpretation of data; in the writing of the manuscript, or in the decision to publish the results. A. G. is an employee of AbbVie Deutschland GmbH & Co.

7.14 References

1. LaFountaine, J. S.; McGinity, J. W.; Williams, R. O. Challenges and Strategies in Thermal Processing of Amorphous Solid Dispersions: A Review. AAPS PharmSciTech 2016, 17, 43–55, doi:10.1208/s12249-015-0393-y.
2. Patil, H.; Tiwari, R. V.; Repka, M. A. Hot-Melt Extrusion: from Theory to Application in Pharmaceutical Formulation. AAPS PharmSciTech 2016, 17, 20–42, doi:10.1208/s12249-015-0360-7.
3. Tiwari, R. V.; Patil, H.; Repka, M. A. Contribution of hot-melt extrusion technology to advance drug delivery in the 21st century. Expert Opin. Drug Deliv. 2016, 13, 451–464, doi:10.1517/17425247.2016.1126246.

4. Agrawal, A. M.; Dudhedia, M. S.; Zimny, E. Hot Melt Extrusion: Development of an Amorphous Solid Dispersion for an Insoluble Drug from Mini-scale to Clinical Scale. AAPS PharmSciTech 2016, 17, 133–147, doi:10.1208/s12249-015-0425-7.

5. Yang, F.; Su, Y.; Zhang, J.; DiNunzio, J.; Leone, A.; Huang, C.; Brown, C. D. Rheology Guided Rational Selection of Processing Temperature To Prepare Copovidone–Nifedipine Amorphous Solid Dispersions via Hot Melt Extrusion (HME). Mol. Pharm. 2016, 13, 3494–3505, doi:10.1021/acs.molpharmaceut.6b00516.

6. Chan, S.-Y.; Qi, S.; Craig, D. Q. M. An investigation into the influence of drug–polymer interactions on the miscibility, processability and structure of polyvinylpyrrolidone-based hot melt extrusion formulations. Int. J. Pharm. 2015, 496, 95–106, doi:10.1016/j.ijpharm.2015.09.063.

7. Zecevic, D. E.; Wagner, K. G. Rational Development of Solid Dispersions via Hot-Melt Extrusion Using Screening, Material Characterization, and Numeric Simulation Tools. J. Pharm. Sci. 2013, 102, 2297–2310, doi:10.1002/jps.23592.

8. Thiry, J.; Krier, F.; Evrard, B. A review of pharmaceutical extrusion: Critical process parameters and scaling-up. Int. J. Pharm. 2015, 479, 227–240, doi:10.1016/j.ijpharm.2014.12.036.

9. Zecevic, D. E.; Evans, R. C.; Paulsen, K.; Wagner, K. G. From benchtop to pilot scale–experimental study and computational assessment of a hot-melt extrusion scale-up of a solid dispersion of dipyridamole and copovidone. Int. J. Pharm. 2018, 537, 132–139, doi:10.1016/j.ijpharm.2017.12.033.

10. Grimard, J.; Dewasme, L.; Vande Wouwer, A. A Review of Dynamic Models of Hot-Melt Extrusion. Processes 2016, 4, 19, doi:10.3390/pr4020019.

11. Rantanen, J.; Khinast, J. The Future of Pharmaceutical Manufacturing Sciences. J. Pharm. Sci. 2015, 104, 3612–3638, doi:10.1002/jps.24594.

12. Gaspar-Cunha, A.; Poulesquen, A.; Vergnes, B.; Covas, J. A. Optimization of processing conditions for polymer twin-screw extrusion. Int. Polym. Process. 2002, 17, 201–213.

13. Durin, A.; De Micheli, P.; Nguyen, H.-C.; David, C.; Valette, R.; Vergnes, B. Comparison between 1D and 3D Approaches for Twin-Screw Extrusion Simulation. Int. Polym. Process. 2014, 29, 641–648.

14. Gaspar-Cunha, A.; Covas, J. A.; Vergnes, B. Defining the configuration of co-rotating twin-screw extruders with multiobjective evolutionary algorithms. Polym. Eng. Sci. 2005, 45, 1159–1173, doi:10.1002/pen.20391.

15. Sarhangi Fard, A.; Anderson, P. D. Simulation of distributive mixing inside mixing elements of co-rotating twin-screw extruders. Comput. Fluids 2013, 87, 79–91, doi:10.1016/j.compfluid.2013.01.030.

16. Lozano, T.; Lafleur, P. G.; Grmela, M.; Vergnes, B. Modeling filler dispersion along a twin-screw extruder. Int. Polym. Process. 2003, 18, 12–19.

17. Malik, M.; Kalyon, D. M.; Golba Jr, J. C. Simulation of co-rotating twin screw extrusion process subject to pressure-dependent wall slip at barrel and screw surfaces: 3D FEM Analysis for combinations of forward-and reverse-conveying screw elements. Int. Polym. Process. 2014, 29, 51–62.

18. Zhang, X.-M.; Feng, L.-F.; Hoppe, S.; Hu, G.-H. Local residence time, residence revolution, and residence volume distributions in twin-screw extruders. Polym. Eng. Sci. 2008, 48, 19–28, doi:10.1002/pen.20812.

19. Gao, J.; Walsh, G. C.; Bigio, D.; Briber, R. M.; Wetzel, M. D. Residence-time distribution model for twin-screw extruders. AIChE J. 1999, 45, 2541–2549.

20. Bochmann, E. S.; Üstüner, E. E.; Gryczke, A.; Wagner, K. G. Predicting melt rheology for hot-melt extrusion by means of a simple Tg -measurement. Eur. J. Pharm. Biopharm. 2017, 119, 47–55, doi:10.1016/j.ejpb.2017.05.010.

21. Bochmann, E. S.; Steffens, K. E.; Gryczke, A.; Wagner, K. G. Numerical simulation of hot-melt extrusion processes for amorphous solid dispersions using model-based melt viscosity. Eur. J. Pharm. Biopharm. 2018, 124, 34–42, doi:10.1016/j.ejpb.2017.12.001.

22. Bochmann, E. S.; Neumann, D.; Gryczke, A.; Wagner, K. G. Micro-scale prediction method for API-solubility in polymeric matrices and process model for forming amorphous solid dispersion by hot-melt extrusion. Eur. J. Pharm. Biopharm. 2016, 107, 40–48, doi:10.1016/j.ejpb.2016.06.015.

23. Prudic, A.; Ji, Y.; Sadowski, G. Thermodynamic Phase Behavior of API/Polymer Solid Dispersions. Mol. Pharm. 2014, 11, 2294–2304, doi:10.1021/mp400729x.

24. Marsac, P. J.; Shamblin, S. L.; Taylor, L. S. Theoretical and Practical Approaches for Prediction of Drug–Polymer Miscibility and Solubility. Pharm. Res. 2006, 23, 2417–2426, doi:10.1007/s11095-006-9063-9.

25. Mahieu, A.; Willart, J.-F.; Dudognon, E.; Danède, F.; Descamps, M. A New Protocol To Determine the Solubility of Drugs into Polymer Matrixes. Mol. Pharm. 2013, 10, 560–566, doi:10.1021/mp3002254.
26. Kim, S.; Thiessen, P. A.; Bolton, E. E.; Chen, J.; Fu, G.; Gindulyte, A.; Han, L.; He, J.; He, S.; Shoemaker, B. A.; Wang, J.; Yu, B.; Zhang, J.; Bryant, S. H. PubChem Substance and Compound databases. Nucleic Acids Res. 2016, 44, D1202–D1213, doi:10.1093/nar/gkv951.
27. Brostow, W.; Chiu, R.; Kalogeras, I. M.; Vassilikou-Dova, A. Prediction of glass transition temperatures: Binary blends and copolymers. Mater. Lett. 2008, 62, 3152–3155, doi:10.1016/j.matlet.2008.02.008.
28. Couchman, P. R.; Karasz, F. E. A classical thermodynamic discussion of the effect of composition on glass-transition temperatures. Macromolecules 1978, 11, 117–119.
29. Carreau, P. J. Rheological Equations from Molecular Network Theories. Trans. Soc. Rheol. 1972, 16, 99–127, doi:10.1122/1.549276.
30. Yasuda, Kenji Investigation of the analogies between viscometric and linear viscoelastic properties of polystyrene fluids. Ph.D. thesis, Massachusetts Inst. of Technology: Cambridge, 1979.
31. Doolittle, A. K. Studies in Newtonian Flow. II. The Dependence of the Viscosity of Liquids on Free-Space. J. Appl. Phys. 1951, 22, 1471–1475, doi:10.1063/1.1699894.
32. Williams, M. L.; Landel, R. F.; Ferry, J. D. The Temperature Dependence of Relaxation Mechanisms in Amorphous Polymers and Other Glass-forming Liquids. J. Am. Chem. Soc. 1955, 77, 3701–3707, doi:10.1021/ja01619a008.
33. Vergnes, B.; Valle, G. D.; Delamare, L. A global computer software for polymer flows in corotating twin screw extruders. Polym. Eng. Sci. 1998, 38, 1781–1792.
34. Teixeira, C.; Gaspar-Cunha, A.; Covas, J. A. Flow and Heat Transfer Along the Length of a Co-rotating Twin Screw Extruder. Polym.-Plast. Technol. Eng. 2012, 51, 1567–1577, doi:10.1080/03602559.2012.716477.
35. Carneiro, O. S.; Covas, J. A.; Vergnes, B. Experimental and theoretical study of twin-screw extrusion of polypropylene. J. Appl. Polym. Sci. 2000, 78, 1419–1430.

36. Baird, J. A.; Taylor, L. S. Evaluation of amorphous solid dispersion properties using thermal analysis techniques. Adv. Drug Deliv. Rev. 2012, 64, 396–421, doi:10.1016/j.addr.2011.07.009.

37. Kohlgrüber, K.; Bierdel, M. Co-rotating twin-screw extruders: fundamentals, technology, and applications; first edition, Carl Hanser Publishers ; Hanser Gardner Publications: Munich [Germany] : Cincinnati, Ohio, 2008; 72-74; ISBN 978-1-56990-422-0.

8 Summary and outlook

8.1 Solubility prediction of APIs in polymer melts

A micro-scale prediction model to define the solubility of an API in a polymeric matrix in temperature-dependency by differential scanning calorimetry (DSC) was established. It consists of an annealing step and a subsequent analysis of the glass transition temperature (T_g). By using a complex mathematical model (BCKV-equation), the soluble API fraction can be determined by employing the API/polymer ratio-dependent T_g curve progression. By using melt-rheological data and XRPD, the validity of the annealing step to allow the API-polymer blend to equilibrate at this temperature, was confirmed. However, further trials showed that the prediction model was not able to correlate to a processing temperature within the HME process. Furthermore, a connection between the deviation from Couchman-Karasz equation as a hint for API solubility (e.g. specific interactions) in the polymeric matrix was not confirmed. Overall, our DSC methodology to identify the API solubility within a polymeric matrix and to estimate a temperature-dependent phase diagram for extrapolating the solubility to ambient condition was successfully established. It simplifies the formulation screening for ASD by hot-melt extrusion.

A data review on the variety of available API solubility in literature was performed. Data out of the data review were compared to our own solubility prediction model and showed good agreement. The entire data set comprised seven polymers, commonly used for forming ASD, 37 APIs and two sugar derivates. The prediction models used in literature were mainly the melting point depression method, dissolution endpoint measurements, indirect solubility determination by T_g and the use of low molecular weight analogues. It was observed that the resulted API solubility depended less on the method used, but rather on the working group and authors who conducted the measurements. Due to difficulties in enabling an equilibrated state prior the API solubility determination, the characterization might be generally prone to errors.

Regarding molecular weight, no connection or tendency of API solubility on the molecular weight of PVP was observed. Furthermore, the highest API solubility were observed for PVP, the poorest for PVAc. Therefore, the API solubility in the copolymer copovidone (PVP and PVAc) depended on the PVP/PVAc ratio used. In the case of SOL, the API solubility was always comparable to COP. PMMA, PEG and HPMC grades achieved a lower solubility as well, especially compared to PVP.

In conclusion, a data set for training new developed solubility prediction models was established. It can serve for validation and training of even such systems, which are based on using only the physicochemical properties of a desired API. The establishment and validation of such prediction models is still ongoing work.

8.2 Hot-melt extrusion simulation with model-based melt viscosity

A correlation between glass transition temperature and melt viscosity in temperature / angular frequency-dependency of an amorphous solid dispersion (ASD) was successfully established. This correlation was largely independent of the added active pharmaceutical ingredient (API) or plasticizer to copovidone. Negligible dependencies on molecular weight, recrystallization tendency, weight fraction (up to 30%) and plasticizing effect were found. However, a positive deviation from the theoretical Couchman-Karasz weight fraction-dependent progression of T_g might influence the accuracy of the predicted melt viscosity. Furthermore, hints of a connection between variable *b* of the T_g-viscosity correlation (Eq. 5.7) and the API solubility in the polymeric matrix were found. A high API solubility may increase the plasticization in the polymeric matrix, whereas a non-soluble API may lead to a higher melt viscosity than estimated. Unfortunately, the present data set does not allow a solubility-dependent (e.g. specific interaction-dependent) consideration of the T_g-viscosity correlation, but it is an important factor to improve our established estimation of melt viscosity. Furthermore, the T_g-viscosity correlation is polymer-dependent. Thus, building up a data base of the most commonly used pharma polymers would improve the application of the model-based melt viscosity on numerical hot-melt extrusion (HME) simulation, too.

The application of the T_g-viscosity correlation in hot-melt extrusion 1D numerical process simulation was verified in dependence of energy consumption and residence time distribution. The use of model-based melt viscosity and further physicochemical parameters of the pure polymeric matrix in HME simulation led to similar results as the use of experimental melt viscosity in a conventional simulation procedure up to 30% API weight fraction. A proof of concept with APIs, which were not considered in establishing the T_g-viscosity correlation, confirmed the findings. In the case of mean residence time (MRT), an increase in dependence of an increase in API weight fraction was observed. The influence of melt viscosity was negligible. Instead, the simulation procedure with model-based melt viscosity was only verified by using a small-scale extruder (12 mm screw diameter) with limited variations in process conditions. Therefore, trials on large-scale extruders in a wider set of process conditions should be conducted. The use of model-based melt viscosity has been verified by using amorphous solid dispersions only. The applicability for formulation with solid particle fractions needs to be further evaluated.

In conclusion, a method to “short-cut” rheological measurements for the use in HME numerical simulation to produce ASDs was established. It reduces the effort in measurement down to a T_g-determination by DSC and rheological trials with the pure polymeric matrix, thus it simplifies the application of 1D HME simulation. Overall, our procedure enables the estimation of a good starting point for HME trials in early formulation development at reduced material and costs. It supports the rational development for forming amorphous solid dispersions by means of HME and reduces experimental trials to define the best formulation and HME process conditions.

9 Publications

Parts of this work are already published as:

Articles:

- Bochmann, E.S., Gryczke, A., Wagner*, K.G.;*Validation of Model-Based Melt Viscosity in Hot-Melt Extrusion Numerical Simulation*, Pharmaceutics 10(3), 132; 2018; doi.org/10.3390/pharmaceutics10030132
- Bochmann, E.S., Steffens, K.S., Gryczke, A., Wagner*, K.G.; *Numerical simulation of hot-melt extrusion processes for amorphous solid dispersions using model-based melt viscosity*; Eur. J. Pharm. Biopharm. 124, 34-42; 2018; doi:10.1016/j.ejpb.2017.12.001
- Bochmann, E.S., Üstüner, E.E., Gryczke, A., Wagner*, K.G.; *Predicting melt rheology for hot-melt extrusion by means of a simple T_g-measurement*; Eur. J. Pharm. Biopharm. 119, 47-55; 2017; doi:10.1016/j.ejpb.2017.05.010
- Bochmann, E.S., Neumann, D., Gryczke, A., Wagner*, K.G.; *Micro-scale prediction method for API-solubility in polymeric matrices and process model for forming amorphous solid dispersion by hot-melt extrusion*; Eur. J. Pharm. Biopharm. 107, 40–48; 2016; doi:10.1016/j.ejpb.2016.06.015

Abstracts (Conference participation):

- Bochmann*, E., Wagner, K.G.; *Hot-melt extrusion simulation with model-based input data for amorphous solid dispersion*; 11th PBP World Meeting, Granada, Spain, March 2018
- Bochmann*, E., Wagner, K.G.; *Micro-scale prediction method for API-solubility in polymeric matrices and stability thereof*; 10th PBP World Meeting, Glasgow, Scotland, April 2016